Tropical cirrus in high-resolution global and regional models

Samantha M. Turbeville

A dissertation
submitted in partial fulfillment of the
requirements for the degree of

Doctor of Philosophy

University of Washington

2024

Reading Committee:

Thomas P. Ackerman, Chair

Peter N. Blossey

Benjamin R. Hillman

Program Authorized to Offer Degree:
Atmospheric Sciences, UW

University of Washington

Abstract

Tropical cirrus in high-resolution global and regional models

Samantha M. Turbeville

Chair of the Supervisory Committee:
Professor Emeritus Thomas P. Ackerman
Atmospheric Sciences

Cirrus clouds remain a large source of uncertainty in predictions of future climate. It is difficult to simulate cirrus because they have very thin optical depths yet cover large horizontal extents. Representation of cirrus in models is difficult to verify due to the limited observations that are comparable to model output. Yet as models continue to increase horizontal and vertical resolutions, cirrus cloud microphysics and parameterizations become an increasingly important driver of model uncertainty. This dissertation is part of a recent effort to reduce uncertainties from high clouds and improve understanding of TTL cirrus. We use high-resolution models on global and regional scales to understand the contribution of ice microphysics and cirrus clouds to the model spread or uncertainty. We investigate the origins of cirrus clouds in high-resolution simulations of radiative convective equilibrium. The origins of cirrus have been a source of debate for decades and this dissertation provides valuable insight into the role of convection in cirrus cloud formation. While convection is a key source of cirrus and water vapor in the upper-troposphere, there are many in-situ formed cirrus that persist far from convection.

While the models generally represent large-scale tropical convection with fidelity, there are large regional differences in cloud properties and top-of-atmosphere radiative fluxes. We focus on the Tropical Western Pacific (TWP) as a case study for the local and small-scale features available with the high spatiotemporal resolution of GSRMs. Each model simulates unique cloud characteristics that are persistent across seasons. We show that these models simulate the difficult-to-observe thin tropical tropopause layer (TTL) cirrus. The models typically scatter around observations but have persistent biases, which stem from the different microphysics and dynamics used in each model. In order to separate microphysical and dynamical effects in the models, we use a single model regional domain sensitivity study to expose the role of microphysics on tropical cirrus. Microphysics can play a significant role in cirrus properties that can have a disproportionate impact on top-of-atmosphere (TOA) radiative fluxes. Sensitivity to ice microphysics seems to explain some of the model spread.

Furthermore, we explore how the ice nucleation scheme and the presence of large-scale ascent impacts cirrus clouds in simulations with convective organization. We introduce passive tracers to the model in order to investigate the origin and life cycle of cirrus clouds. The structure and degree of convective organization seems to play a key role in the amount of in-situ cirrus in these simulations. While the response of anvil clouds is similar to other RCE models when the SST is increased by 4K, the response of in-situ cirrus is uncertain; they decrease in frequency of occurrence in two of three simulations. Nonetheless, all simulations show a warming of in-situ cirrus clouds when the SST is increased by 4K.

TABLE OF CONTENTS

LIST OF FIGURES

Chapter 1

INTRODUCTION

1.1 Cirrus clouds

Tropical cirrus clouds, especially those near the tropopause, are some of the highest on Earth. They occur at extremely cold temperatures and have a disproportionately large effect on radiation with their small yet strong warming effect (Ackerman et al., 1988; Hartmann & Berry, 2017). Jensen et al. (1996) noted the persistence of near-tropopause thin cirrus. The extremely cold temperatures in the upper troposphere impact radiation significantly when clouds are present through the absorption and re-emission of LW radiation at much lower temperatures than anywhere else on Earth.

The tropical tropopause layer (TTL, also known as the tropopause transition layer) was first introduced in Highwood and Hoskins (1998) as a transitional zone with properties of both the troposphere and stratosphere. The TTL is driven both by dynamics and radiative processes leading the TTL to have its unique structure. The TTL is the $14 - 18$ km layer in the tropics that has strong implications for water vapor entering the stratosphere, acting as a "gate to the stratosphere" (Fueglistaler et al., 2009). The presence of clouds in the TTL has been shown to "freeze-dry" the stratosphere; clouds form in the TTL, reducing the supersaturation of the air parcel and effectively dehydrating the TTL and any air rising across the tropopause (Jensen, 2004; Holton & Gettelman, 2001). It can be difficult to observe the impacts of cirrus on water vapor directly since there are no co-located satellite products and aircraft measurements are sparse and cannot track the life cyle of a cirrus cloud. Thus, models can be a useful tool to studying TTL cirrus and (de)hydration. The amount of ice reaching the stratosphere also depends on the ice habit of the cirrus clouds (Lamraoui et al., 2023), which depend on the origin and microphysical properties (as described in Chapter 1.1.1).

The vertical structure of tropical clouds is complex and important for its impact on rainfall, radiation, and water vapor (Liou, 1986; Sassen et al., 2009). Cirrus clouds have a warming effect at the top-of-atmosphere by absorbing LW radiation from below and re-emitting at the extremely cold temperatures in the upper troposphere, reducing the outgoing LW radiation (OLR) that can escape to space. TTL cirrus also have a local warming effect on the TTL through cloud-radiative heating (Fu et al., 2018).

There are several studies which attempt to quantify the role of convection in cirrus cloud formation. Massie et al. (2002) find that cirrus in observations were detrained from convection about half of the time. Luo and Rossow (2004) also found that in-situ cirrus are numerous and have their own dynamics and lifecycle. This dissertation also attempts to quantify the fraction of in-situ cirrus and the potential role (or lack thereof) of convection. Due to the difficulties of observing and measuring cirrus, we take advantage of the high-resolution output from models to quantify the impact of convection on cirrus (see Chapter 4).

1.1.1 Microphysics of cirrus

From their small scale processes (individual ice crystals are micrometers in diameter) to their large horizontal expanse (1000s of kilometers), cirrus clouds remain a challenge in computer models (Morrison et al., 2020). This section describes the microphysical processes relevant for cirrus clouds and sets up the historical context for the problem of ice microphysics. These processes are parameterized in all storm-resolving models. We discuss how these parameterizations impact model uncertainty related to cirrus.

Krämer et al. (2016) described the microphysical properties of cirrus clouds using 15 years of aircraft measurements from 17 field campaigns resulting in about 94 hours in cirrus clouds. The cirrus are also broken into liquid-origin and in-situ origin

(Lawson et al., 2019; Krämer et al., 2016). Krämer et al. (2016) generally find that the liquid-origin cirrus have higher ice water content (IWC) and ice mass radius (R_{ice}) and that in-situ cirrus have two mechanisms of formation: slow and fast updrafts. TTL cirrus fall into the former category as a special case of slow large-scale ascent, but are not included in their models. Slow large-scale updrafts tend to have low IWC cirrus with few but large ice crystals. Fast updraft cirrus tend to have larger IWC and high ice number, N_i. Jensen et al. (2009) also emphasized the importance of small ice crystals in tropical anvil cirrus in setting the radiative heating rates in the recently detrained anvil cirrus. In-situ cirrus have distinct ice habits, mostly rosettes, while anvil cirrus contain more columns and aggregates (Lawson et al., 2019). They also found that subvisible TTL cirrus may have more plates and quasi-spherical ice particles. The presence of ice nucleating particles (INP) is also key to properties of cirrus present at a given moment (Beer et al., 2024; Hawker et al., 2021). We compare some of our model results in Chapters 3 and 4 to the climatology from these aircraft campaigns following Krämer et al. (2020).

From the late 1980's, this problem of how cirrus interact with water vapor and radiation has been persistent. Ackerman et al. (1988) and Lilly (1988) began the scientific journey into cirrus cloud dynamics and heating rates. Due to the complex processes and relationships between ice and radiation, progress has been slow and there are still large uncertainties associated with cirrus clouds. As much as we have improved our knowledge of cirrus clouds through in-situ observations and satellite measurements, there is still a gap in how to represent such processes in models. Many modern schemes use a bulk microphysics, which defines the ice distribution in a single model grid box, rather than following the life cycle of individual ice crystals. Sullivan and Voigt (2021) found that using a two moment bulk microphysics scheme, which predicts both ice mass (q_{ice}) and ice number (N_{ice}), significantly improves simulations of ice clouds over one moment schemes. We explore cirrus sensitivities using a two moment bulk microphysics scheme in Chapters 3 and 4.

Cirrus clouds also introduce variability from the different types of ice present in anvil outflow and in-situ cirrus (Krämer et al., 2016, 2020; Lamraoui et al., 2023). Atlas et al. (2024) found that changing the microphysics scheme (one of which was P3 used in Chapters 3 and 4) caused up to 20 W/m^2 changes in the LW cloud radiative effect, which was dominated by the cirrus cloud impacts. Using the radiation is a common way to evaluate the cloud microphysics due to the explicit coupling between the two (e.g., Hashino et al., 2013; Sullivan & Voigt, 2021; Seiki et al., 2022; Atlas et al., 2024). We will use top-of-atmosphere radiation in each chapter to present our results in context of each other.

1.1.2 Key parameters in the microphysics for cirrus clouds

Here, the key parameters related to cirrus cloud processes in model microphysics are outlined. Chapter 3.1 goes into greater detail into each parameter and process as it pertains to my modeling study.

Since tropical cirrus are slow to dissipate in the extremely cold temperatures of the upper troposphere and TTL, ice sedimentation plays a significant role as a cloud sink for tropical cirrus (Seeley et al., 2019) and contributes significantly to model variability in both GCMs and GSRMs (e.g., Heymsfield & Donner, 1990; Sanderson et al., 2008; Lamraoui et al., 2023; Hong et al., 2009). Ice sedimentation depends on assumptions of particle size distribution, ice crystal habit, ice mass radius, and terminal velocity (Naumann et al., 2024). Ice fall speeds are a dominant sensitivity for cloud condensates in GSRMs regardless of the cloud microphysics scheme (Naumann et al., 2024). Assumptions of ice crystal properties not only impact cloud sinks such as ice sedimentation but also cloud sources such as vapor deposition rate and ice nucleation. Lots of recent progress has been made to study ice crystals in a laboratory or cloud chamber (Möhler et al., 2006; Lamb et al., 2023; Schneider et al., 2021), but there are still a lot of uncertainties in the measurements and gaps in theory, which cascade into modeled uncertainty as assumptions are made for the bulk characteristics of ice within a model grid box (Morrison et al., 2020).

Another sensitivity for cirrus clouds is the presence of large-scale ascent. Proposed by Jensen et al. (1996), cirrus cloud formation may be encouraged by the presence of large-scale ascent. Large-scale ascent is especially relevant for tropical cirrus which occur in the rising branch of the Brewer-Dobson Circulation. The Tropical Western Pacific (TWP) region experiences large-scale ascent from the Walker circulation as well (e.g., Lin et al., 2013; Blossey et al., 2010; Kuang & Bretherton, 2004). Many RCE-type models in limited domains do not recreate a large-scale ascent that is present in global models like GCMs and GSRMs (Wing et al., 2018).

We explore the effect of these microphysical parameters and processes in Chapter 3 in a sensitivity study using a small domain model.

The problem of ice microphysics is expansive and multi-faceted as the scales range from micro to planetary. It brings together field campaigns, laboratory measurements, satellite data, theory, and models. Cirrus clouds are intertwined with the thermodynamic background of the atmosphere, large-scale circulations, convective organization, atmospheric dynamics, turbulence, aerosols, and more. Microphyiscal parameterization is not a problem that will go away with further increases to horizontal or vertical resolutions since individual ice crystals occur on scales of microns (Morrison et al., 2020). Morrison et al. (2020) describe the problem of quantifying microphysical uncertainties as “very difficult” yet quantification of uncertainties is necessary for model improvement. This dissertation quantifies some of these uncertainties in GSRMs and limited domain convection-permitting models (CPMs). Randall et al. (2003) claimed that cloud microphysics is “a problem that refuses to die” and is evident in the current state of microphysics in GSRMs, which are described in more detail in Seiki et al. (2022).

1.2 DYAMOND

DYAMOND (DYnamics of the Atmospheric general circulation Modeled On Non-hydrostatic Domains; Stevens et al., 2019) is an intercomparison of several GSRMs that were initialized from reanalysis and run freely for 40 days. Most models have explicit deep convection (many still have parameterized cumulus schemes for shallow convection). There were two phases of DYAMOND: (DY1) boreal summer simulations initialized on 1 August 2016, and (DY2) boreal winter simulations initialized on 20 January 2020. The DYAMOND models generally resolve vertical velocity fields, shifts in circulation, and the diurnal cycle of precipitation better than GCMs (Stevens et al., 2020); however, they still need improvement in their portrayal of clouds from deep convection to cirrus clouds (Nugent et al., 2022; Turbeville et al., 2022). More information on the models in DYAMOND is provided in Table 2.1.

This section summarizes the results from my Master's thesis work, culminating in a two-part publication, which shaped the work for my PhD. Nugent et al. (2022, hereafter DY1 P1) found that convection in the DYAMOND models reasonably simulates convective organization and rainfall despite a diverse vertical cloud structure, especially in the upper troposphere. DY1 P1 emphasized deep convection as the primary source of water into the TTL in these models noting the intermodel spread depends on the model dynamics and microphysics (see the spread in model microphysics through hydrometeor types and dynamics through updraft speed in Figure 10 and 13a in DY1 P1). The second paper of the set explored the properties of cirrus clouds after formation. Turbeville et al. (2022, hereafter DY1 P2) found that the models scatter around observational values; sometimes significantly under- or overpredicting relative to climatology. The DYAMOND models typically balance each other out with models on either sides of the mean, meaning the models capture the current climate on the whole but have large variations and internal biases. The large model spread is driven by differences in model dynamics and microphysics (DY1 P2).

One goal of this dissertation is to determine how much of this model spread could be the result of differing microphysics: what is the role of microphysics in setting the inter-model spread in GSRM intercomparisons?

We describe our results using the DYAMOND 2 models in Chapter 2 with a section on the comparison between DYAMOND 1 and 2 for models that participated in both phases (Ch. 2.3.2).

1.2.1 Other results from DYAMOND

Satoh et al. (2019) was the first to compare several GSRMs, emphasizing the improvements over GCMs while providing a more physical framework for understanding model behavior. The intermodel spread is reduced in GSRMs compared to GCMs (Lang et al., 2021) through they cite cloud microphysics as a large source of intermodel spread. Naumann et al. (2024) also explore the role of microphysics on cloud condensate in the ICON GSRM, finding a significant variability from the microphysics on cloud structure.

The diurnal cycle of precipitation is significantly improved in both the timing of convection over land and the amplitude of the diurnal cycle (Song et al., 2024). The diurnal cycle of mesoscale convective systems in GSRMs is also improved both in their initiation and maturation phases (Feng et al., 2023). GSRMs are also a promising tool for studying tropical cyclones but need further development. In DYAMOND, tropical cyclones appear realistic but vary greatly model-to-model in their representation of tropical cyclone number, intensity, size, and structure (Judt et al., 2021). DYAMOND models also provide an excellent resource for studying precipitation extremes, ITCZ, low clouds, waves, and more (see the Journal of the Meteorological Society of Japan (JMSJ) Special Edition on the DYAMOND initiative).

In this dissertation, I investigate the properties of cirrus clouds in GSRMs and their radiative impact. Before our work in DY1 P1 and P2, it was unclear whether these GSRMs were capable of simulating thin TTL cirrus, but now we can definitively say that these models represent cirrus clouds and prove to be a nice framework for understanding various processes related tropical cirrus in an attempt to explain the large model spread.

1.3 Outline of this dissertation

Chapter 2 provides an overview of an intercomparison of the properties of thin cirrus produced in the DYAMOND models. This chapter answers: how well do GSRMs represent tropical cirrus? From the convection that drives cirrus cloud formation to the spatial and vertical distribution of cirrus, we compare the DYAMOND models against observations when possible by using top-of-atmosphere radiative fluxes as our main comparison tool. We see a large inter-model spread in many of the metrics related to clouds, especially top-of-atmosphere radiative fluxes. We identify clouds as a main source of variability, both convective and cirrus clouds. Convective clouds vary significantly in the models from vertical structure to frequency of occurrence. While less obvious, differences in cirrus clouds in the models also play a key role in the inter-model spread, whose small but persistent LW radiative impacts are significant. These differences in cirrus likely result from the different model dynamics and microphysics.

In order to understand how much ice microphysics matter for cirrus clouds, we perform a single model microphysics parameter sensitivity study. Chapter 3 describes the results of our microphysical parameter sensitivity study. By using a single model on a small domain, we keep the model's dynamics fairly consistent. We adjust the process rates for sedimentation and vapor deposition of ice. Specifically, we focus on cirrus processes by limiting our change to small ice, which can impact top-of-atmosphere radiative fluxes up to 4 W/m^2. We analyze the impact of an updated ice nucleation scheme that includes homogeneous and heterogeneous freezing. Then we impose a slow mean large-scale ascent and change the SST by ±4K. This chapter answers how cirrus clouds respond to different model setups.

Finally, Chapter 4 expands on the role of microphysics, specifically ice nucleation and slow mean ascent, on the cirrus life cycle in a large domain simulation. This chapter answers the question about cirrus cloud origins. How much cirrus is formed in-situ or detrained directly from convection? And how does the lifecycle impact cirrus cloud properties? We see a lot of cirrus clouds continue to persist more than 5 hours after convection and some even more than two days from convection. We present a case study of TTL cirrus formed in-situ then show statistics from three different model setups and with +4K SST simulations. These small changes to cirrus impact the large domain simulations substantially in terms of convective structure and LW radiation. Due to the model setup, we can also infer the role of convective organization on in-situ cirrus formation.

Finally, we discuss the results from the previous chapters and their implications for this field of research in Chapter 5. We also discuss several possible directions for future work.

Chapter 2

DYAMOND INTERCOMPARISON OF TROPICAL CIRRUS

2.1 Introduction

Cirrus clouds cover a substantial area of the tropics and are significant for several aspects of Earth's climate system. Cirrus are closely related to deep convection and may be formed directly from anvil outflow or indirectly from gravity waves (Gasparini et al., 2023; Sassen et al., 2009). Different formation mechanisms drive different cloud properties (Krämer et al., 2016; Weng et al., 2024) that impact the top-of-atmosphere radiative fluxes and the local heating within the clouds. Large-scale circulations impact cirrus clouds, which may feedback on these circulations by strengthening the ascent and widening the descending branches of the Hadley cells (Albern et al., 2018; Su et al., 2017). These complex processes occur across a range of scales from individual ice crystals at the micron scale to cirrus cloud decks spanning hundreds of kilometers. Hence, modeling cirrus clouds is very challenging, but crucial to addressing uncertainty in climate sensitivity (Sherwood et al., 2020; Sokol et al., 2024; Hartmann & Berry, 2017; Atlas et al., 2024).

In the tropics, cirrus clouds occur frequently in the tropical tropopause layer (TTL; 14 km to 18 km). The TTL is a transitional region from the upper troposphere to the lower stratosphere, having intermediate properties of both (Fueglistaler et al., 2009). Due to generally coarse horizontal and vertical resolution in the upper troposphere-lower stratosphere (UTLS; typically 12 km to 20 km), general circulation models (GCMs) cannot resolve the complex processes of clouds, gravity waves, and water vapor occurring in the upper troposphere and TTL. Clouds in the UTLS impact the top-of-atmosphere radiation balance and radiatively heat the UTLS, which impacts the amount of stratospheric water vapor and circulation in the tropics (Jensen et al., 1996; Haladay & Stephens, 2009; Solomon et al., 2010). Models that are able to resolve explicit convection may allow cirrus to form more naturally. However, cirrus cloud properties and lifetimes in the tropics are highly sensitive to ice microphysical schemes (Atlas et al., 2024). Many ice microphysics schemes use ice microphysics for TTL cirrus that were designed to simulate cirrus at less extreme temperatures (lower altitude), which neglects important physical processes for and environmental drivers of cirrus cloud formation and evolution (Gasparini et al., 2023; Kärcher, 2022).

As computing resources increase, it becomes feasible to run models with high enough resolution to represent deep convective storms explicitly at global scales. We must then diagnose model biases and areas for improvement to continue developing these global storm-resolving models (GSRMs). The DYAMOND (DYnamics of the Atmospheric general circulation Modeled On Non-hydrostatic Domains; Stevens et al., 2019) initiative collected output from several GSRMs that were initialized from reanalysis and run freely for 40 days (Stevens et al., 2019). The DYAMOND project provides an opportunity to analyze the current state of GSRMs, both individually and compared to other models of this type.

The DYAMOND models generally resolve vertical velocity fields, shifts in circulation, and the diurnal cycle of precipitation better than GCMs (Stevens et al., 2020); however, they still need improvement in their portrayal of clouds from deep convection to cirrus clouds. Feng et al. (2023) show that MCSs in DYAMOND capture some characteristics of MCSs, such as the diurnal cycle, but overestimate convective precipitation and precipitation intensity from MCSs. Some models have more isolated deep convective systems, especially over convectively active ocean regions (Feng et al., 2023). Previous work by Nugent et al. (2022) and Turbeville et al. (2022) found a large spread in DYAMOND 1 models relating to tropical clouds, especially overshooting convection and cirrus. They showed that the variability of cloud properties comes from a combination of microphysical and dynamical differences in the model though it is impossible to quantify the contribution from each due to the format of the model comparison. This study expands on these previous results and focuses on the distribution and vertical structure of tropical cirrus clouds in DYAMOND 1 and 2. We analyze variables related to cirrus clouds such as convection, precipitation, and radiation at the top of the atmosphere (TOA) to build a conceptual picture of tropical clouds in these models.

The DYAMOND models simulate two seasons: Phase 1 from August to September 2016 and Phase 2 from January to February 2020. In section 2.3.2, we compare the two phases of DYAMOND to climatology from Sassen et al. (2009) who found that cirrus are observed more frequently at night and in boreal winter. However, not all differences between phases of DYAMOND are from the change in season because many models had significant development, which changed the cloud characteristics. We highlight developments related to convection and cirrus clouds specifically.

In section 2.2, we describe the data, model output, and domain. The results start with an overview of the cloud characteristics in the entire tropics from 30°N–30°S in section 2.3.1. Then we dive deeper into the vertical structure of clouds and the environment in a subsection of the Tropical Western Pacific (section 2.3.2) and compare the seasonality between DYAMOND 1 and 2. Finally, section 2.3.3 explores the differences in TTL cirrus in the models.

2.2 Description of model output, data, and study domain

One of our principal goals is to assess the quality of cirrus simulations. Data on clouds in the tropical upper troposphere and TTL is limited. Satellite data provides the most uniform coverage in the tropics and is our primary tool for comparison to model output.

2.2.1 DYAMOND Models

In previous studies, Nugent et al. (2022) and Turbeville et al. (2022) investigated the life cycle of tropical convection and cirrus in models that participated in the first phase of DYAMOND (hereafter DYAMOND 1; Stevens et al., 2019). This study incorporates results from the second phase of DYAMOND, which took place in boreal winter (hereafter DYAMOND 2). The DYAMOND 2 simulations were initialized on 20 January 2020 at 0 UTC from ECMWF reanalysis and ran freely for 40 days (no nudging). The various models, identified in Table 2.1, were run at horizontal resolutions of less than 5 km. This high horizontal resolution allows most models to turn off parameterizations for deep convection and shallow cumulus parameterizations; however, some models have a modified deep convective and shallow cumulus parameterization. See Table 2.1 for more information on the setup of the models. The models have different microphysics schemes, which vary greatly in their treatment of ice clouds such as cirrus. Seiki et al. (2022) provides an excellent description of the cloud microphysics used in each of the DYAMOND models. Most models have a single moment bulk microphysics scheme except for SCREAM's double moment microphysics and MPAS's hybrid microphysics (predicts number concentration for cloud water and ice only). Most models have 6 categories of hydrometeors (water vapor, cloud water, rain, cloud ice, snow, and graupel), but ARP, IFS, and UM have 5 categories (excludes graupel) and SCREAM has 4 categories (the ice category accounts for different particle sizes). We evaluate nine DYAMOND models against satellite data and reanalysis to see how well models represent the current climate.

Differences in model set-up between DYAMOND phases

The models that participated in both phases of DYAMOND are ARP, GEOS, FV3/SHiELD, ICON, IFS, MPAS, NICAM, SAM, and UM. The notable model differences between the two phases of DYAMOND are listed in Table 2.2. More detailed information on

Table 2.1: Models from DYAMOND Phase 2 listed with their horizontal resolution at the equator (dx); number of vertical levels (nlevs); number of vertical levels in the TTL (nlevs TTL); microphysics scheme and references (mphys); number of moments in microphysics scheme (mom); which types of cumulus parameterizations (CP) are used (D: deep; S: shallow, N: none); whether the atmosphere model is coupled to an ocean model; and further references for the model.

Model	dx	nlevs	TTL nlevs	mphys	mom	CP?	Coupled?	References
ARP	2.5 km	75 (60)	8	modified LAM model AROME	1	N	N	Voldoire et al. (2017)
GEOS	3 km	181	22	1 MOM 6 cat	1	D, S	N	Putman and Lin (2007); Putman and Suarez (2011)
ICON-NWP	2.5 km	77	8	Baldauf et al. (2011)	1	N	N	Klocke et al. (2017) Zängl et al. (2015)
IFS	4 km	137	15	ECMWF scheme	1	S	Y	ECMWF (2020)
MPAS	3.75 km	55	N/A	Thompson WRF Single-Moment 6-Class	1.5	D, S	N	Skamarock et al. (2012)
SAM	4 km	61	8	SAM 1 MOM	1	N	N	Khairoutdinov et al. (2022)
SCREAM	3.3 km	128	18	P3	2	N	N	Caldwell et al. (2021)
SHiELD	3 km	79	8	GFDL MP v3 (Zhou et al., 2022)	1	S	N	Harris et al. (2021, 2023)
UM	4.5 km	55	7	Modified Wilson and Ballard (1999); Ice (Baran et al., 2016)	1	S	N	Walters et al. (2019)

the differences can be found in the *Supplementary Materials S1-S8*.

Differences between mode setup in DYAMOND 1 and 2 are small for IFS, ICON, and UM, which had few significant changes between runs. In contrast, differences in models like SAM and FV3/SHiELD may be due to changes in the model itself. Although it is difficult to determine whether differences between DYAMOND 1 and 2 are due to model setup or seasonality, we will attempt to note which models had significant model development when comparing the radiative and cloud properties in each model.

2.2.2 Data

This study uses data from four satellite products with retrievals of cloud, precipitation, and radiative fluxes (details described below). We typically compare to climatology since the DYAMOND models are free-running and will not follow the same weather

Table 2.2: List of models that participated in both phases of DYAMOND and the major differences between the simulations that are known. More details can be found in Supplementary Information S1-S8.

Model	Differences
ARP	Microphysics tuned for high-resolution non-hydrostatic modeling
GEOS[1]	Poor version of microphysics in DYAMOND 1
FV3/SHiELD	Many significant changes
ICON	No significant changes
IFS	Small changes
NICAM[1]	Error in DYAMOND 2
SAM	Improved temperature profile used for precipitation-related coefficients
UM	None

[1] Removed from our analysis.

patterns as in the 2020 data.

The CERES-CloudSat-CALIPSO-MODIS (CCCM) product provides collocated cloud microphysics and TOA radiative fluxes with a horizontal footprint of roughly 30 km (Kato et al., 2010, 2011). We use three months of data over three years for comparison to DYAMOND, specifically July–September during the years 2007–2010 for DYAMOND 1 and January–March during 2008–2011 for DYAMOND 2 comparisons. The daytime values for TOA shortwave and longwave radiation as well as cloud top height are used in this study. Additionally, we coarsened the model output to $0.3° \times 0.3°$ to match the footprint of CCCM for the radiation comparison but left the models at native resolution for the cloud top height analysis.

The liDAR-raDAR (DARDAR) product (Deng et al., 2013) combines CloudSat, CALIPSO, and MODIS satellite measurements to derive microphysical properties of cirrus clouds over a broad range of optical thicknesses with a fine horizontal spacing of

~1.1 km and a vertical resolution of 60 m (Deng et al., 2013; Sokol & Hartmann, 2020). DARDAR has a higher retrieval uncertainty for optically thin cirrus layers, which are detected only by the lidar (Cazenave et al., 2019). We use both daytime and nighttime values from the 2009 July to September dataset to compare to DYAMOND 1. For DYAMOND 2 comparisons, we have data from February for eight years (2007 − 2017 with two years missing). The GSRM output is not coarsened for comparisons with DARDAR, which has a similar footprint to the model grid.

We use LW and SW radiative fluxes at TOA from the CERES SYN1deg product (Doelling et al., 2013, 2016), available from 2000–2019. The data has a 1° × 1° horizontal resolution with an approximate uncertainty of 3 W m^{-2} (Kato et al., 2018). We seasonally subset this data to 1 August to 10 September of each year for DYAMOND boreal summer comparisons and 20 January to 28 February for DYAMOND boreal winter comparisons. We use observations of precipitation from the Global Precipitation Measurement (GPM) Integrated Multi-Satellite Retrievals for GPM (IMERG) on a $0.1^\circ \times 0.1^\circ$ grid and 30-minute output frequency (J. Tan et al., 2019; Huffman et al., 2015). The precipitation data matches the DYAMOND 2 simulation period from 20 January to 28 February 2020.

2.2.3 Study Domains

This study focuses on two main regions of climatic interest: the global tropics (GT; 30°N−30°S) and the tropical western Pacific (TWP; 143°E−153°E, 5°S−5°N) as shown in Figure 2.1.

Global tropics (GT)

This analysis uses data to evaluate model output from the global tropics (GT; 30°N−30°S). The model output is coarsened 1° × 1° for comparison to the gridded near 1° × 1° satellite data for the TOA radiation and precipitation analysis. To calculate the thin

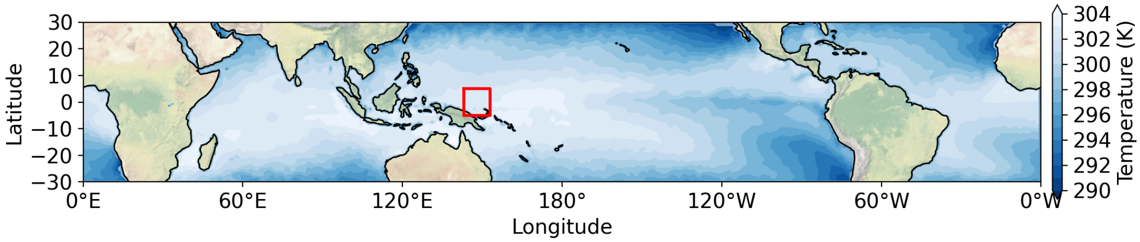

Figure 2.1: Study domain is plotted with sea surface temperature from 20 January 2020 00 UTC, the initial condition for DYAMOND 2. The 10° × 10° TWP region (outlined in red) is used for an in-depth small-domain analysis.

cirrus fraction, we use the native grid data ice water path (IWP) to threshold the cloud fraction which is then coarsened to 1° squared for plotting and comparison.

Tropical Western Pacific (TWP)

We do an in-depth analysis of the small-scale and local features of GSRMs by using a small 10° × 10° region in the convectively active Tropical Western Pacific (TWP; 143°E−153°E, 5°N−5°S), which is outlined by the red box in Figure 2.1. This domain matches the TWP analysis from Turbeville et al. (2022), which used DYAMOND 1 model output. The TWP is convectively active year-round and has the key feature that the SW cloud radiative effects (CRE) from convection are approximately balanced by LW CRE from cirrus clouds (Hartmann & Berry, 2017; Hartmann et al., 2018). Thus, models must be able to reproduce the cloud properties in this region. We analyze tropical clouds and TTL cirrus in DYAMOND 2 and compare it to available output from DYAMOND 1 (section 2.3.2).

2.3 Results

Results are broken into two distinct parts: 1) statistics of global tropical convection and cirrus clouds in DYAMOND 2, and 2) a regional study in the TWP between DYAMOND 1 and 2. We note major model developments that may impact the seasonal comparison between DYAMOND 1 and 2. Lastly, we analyze the TTL cirrus produced in the models and how they relate to the background thermodynamic state of the TTL in DYAMOND 2.

2.3.1 Global tropics

In order to determine how well the DYAMOND models simulate large-scale convective features, we compare OLR, precipitation, and cirrus cloud fraction statistics in the tropical band from 30°N to 30°S. The differences in radiation fluxes at the top of atmosphere can expose the differences in microphysics through its impact on cloud radiative forcing (Seiki et al., 2022; Atlas et al., 2024).

The climatological distribution of outgoing longwave radiation (OLR) at TOA in the tropics has three local minima: the Maritime continent/western Pacific Ocean, continental Amazon, and south-central Africa. Most models underestimate the convection over land in the Amazon or African regions (Figure 2.2); ARP closely matches climatology over land. Half of the models also underestimate convection in the South Pacific Convergence Zone (SPCZ). Aside from SCREAM, most models have a shift in the location of convection in the Indian Ocean towards the southwest, which is not unexpected since the 2020 data also shows this particular variation from climatology.

The standard deviation of 13 years of CERES data for January–March (JFM) is around 20 $\mathrm{W/m^2}$ in the Maritime Continent and TWP regions with a maximum east of the TWP box at 30 $\mathrm{W/m^2}$ (not shown). Thus, it is not surprising to see ± 20 $\mathrm{W/m^2}$ model differences (grayed out in Figure 2.2) due to the free-running behavior of the models. However, the model differences from observations in some regions exceed 100 $\mathrm{W/m^2}$ in magnitude. The spatiotemporal mean values of OLR in the global tropics range from 250.8 $\mathrm{W/m^2}$ in MPAS to 272.1 $\mathrm{W/m^2}$ in SAM. While the climatological mean falls within the model spread at 258 $\mathrm{W/m^2}$, the majority of the models (all but MPAS and ARP) simulate a mean OLR larger than CERES (Figure 2.3a).

The models do have some individual large-scale and local differences from climatology: SAM and IFS have too little convection across the tropics; SCREAM has too little anvil and convective clouds in convectively active regions; GEOS has an ITCZ that is too narrow and an SPCZ that is too weak; MPAS has extremely low OLR in the west-central Pacific which is only partially counteracted by weak convection over land; the other models (ICON, UM, SHiELD, and ARP) match the tropical mean OLR within 8 W/m^2 with larger regional differences.

Despite convection occurring in slightly different locations in each model, the cumulative tropical precipitation is uniform between 107 mm and 127 mm by the end of the simulations, excluding MPAS which has anomalously low precipitation (Figure 2.3a). All the models other than MPAS overestimate accumulated precipitation compared to the IMERG observations, which measured 99 mm of precipitation accumulated from 30 January to 28 February 2020.

The energy budget in the tropics roughly balances precipitation with radiative cooling. As a saturated air parcel rises, it will condense to form cloud particles in the liquid or ice phases which may then sediment out to form precipitation if it reaches the ground before sublimating. Precipitation rates are affected by both moisture and cloud sources/sinks where differences in cloud ice may be significant (Gao et al., 2005). Since the models have similar moisture profiles in the tropics, differences arise mainly from the cloud ice microphysics in the model. Models with higher rain rates comparatively inhibit convection. For example, MPAS accumulates very little precipitation meaning that less cloud condensate sediments as precipitation and falls to the surface than in other models; in the absence of a strong cloud sink from precipitation, more cloud ice reaches the upper troposphere and spreads into anvil clouds contributing to the low mean OLR. MPAS is an extreme example of this in the tropics. Most other models have a higher OLR and a higher precipitation, hence they precipitate more effectively so less cloud condensate reaches the upper troposphere.

Schumacher and Houze (2003) found that the stratiform to convective precipitation ratio in the tropics (20°N-20°S) is about 24% using observations from TRMM.

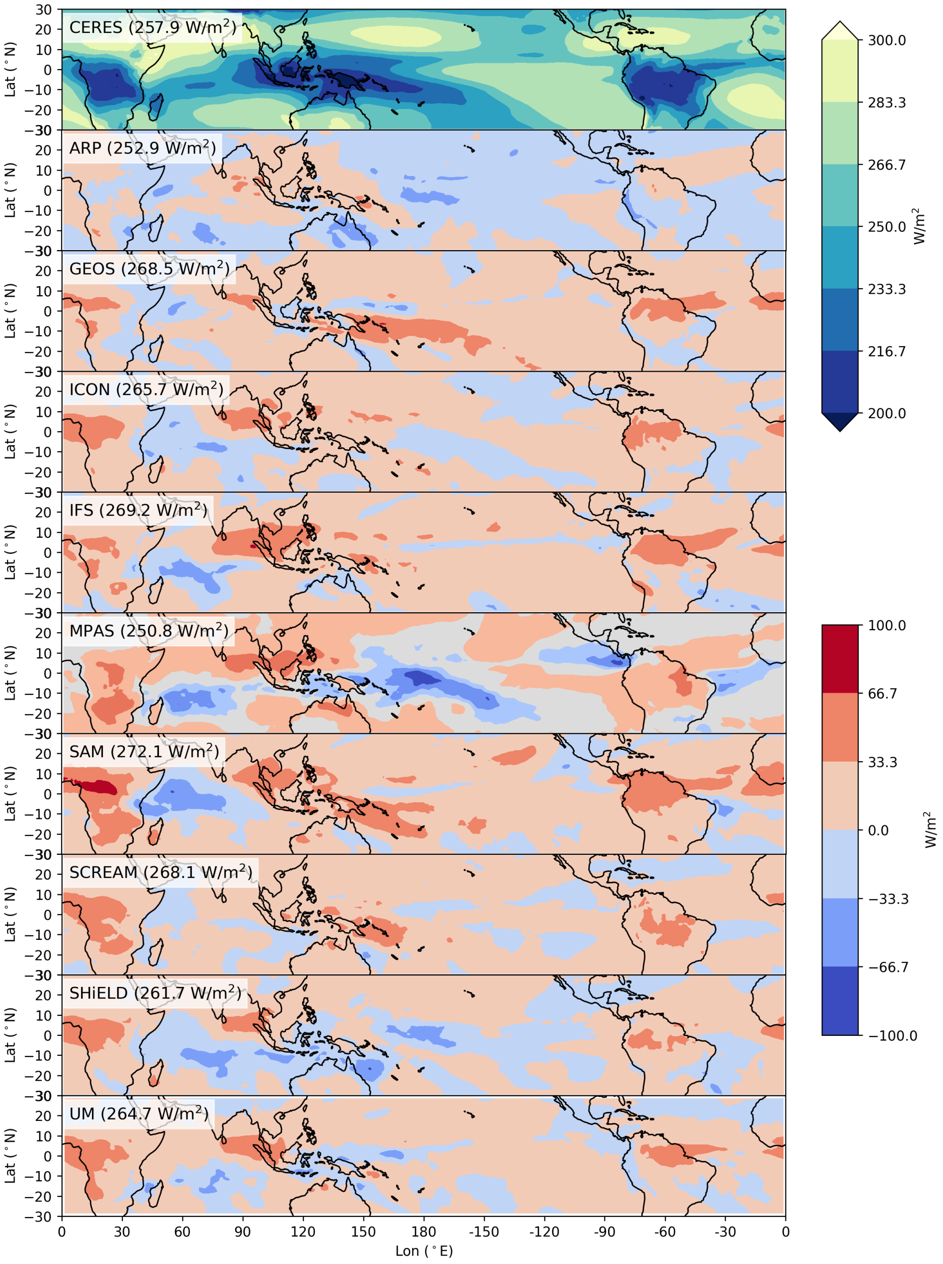

Figure 2.2: Observed mean OLR from CERES from the months of January, February, and March during each year from 2001 to 2013 is shown in the top panel. Model output coarsened to 1° and averaged over the last 30 days of the simulation period is plotted as the difference from observations in panels below. The model name and spatiotemporal mean of OLR are noted in the upper left corner of each panel. The warmer colors indicate that the models have a higher mean OLR than the data at that location over the 30 days, and vice versa for cooler colors.

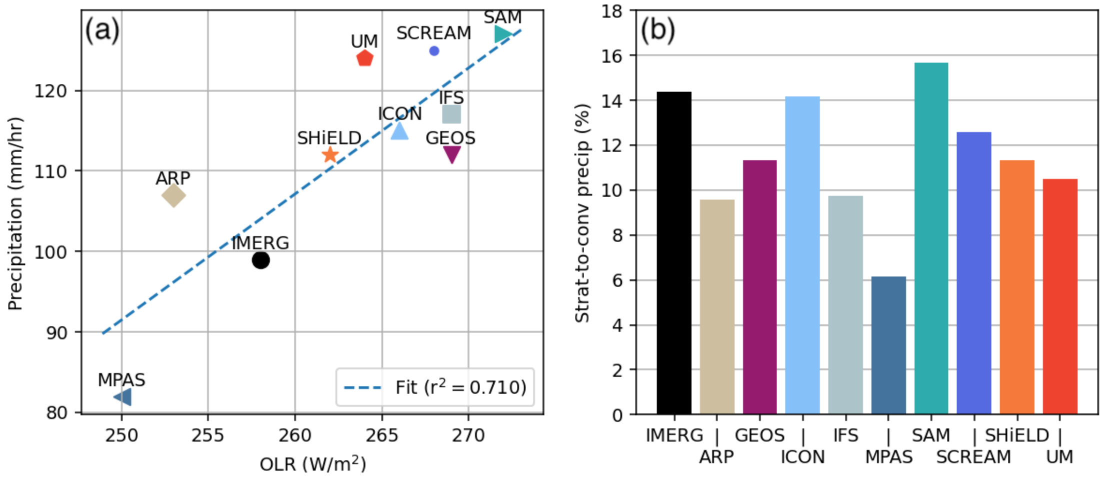

Figure 2.3: (a) Daily mean accumulated precipitation over the tropical band from 30°N to 30°S. The first ten days are ignored as spin-up. (b) The stratiform to convective precipitation ratio is plotted as a percent with the models listed from highest to lowest accumulated precipitation from left to right.

Data from IMERG from 30°N-30°S during the DYAMOND 2 period shows that about 14% of precipitation is from stratiform clouds, where stratiform precipitation is weaker than 1 mm/hr. We use this threshold in the models as well, which is shown in Figure 2.3. While IMERG has been shown to overestimate precipitation overall and underestimate light precipitation (Bolvin et al., 2021; Pradhan et al., 2022), some models (in particular, SAM, SCREAM, and ICON) agree well with IMERG. However, most models underestimate the fraction of overall precipitation that is stratiform, consistent with results from Feng et al. (2023).

The model biases in OLR are consistent with the frequency distribution of IWP in the tropics as seen in Figure 2.4. Notably, IFS has very little ice greater than 1 kg/m^2, leading to the warm bias in OLR. While SCREAM has fewer anvils (intermediary values of IWP around 1e-2 kg/m^2), it has more 1° × 1° boxes with large IWP (likely associated with convection). Most models simulate small amounts of IWP ($\leq 1e-4$ kg/m^2), which are not included in DARDAR retrievals.

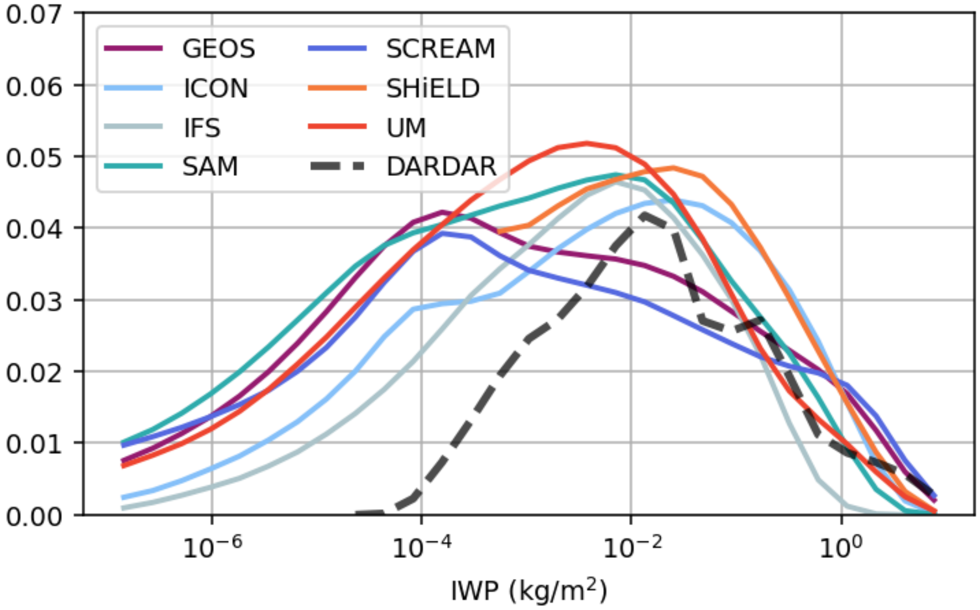

Figure 2.4: Normalized histograms of ice water path (IWP) in the tropics after the model output was coarsened to 1° squared. SHiELD (orange) is inaccurate below 10^{-3} kg/m^2 and thus not included here. DARDAR here includes IWP from 30°N−30°S from nine Februaries and is not coarsened here.

Now that we have established the general convective characteristics of the DYAMOND 2 models, we compare the properties of ice clouds by using IWP as a proxy for ice cloud type. Thin cirrus clouds are defined as 1e-4 kg/m^2 $\leq$ IWP $<$ 0.1 kg/m^2, following Sokol and Hartmann (2020) and Turbeville et al. (2022). This threshold is used on the native grid to get cloud fraction which is then averaged to 1° squared boxes and has a small sensitivity to the choice used for the upper bound but a larger sensitivity for the lower bound (our definition of clear sky) since most models produce prolific amounts of small IWPs. The observed maximum in observations from Sassen et al. (2009, Fig. 1) occurs over the tropical ocean from the eastern Indian Ocean to the western Pacific with local maxima over continental Amazon and Africa. Sassen et al. (2009) found that thin cirrus are strongly correlated with deep convection cloud fraction and cover broader regions around convective areas. We show similar results in Figure 2.5, which shows side-by-side plots of thin cirrus cloud fraction and mean precipitation rates (a proxy for convection).

GEOS and SCREAM simulate three local maxima in cirrus cloud fraction in the same three regions as observed; however, the maximum over the tropical ocean is subdued in both. Most models generate a large swath of cirrus clouds extending from continental Africa in the west to the south-central Pacific Ocean along the SPCZ, not distinguishing the three different regions of cirrus related to convection. However, there is a strong correlation between cirrus clouds and convection as noted by Sassen et al. (2009). In agreement with the lower mean OLR showing in Indian Ocean in Figure 2.2, there are more cirrus clouds over the Indian Ocean than observed in climatology in Sassen et al. (2009, Fig. 1 & 2). The DYAMOND models also have a higher cirrus cloud fraction at the edges of convective areas, especially in UM from a combination of too much anvil cirrus spread and too few grid boxes with small IWPs; UM tends to favor thicker anvil with more substantial IWPs. Perhaps the higher fraction of cirrus at the edge of convection is related to the phenomena of increased deep convection at the edge of convection described in (Windmiller & Hohenegger, 2019).

2.3.2 DYAMOND 1 vs DYAMOND 2

Most models participated in both DYAMOND 1 and 2 by submitting 40-day free-running simulations. DYAMOND 1 simulates 01 August to 10 September 2016; DYAMOND 2 simulates 20 January to 28 February 2020. There are two contributors to the differences between models in the two phases of DYAMOND: (1) the season via the initial conditions and prescribed SSTs, and (2) significant model development that impacted tropical high clouds. Some models made negligible changes to the model setup, dynamics, or microphysics; however, others had significant model development in the three years between DYAMOND 1 and 2 submissions. The developments most important for tropical cirrus clouds are listed in Table 2.2. The

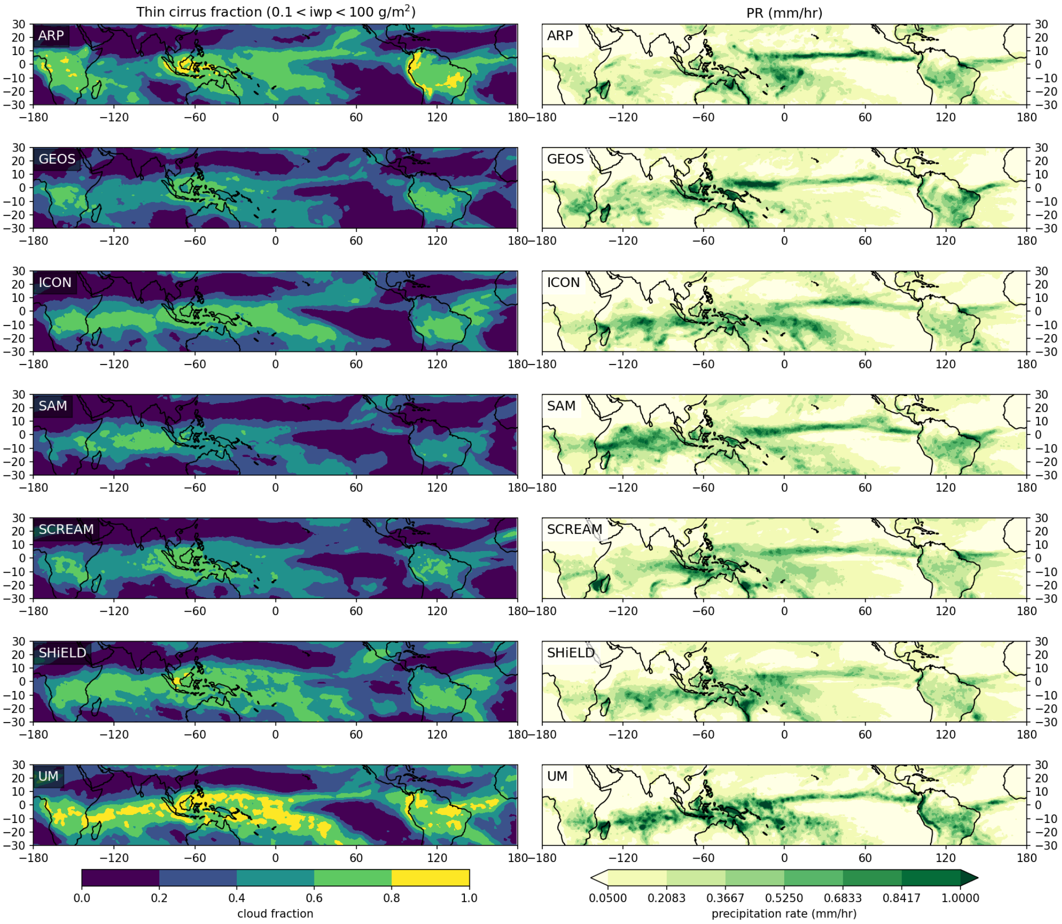

Figure 2.5: Thin cirrus cloud fraction (1e−4 kg/m^2 $\leq$ IWP $<$ 0.1 kg/m^2) is plotted on the left for each model (label in top left of each panel). The mean precipitation rate is plotted on the right for comparison to regions of frequent deep convection.

analysis in the following section uses a regional subset from the TWP (143°E−153°E, 5°N−5°S); the impact of this domain choice is discussed below.

Aside from SAM and MPAS, the models are qualitatively similar in the TWP between DYAMOND 1 and 2 (i.e., those with a relatively high mean OLR in DYAMOND 1 like ARP, ICON, and IFS also have a high mean OLR in DYAMOND 2). Hence, we are making a decent comparison between DYAMOND 1 and 2 using the TWP region. The impact of choosing a small domain like the TWP can increase the variance among the models. For example, MPAS and UM have lower mean OLR in the TWP while the other models (in order of mean OLR: SHiELD, GEOS, SAM, ICON, SCREAM, ARP, and IFS) have a slightly high mean OLR compared to climatology. CERES has a standard deviation of ±20 W/m^2 in the TWP; we can expect the models to vary by around 20 W/m^2 due to differences in weather patterns. Models like UM, SHiELD, SAM, and ICON are within this range of observed OLR in the TWP, but models like SCREAM, ARP, and IFS tend to produce higher mean OLR in the TWP than we would expect from their relative GT mean; on the other hand, MPAS has a large negative local difference in OLR in the TWP. The mean values of OLR for the global tropics, TWP, and local differences between the two regions are listed in Table S1. Furthermore, we note a slightly positive MJO and El Niño during February 2020 compared to the climatology used in our results. In the CERES data from February 2020, there is a slight eastward shift of convection in the west Pacific compared to climatology, which only a couple of models capture (Figure 2.2).

Radiative fluxes in the TWP

The long-term cloud radiative balance in the TWP is near zero due to the infrequent but strong SW impacts of deep convection balanced by the long-lasting but weak impacts of cirrus clouds (e.g., Hartmann & Berry, 2017; Wall & Hartmann, 2018; Gasparini et al., 2019). The dashed line in Figure 2.6 fits 20 years of observational data from CERES across seasons and approximates the LW to SW radiative balance, which is known to be in net radiative balance in this region (Hartmann & Berry, 2017). There is a clear shift in the observed OLR and reflected SW radiation between seasons; the boreal winter (Figure 2.6 open black circles) has a generally lower OLR and higher reflected SW radiation at TOA compared to the boreal summer (Figure 2.6 closed black circles) over 20 years of observations. Most models qualitatively capture the seasonal shift in TOA radiation, having a similar slope to the observational best fit. SAM, which had major model developments between DYAMOND 1 and 2, is an outlier in terms of slope.

While some models fall within the observed range of either SWU or OLR, they do not capture the observed balance between SW and LW radiative fluxes (e.g., FV3/SHiELD, GEOS, NICAM). Other models such as ARP, IFS, and ICON are on the limits of what is observed for reflected SW and OLR. This lack of balance is likely due to a combination of a short simulation period, a small analysis domain, and a lack of tuning to achieve global radiative balance. Despite these issues, the models are reasonably close to the data. The seasonal shifts in FV3/SHiELD, ICON, IFS, and ARP are nearly parallel to the dashed line. FV3 had major model development to become SHiELD but that does not seem to change the characteristic model behavior in the convectively active TWP region from DYAMOND 1 to 2.

Although some models simulate the shift between seasons with the correct direction and slope, there are still inherent model biases. The mean OLR and reflected SW radiation are similar for DYAMOND 1 and 2 for each model except SAM and MPAS. In other words, the differences between seasons in a single model is smaller than the differences across models in a single season; this is similar to our earlier findings that the regional differences in tropical cloud populations in a single model are small compared to differences across models (Turbeville et al., 2022). Some models, like ARP, IFS, and ICON, consistently do not simulate enough thick convective or anvil clouds (low reflected SW and high mean OLR). On the other hand, some models (e.g., UM, GEOS) have excessive anvil cloud decks that greatly reduce the mean OLR or thick

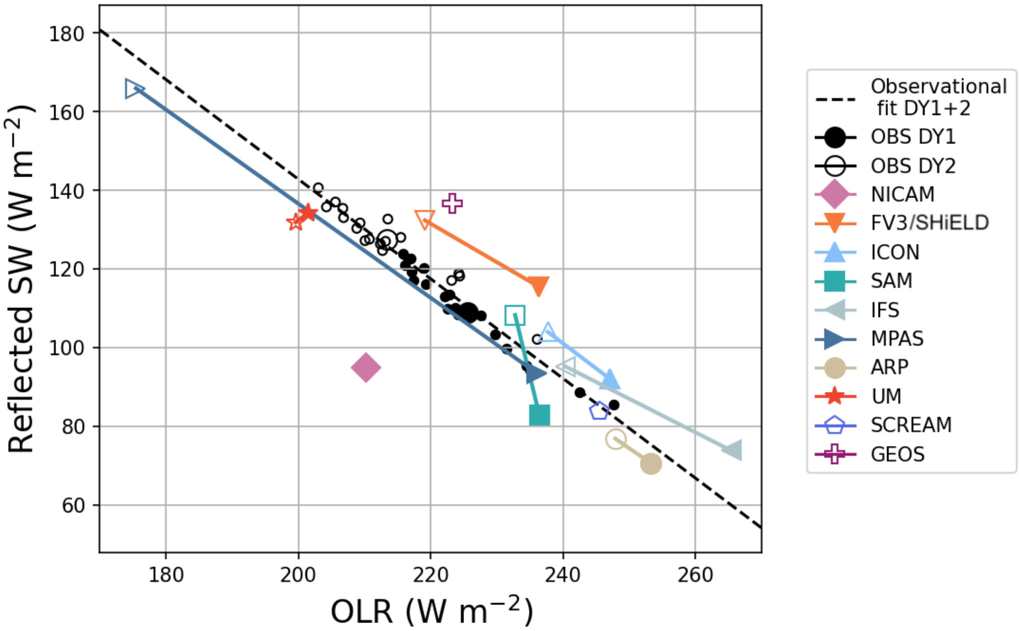

Figure 2.6: Mean OLR (upward LW) is plotted against mean reflected SW radiation (upward SW) at TOA for the TWP region. The models are shown in the colors indicated in the legend with the solid and open symbols for DYAMOND 1 and 2 respectively. The observations from CERES are plotted year by year for both July–August and January–March seasons to match the seasons from DYAMOND boreal summer and winter, respectively. The multiyear mean is plotted as the large solid and open circles for DYAMOND 1 and 2 respectively.

congestus clouds that increase the amount of reflected SW radiation. FV3/SHiELD nicely aligns with the seasonal shift but does not capture the LW-SW balance since it has too much reflected SW per the mean OLR (i.e., clouds are too bright). Once again, SAM and, probably, MPAS had major differences in model setup between the two runs so interpreting their changes is difficult.

The differences in cloud populations present in each model and season are clear when we look at the seasonal shift in the joint albedo-OLR histograms in Figure 2.7.

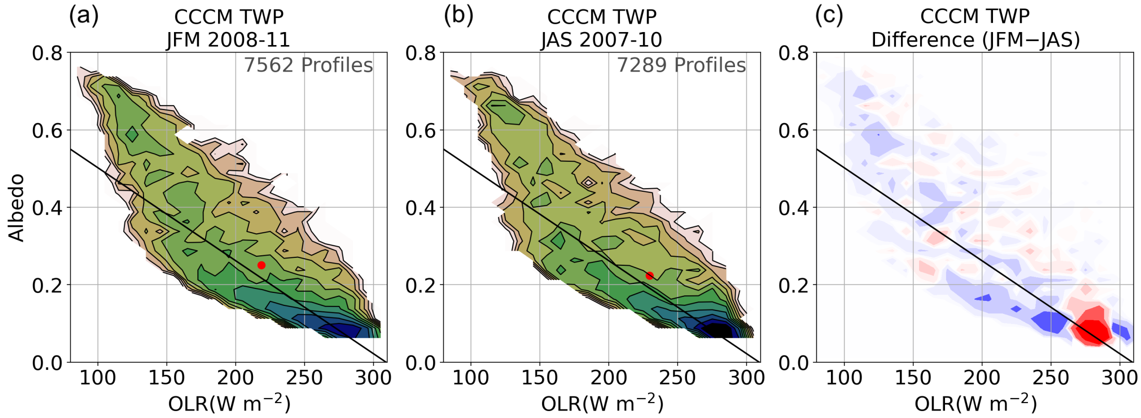

Figure 2.7: The joint albedo-OLR histogram is plotted for observations using CCCM for (a) boreal winter (January–March for comparison with DYAMOND 2), (b) boreal summer (July–September for comparison with DYAMOND 1), and (c) the seasonal difference (a)–(b). The black line denotes the observed balance between LW and SW at TOA in the TWP region from the boreal summer data; this line is replicated on (b), and (c) for visual comparison. The red dot denotes the mean albedo and OLR for the data.

This introduces some nuance to the mean values presented in Figure 2.6 by including the distribution of SW and LW radiative fluxes since albedo is the ratio of reflected to incoming solar radiation. High albedo and low OLR signify deep convection while high OLR and low albedo signify clear sky. The CERES histogram has a banana-like shape stretching from the deep convective region in the top left to the clear sky region in the lower right. Values with intermediary albedo and OLR range from thick anvil clouds extending from deep convection to thin cirrus which can have albedo-OLR values near clear sky. Turbeville et al. (2022) used this joint albedo-OLR histogram to describe differences in cloud populations in DYAMOND 1, which they summarized in a schematic in Figure 4f.

In the observations, both boreal summer and winter joint albedo-OLR histograms have two local maxima at clear sky and deep convective cloud values. The summer and winter histograms look qualitatively similar but when we take the difference between them (Figure 2.7c), some features appear. Red colors show where albedo-OLR pairings are more prevalent in boreal summer and blue colors where they are more prevalent in the winter. The observations have two key differences: (1) the boreal winter data has more convective and anvil clouds (with medium to high albedo and low to medium OLR), (2) the boreal summer data has more concentrated clear-sky values around 275 W/m^2 and 0.1 albedo. There are consistent seasonal shifts of CERES TOA fluxes seen in Figure 2.6. The boreal winter has a wider distribution around the clear sky end of the diagram, perhaps indicating the presence of more thin cirrus in the winter. This is consistent with observations using MISR cloud top height that shows boreal winter tends to have higher cloud tops (more thin cirrus with albedo < 0.3) (Chae & Sherwood, 2010). Chae and Sherwood (2010) also found there were fewer thick clouds (albedo > 0.3) in boreal winter, which differs from the CCCM results here.

Figure 2.8 reproduces the difference plot from Figure 2.7c and compares with models that participated in both DYAMOND 1 and 2. The black contours are the joint histograms for boreal winter, showing that the models have a large variance in the shape of their underlying joint albedo-OLR histogram. The models have similar characteristics between the seasons aside from SAM (See Supplementary Figures S2 and S3 for the joint albedo-OLR histogram of the winter and summer simulations separately).

In Figure 2.8, four models (IFS, FV3/SHiELD, MPAS, and UM) show a shift towards more anvil clouds in the boreal winter, similar to the observations. The models also simulate seasonal shifts and cloud populations that are not apparent in the observations. For example, MPAS and UM also show a shift in the deep convection towards lower OLR and lower albedo in boreal winter. In UM, this shift is likely from higher cloud top heights in the winter with less optically thick deep convective clouds. ARP and ICON show strong yet opposite dipoles in the difference between seasons; ARP has slightly more anvil cirrus in the winter while ICON has

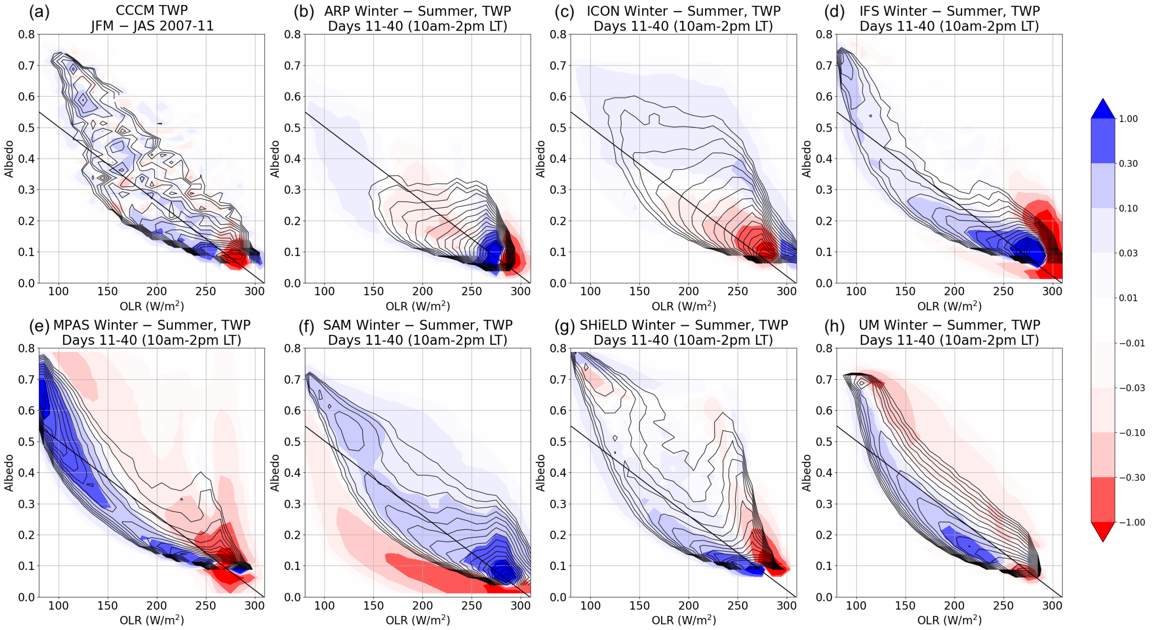

Figure 2.8: The joint albedo-OLR histogram for the boreal winter in the TWP region is shown in the black contours (same contour levels as Figure 2.7a) with the difference between boreal winter (blue colors) and summer (red colors) for (a) observations from CCCM (reproduced from Figure 2.7c), and (b–h) models (the difference between DYAMOND 1 from DYAMOND 2). Note that the models have been coarsened to $0.3° \times 0.3°$ for comparison to CCCM observations. The black line denotes the observed balance between LW and SW at TOA in the TWP region; this line is replicated on the model plots for visual comparison. Recall, that SAM and, likely, MPAS had major differences in model setup between DYAMOND 1 and 2.

less. ARP and ICON both have a joint histogram that is restricted to the lower right corner, rarely simulating $0.3° \times 0.3°$ averaged boxes that reach albedo-OLR values of deep convection (black contours in Figure 2.8b & c).

Vertical structure of clouds

Differences in TOA radiation result from variations in cloud amount and vertical structure across the simulations. The mean vertical profiles of modeled cloud fraction (Figure 2.9a & c) and condensate (Figure 2.9b & d) in the models are shown in Figure

2.9. The differences in the TTL IWC are around an order of magnitude, highlighted by the log scale in Figure 2.9b & d.

Most models simulate a trimodal peak in tropical cloud fraction as observed (e.g., Johnson et al., 1999; M. P. Jensen & Genio, 2006; Kubar & Hartmann, 2008). The DARDAR observations show the range of monthly mean ice cloud condensate across nine years of February data; the DARDAR data matching the DYAMOND 1 (gray dashed line in Figure 2.9b likes within the range of the nine Februaries (gray shading). The models agree on the altitude peak in the cloud fraction (near the base of the TTL) but disagree on its magnitude (from $0.2 - 0.75$). Some of the models (e.g., ARP, ICON, and SAM) underestimate both the cloud fraction and cloud condensate (Figure 2.9) relative to observations. On the other hand, UM greatly overestimates the cloud fraction especially the ice cloud fraction (Figure 2.9c) but falls within the range of observed ice cloud condensate from nine years of DARDAR (Figure 2.9d). FV3/SHiELD closely matches the observations in both DYAMOND 1 and 2. The FV3/SHiELD profiles between DYAMOND 1 and 2 are similar in shape and magnitude, with the largest difference in the upper troposphere. The clouds in SHiELD (DYAMOND 2) increased in frequency above 5 km, but the mean ice cloud mass decreased slightly compared to FV3 (DYAMOND 1). Despite major model development, FV3/SHiELD simulates clouds very similarly across the different simulations.

There is a large spread in the models near the freezing level from near 0 cloud fraction in SAM to 0.4 in UM and nearly two orders of magnitude in cloud water content (a mixture of ice and supercooled liquid above the freezing point and melting snow and liquid below the freezing point). In the TTL (shaded blue in Figure 2.9), the simulated cloud fraction and the ice water content vary by factors of about 4 and 10 across models, respectively. While TTL cirrus may not have a strong impact on TOA radiation, they can influence stratospheric water vapor and TTL temperature (e.g., Fueglistaler et al., 2009; Haladay & Stephens, 2009). The variation of TTL cirrus properties in the models is discussed in more detail in the next section.

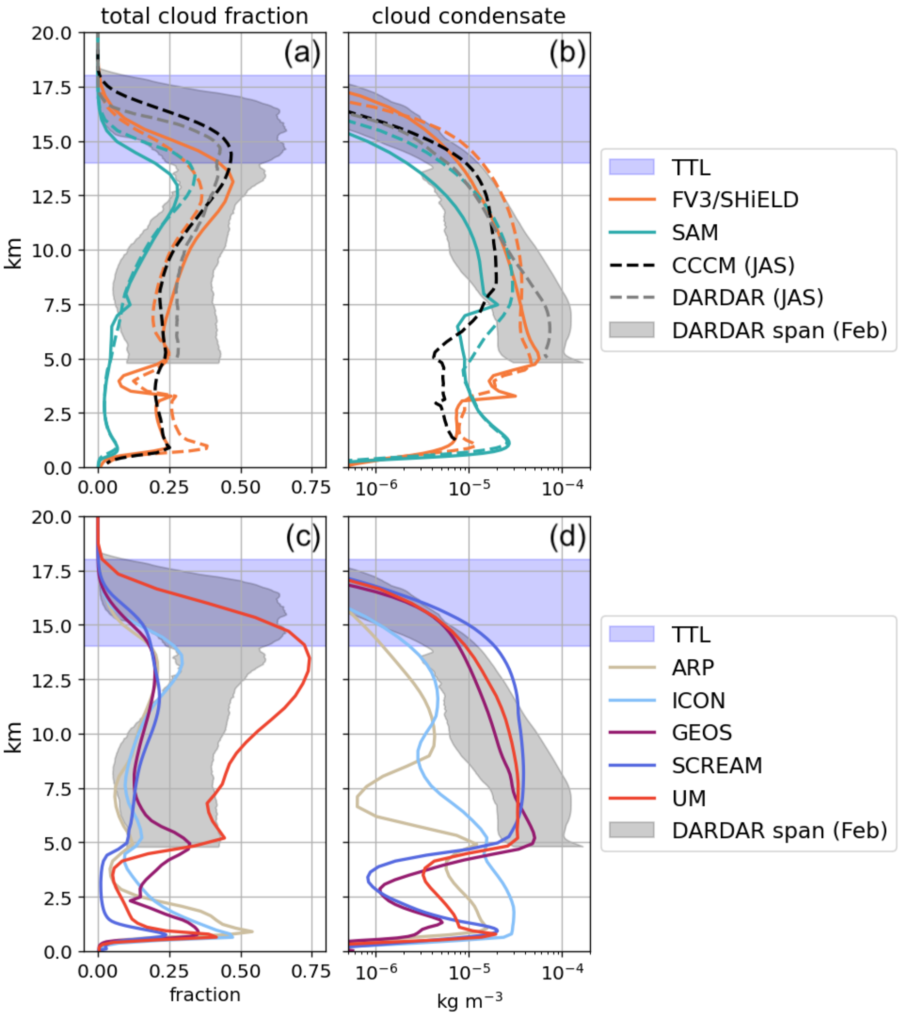

Figure 2.9: The top row compares observations and models from both DYAMOND 1 and 2 for (a) cloud fraction defined as ice water content > 5e−7 kg/m^3 and (b) mean ice water content. The CCCM (black dashed) and DARDAR observations (gray dashed) coincide with the DYAMOND 1 season. The gray shading shows the range of observed ice cloud condensate using DARDAR from each February for nine years. The bottom row compares observations from nine years DARDAR (same as in b) to other models, only in DYAMOND 2 for (c) cloud fraction and (d) mean cloud condensate from the last 30 days of the simulations.

2.3.3 TTL cirrus in the models

Some of the discrepancies in the model output in the UTLS may be related to the relatively short duration (40 days) of these simulations, which may not allow the spin up of the large-scale circulations, such as the Brewer-Dobson Circulation, and stratospheric processes (Fueglistaler et al., 2009; Blossey et al., 2010). Figure 2.10a and b show the temperature from the last five days of the simulations and the temperature drift from the first to last five days. The temperature varies most strongly above the cold point, signifying that the stratosphere is not in equilibrium by the end of the 40-day simulation. However, the temperature drifts differ by as much as 5 K across the models within the TTL, where convective overshoots and thin cirrus influence temperatures (Kuang & Bretherton, 2004; Yang et al., 2010). Nonetheless, these results are encouraging for simulations of TTL cirrus clouds; in the subset of DYAMOND 2 models that we looked at here, thin TTL cirrus clouds occur frequently in the simulation period (Figure 2.11d). The high frequency of clouds reaching the TTL is highest in SCREAM and UM, which also have the highest relative humidity. ICON, ARP, and GEOS have a less clouds with tops in the TTL and a lower relative humidity.

Figure 2.11 shows the joint histogram of cloud top height (CTH) vs OLR (a proxy for the opacity of the cloud at a given height). The top row shows the roughly linear relationship between OLR and cloud top height that we expect for thick clouds; here we use an ice cloud mixing ratio threshold of $1\text{e}{-5}$ kg/m^3. However, when we reduce the threshold by one and then two orders of magnitude (middle and bottom row, respectively), the amount of thinner cirrus (high cloud tops coupled with higher OLR values) increases. A cloud threshold of $1\text{e}{-7}$ kg/m^3 (bottom row) shows a significant amount of thin TTL cirrus that is largely missing from the other two rows.

The observations of cloud top height from CALIPSO may be most comparable to the lowest cloud threshold used with the models (bottom row of Figure 2.11), which

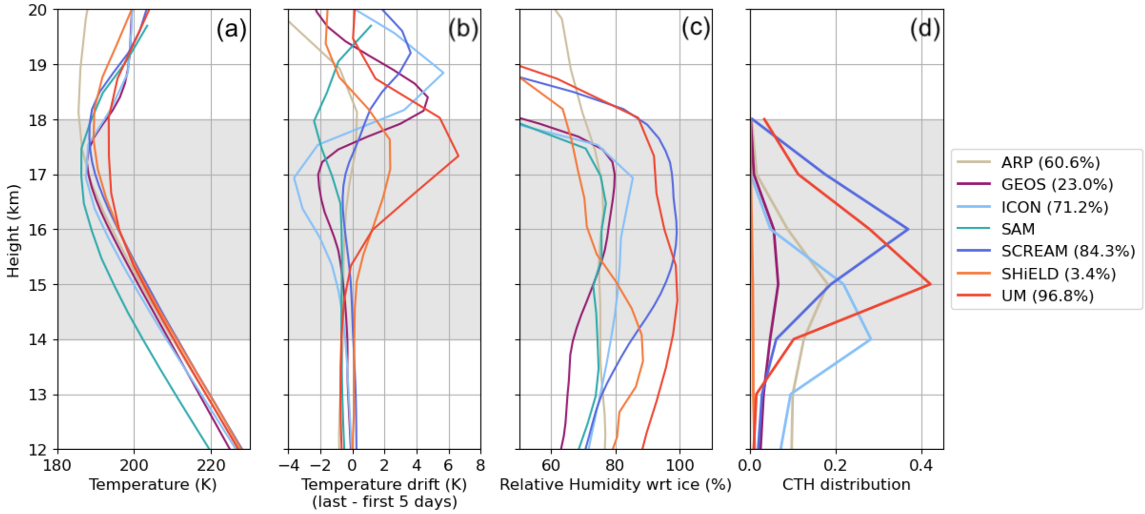

Figure 2.10: (a) The mean profiles of temperature are plotted for each model; (b) the temperature drift is plotted as the difference between the first and last five days of the simulation; (c) the mean profile of relative humidity with respect to ice, which depends on both temperature and water vapor; and (d) the histogram of cloud top height (CTH) with bins every kilometer in altitude and a cloud threshold of 1e−7 kg/m^3 (the cloud cover for clouds with a CTH above 12 km is noted in the legend).

includes more thin cirrus. Where the models have a nearly constant cloud top height across OLR values in the bottom row, the observations have a dip in the cloud top height at intermediary values of OLR using co-located CERES data.

In the models, it is not uncommon for TTL cirrus clouds to occur above thicker clouds, given the relatively low values of OLR that occur with high cloud top height. For example, comparing the rows for a given OLR, the cloud top height increases as the cloud threshold decreases (from top to bottom rows in Figure 2.11). This high frequency of TTL cirrus above thicker clouds has been observed in the tropical Pacific in observations from the Central Equatorial Pacific Experiment (CEPEX; McFarquhar et al., 2000). The peak in the distribution in Figure 2.11 (top row) mostly occurs at deep convective values (high cloud top height and low OLR), but as the cloud threshold decreases the peak in the distribution shifts to the left towards

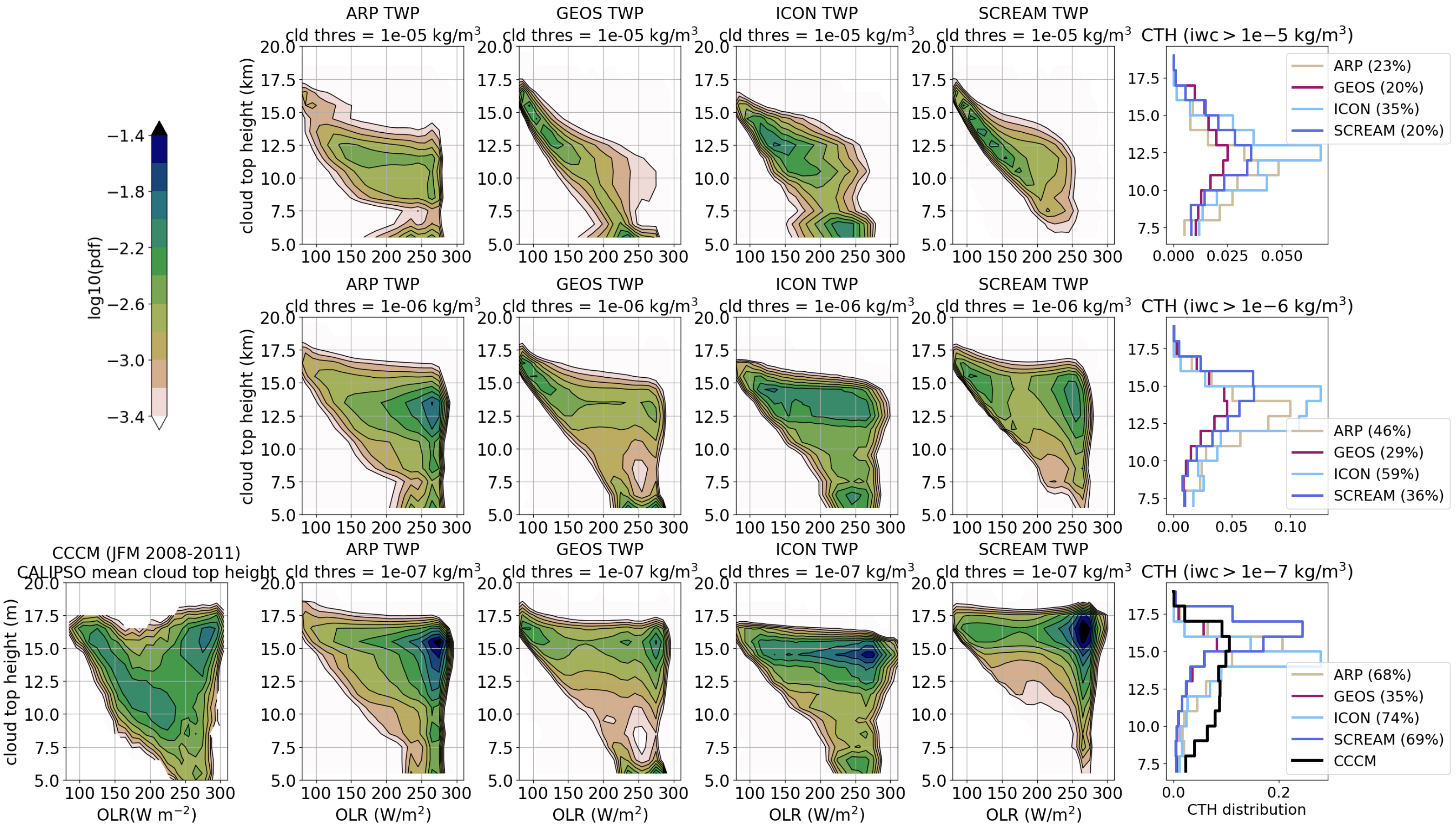

Figure 2.11: This is a joint histogram of OLR vs cloud top height using cloud thresholds of 1×10^{-5} kg/m^3 (top), 1×10^{-6} kg/m^3 (middle), and 1×10^{-7} kg/m^3 (bottom). We focus on clouds above the freezing level around 5 km. The bottom left shows observations from CCCM output of mean cloud top height over a 20 km swath using the lidar from CALIPSO so it is likely closest to our lowest cloud threshold. The next four columns show ARP, GEOS, ICON, and SCREAM. The far right column shows the cloud top height distribution for each row. Note the x-axis changes on each. The cloud cover for clouds above 5 km are noted in the legend.

TTL cirrus values (near 15 km altitude and high OLR; Figure 2.11 bottom row). There is some variance among the models in how they are simulating TTL cirrus. This may be partly related to the fact that SCREAM and GEOS have a higher vertical resolution than ICON and ARP, especially in the TTL region which could contribute to the different distribution of cloud top heights with OLR. SCREAM simulates the TTL cirrus at higher altitudes but at a similar frequency to ARP and ICON. SCREAM also has a higher cold point and relative humidity than the other models included here (Figure 2.10a and c), contributing to the higher TTL cirrus.

Further, we verified that the models are truly simulating thin TTL cirrus by confirming that cloud base heights were mostly above 12.5 km (not shown). In the intermediary stages (middle row in Figure 2.11), these thick cirrus are most likely related to convection whereas the thin TTL cirrus (bottom row in Figure 2.11) seem more detached from the convective cores (especially in SCREAM and GEOS where the local maxima in frequency of occurrences restricted to the upper right corner). These GSRMs, and likely other cloud-resolving models, are simulating thin cirrus that seem to lack a direct connection to convection. There may, however, be a more subtle connection where the outflow produces high humidity layers in the TTL that are then more easily stimulated by gravity waves to form cirrus. The relationship in SCREAM between a higher relative humidity and higher cloud top height for thin cirrus is promising. There is some debate whether TTL cirrus are formed mostly in situ or extruded from deep convection (Jensen et al., 1996; Garrett et al., 2006; Immler, 2008; Virts et al., 2010; Schoeberl et al., 2018; Nugent et al., 2022). Hence, the DYAMOND models provide an excellent basis for showing that models with different dynamics and microphysics simulate TTL cirrus, but they provide few answers regarding the dominant formation mechanisms. Future work using a single cloud-resolving model from DYAMOND and implementing tracers to identify the origin of a cloud parcel may provide a path to quantifying the fraction of TTL cirrus that originate directly from convection or form in situ.

2.4 Conclusions

Output from nine GSRMs that participated in the DYAMOND project was compared to climatology to understand the ability of an individual model to represent the current climate with fidelity. Generally, the models, with only one exception, underestimate convection over land in the Amazon or African regions. Half the models underestimate convection in the SPCZ and shift convection in the Indian and western Pacific ocean regions. All models except one overestimate tropical mean accumulated precipitation compared to the IMERG observations over the 40 days. Most models have too much intense precipitation from convection and under-represent light or stratiform precipitation outside convective clouds.

In agreement with observations, there is a strong correlation between cirrus and convection. Some DYAMOND models have a higher cirrus cloud fraction at the edges of convective areas. It is possible that the models tend to produce convection in certain areas and they trigger convection there sufficiently often, reducing the occurrence of small IWPs and thin anvil cirrus at the location of convection (especially in UM, which has more thin cirrus surrounding the areas of convection). GEOS and SCREAM match the observed local peak in cirrus over the Amazon, Maritime Continent/west Pacific, and Africa. While the cirrus cloud frequency in other models is higher than observed in the Indian Ocean, the models also have more convection occurring there, which supports the presence of more cirrus clouds.

We also compared seven models that participated in both phases of DYAMOND with 2D fields in the Tropical Western Pacific (TWP) region. Four models capture the seasonal shifts in LW and SW TOA radiation (namely, ARP, FV3/SHiELD, ICON, IFS, and MPAS) though they differ in the magnitude of this shift. Other models had major developments that changed the characteristics of the clouds in those models (e.g., SAM). While model biases are dominant, the seasonal shift is robust among the models towards more anvil in boreal winter.

Some models such as ARP, IFS, and UM have large local differences in the TWP compared to the tropical average, so the TWP may not accurately represent the global tropical behavior. However, one advantage to using high-resolution modeling is the detail provided at regional scales. In a region as convectively active as the TWP, these models do simulate the characteristic of tropical convection with some fidelity. However, the unique characteristics and biases of cloud properties in each model are persistent, which needs to be recognized in single model studies when attempting to generalize results. Treating the models as an ensemble provides results more like climatology and represents a range of variability. Thus, there is some hope for using these models for predictions for future climates.

Unlike typical GCMs, GSRMs can represent fine-scale features due to their higher horizontal, vertical, and temporal resolution. One fine-scale feature that we discussed in section 2.3.3 is the ability to represent thin TTL cirrus clouds. While there is much diversity among the models in the mean thermodynamic structure of the UTLS especially considering temperature, moisture, and clouds, the models all simulate some thin TTL cirrus clouds.

We have shown that the models represent a diverse array of tropical clouds, convection, precipitation, and radiative balance. There are strong model biases both across the tropics and in a smaller subset of the Tropical Western Pacific. A single model study must keep these biases in mind; however, as an ensemble, these models represent the current climate with some fidelity and provide a diverse set of realizations. An obvious question is what is responsible for the large model spread in cloud properties in these DYAMOND models. Is it mainly from dynamical responses driven by vertical velocity fields, mesoscale to large-scale circulations, and clear-sky cooling rates? Or is it from ice microphysical processes such as nucleation, ice sedimentation, etc.? An important next step is to quantify the sensitivity from cirrus clouds to climate across global or regional storm-resolving models, as done for single models in Satoh et al. (2018) and Bolot et al. (2023). Sullivan and Voigt (2021) and

Atlas et al. (2024) found that ice microphysics in a single model changed the TOA radiative fluxes greatly. More work can be done to distinguish the internal spread of the multi-model ensemble from the spread due to true parameter uncertainties (the range of vapor deposition rates, the different behaviors of ice due to ice habit, etc.) that will still constrain the contribution of cirrus clouds to our climate sensitivity.

Chapter 3

INVESTIGATING THE ROLE OF MICROPHYSICS ON CIRRUS CLOUDS IN SMALL DOMAIN SIMULATIONS

3.1 Introduction

Despite improvements in representing cloud processes with the shift from GCMs with parameterized convection to GSRMs with explicit convection in non-hydrostatic setups (Satoh et al., 2018), there are still critical gaps in knowledge of ice microphysical rates and processes as well as how to represent such complexity in a bulk microphysics scheme that hinder our ability to reduce cloud uncertainties even further (Morrison et al., 2020). To simulate clouds, the models must reduce the difficult-to-observe processes involved in cloud formation, evolution, and dissipation to a handful of variables to describe the state of the atmosphere such as temperature, humidity, wind speed, ice mass, ice number concentration, ice crystal habit, aerosol properties. These seemingly small uncertainties in ice microphysics can impact the cloud radiative effect at the top-of-atmosphere by as much as a factor of four (Sullivan & Voigt, 2021).

Much work has been done to identify the largest sources of uncertainty in clouds. For example, in the ICON model, autoconversion of ice to snow is the largest source of variability in ice microphysics and has a large impact on the radiative properties of clouds (Sullivan & Voigt, 2021). The different processes of frozen hydrometeors and conversion between them is a large source of uncertainty in cloud microphysics (e.g., McCumber et al., 1991; Bryan & Morrison, 2012; Adams-Selin et al., 2013; Bao et al., 2019). We avoid this autoconversion problem by using a single-category microphysics scheme (P3 Morrison & Milbrandt, 2015). Using a single ice category has been shown to improve the ice water content in high level clouds and their radiative impact (Zhao et al., 2017). By using P3 microphysics, we focus on cloud microphysical uncertainties that are more physics-related such as ice sedimentation rates, vapor depositional growth, and ice nucleation.

The goal of this chapter is to understand processes key for simulating cirrus clouds and how they impact the formation and life cycle of cirrus clouds. Below we list the key parameters for our sensitivity study using SCREAM as well as other important processes for cirrus clouds like large-scale ascent. Lastly, we consider the impact of changing SSTs to give us context for the spread in the current climate from microphysics.

3.1.1 Ice sedimentation

Climate simulations from GCMs to weather forecasting models are known to be sensitive to ice crystal fall speed (e.g., Heymsfield & Donner, 1990; Sanderson et al., 2008; Lamraoui et al., 2023), which is strongly influenced by assumptions of vapor growth, ice crystal habit, and particle size distribution (Morrison et al., 2020; Wang et al., 2020). Cirrus cloud coverage, cirrus cloud radiative effects (CRE), and upper troposphere-lower stratosphere (UTLS) humidity are also strongly influenced by ice sedimentation and contribute significantly to climate feedback uncertainties (Mitchell et al., 2011). Sullivan et al. (2022) found that different life cycles of ice nucleation, growth, and sedimentation exist and impact the radiative properties. The speed at which ice falls strongly impacts the global radiation budget (Mitchell et al., 2008; Saito et al., 2017), as well as other microphysical processes such as collisional growth and vapor deposition (Seiki & Ohno, 2022). It has been shown that cloud sinks are key to the lifetime of clouds in the upper troposphere, and thus the shape of the cloud fraction profiles (Seeley et al., 2019). The cloud condensates in the upper troposphere are slow to evaporate or sublimate due to the extremely cold temperatures as a result of Clausius-Clapeyron and a generally high relative humidity (e.g., Romps, 2014). Since evaporation is slow in the upper troposphere, ice sedimentation may play a more active role in the dissipation of anvil and cirrus clouds. Hong et al. (2009) showed that ice sedimentation and ice microphysics from two different bulk schemes were key to the sensitivity of convection in squall lines using idealized and cloud-resolving models.

3.1.2 Vapor deposition

Like the sedimentation rate, the vapor depositional growth rate can depend on the ice crystal habit assumed; simulations are sensitive to vapor depositional growth and, by association, ice habit assumptions (Morrison et al., 2020; Sulia et al., 2014; Woods et al., 2007). The assumed habit of the ice crystal can also significantly impact the ice particle size distribution and number concentration, which then impacts the ice sedimentation, latent, and radiative heating rates (Lamraoui et al., 2023). Modeled cirrus clouds have also shown sensitivity to surface kinetic processes that influence vapor depositional growth (Zhang & Harrington, 2015).

3.1.3 Ice nucleation

Several studies have shown that simulations of cirrus clouds are highly sensitive to the choice of ice nucleation scheme by including homogeneous and heterogeneous freezing, ice nucleation mechanisms (immersion, deposition, etc.), and assumed aerosol properties (ice nucleating particles and aerosol type) (e.g., Fridlind et al., 2012; Paukert et al., 2017; Zhang et al., 2014; Morrison et al., 2020). Parameterizations that incorporate lab measurements can reduce the errors in the model simulation (Kulkarni et al., 2012; Kärcher, 2022). In GCMs, even variables not directly linked to ice properties like liquid water path, cloud forcing, and precipitation were sensitive to ice nucleation (Gettelman et al., 2012; Sulia et al., 2014; I. Tan & Storelvmo, 2016; Morrison et al., 2020). Kärcher (2022) showed that using a more physically-based ice nucleation scheme allowed them to conclude that nucleation inside already formed cirrus must have high updraft speeds. In particular, we use the same nucleation as in (Gasparini et al., in prep.) which slightly modified the Liu and Penner (2005, hereafter LP2005) for homogeneous freezing and heterogeneous-homogeneous freezing competition. We also added cirrus depositional freezing from (Möhler et al., 2006). In this study, we test the impact of updating the ice nucleation scheme from 1986 to a more modern and cirrus-aware scheme from 2005 (Cooper, 1986; Liu & Penner, 2005).

3.1.4 Large-scale ascent

Large-scale ascent and deep convective influence on the thermodynamic structure of the upper tropospheric and lower stratosphere (UTLS) is also important. In regional models, large-scale circulations are not present yet the mean ascent from these circulation patterns can have a large impact on the clouds present, especially cirrus in the tropical oceans. Regions like the West Pacific and Indian Oceans have a slow mean ascent that impacts the UTLS thermodynamic structure. Lin et al. (2013) calculates the vertical ascent and upward mass flux in the UTLS from radiative heating profiles. They calculate an annual mean vertical velocity of 0.77 mm/s and 0.13 mm/s at 120 hPa (15.5 km) and 60 hPa (19.5 km) respectively. Blossey et al. (2010) show that the water vapor and water isotopologues depend on the strength and seasonal cycle of the Brewer-Dobson Circulation (BDC), cirrus cloud fraction, and deep convection. Cirrus conversely depend on the relative humidity of the air in the upper troposphere to nucleate new ice particles. Kuang and Bretherton (2004) state that the role of convection interacts with those of large-scale ascent and radiative heating in setting the thermal structure of the TTL cannot be ignored as previously assumed.

3.1.5 A cirrus sensitivity study

On global scales in high-resolution cloud-resolving models (CRMs), ice microphysics may play a large role in the diversity of clouds (Sullivan & Voigt, 2021; Nugent et al., 2022; Turbeville et al., 2022; Atlas et al., 2024). Nugent et al. (2022) found that the ice mass in the TTL in each DYAMOND model varied by a few orders of magnitude, which strongly influenced the cloud radiative effects. Turbeville et al. (2022) highlighted that the different microphysics and dynamics in the model are impossible to separate, so the role of microphysics is opaque in the DYAMOND model output. Thus, in this study, we use a single model, SCREAM, with a single dynamical setup and vary the treatment of processes within the microphysics to determine the role of ice microphysics and what aspects of the microphysics matter for simulations of cirrus clouds. We first analyze the impact of changing the rates of ice sedimentation and vapor deposition. Then we look at how large-scale ascent is important for the formation of thin TTL cirrus. Next, we show that updating the representation of ice nucleation can have a major impact on the properties of cirrus clouds. Finally, we investigate how changing sea surface temperatures (SSTs) impact clouds and top-of-atmosphere (TOA) radiative fluxes.

The next section describes the methods and model used for this microphysics parameter sensitivity study to better understand the role of microphysics on tropical cirrus cloud simulations. Then we show the analysis leading to our conclusions about key parameters for cirrus cloud simulations.

3.2 Model setup and evaluation methods

3.2.1 Description of small domain SCREAM

For this study, we use the Simple Cloud-Resolving E3SM Atmosphere Model (SCREAM; Caldwell et al., 2021) with P3 microphysics (Morrison & Milbrandt, 2015). P3 is a double-moment bulk microphysics scheme, representing both cloud mixing ratios and liquid/ice number concentration for vapor, cloud water, rain, and cloud ice. The single ice category can adjust the particle size distribution based on the type of ice present in the grid box so it does not separate the ice into snow and graupel types. Atlas et al. (2024) showed different microphysics schemes used in a single model can cause large differences in the cloud radiative effects and that P3's representation of

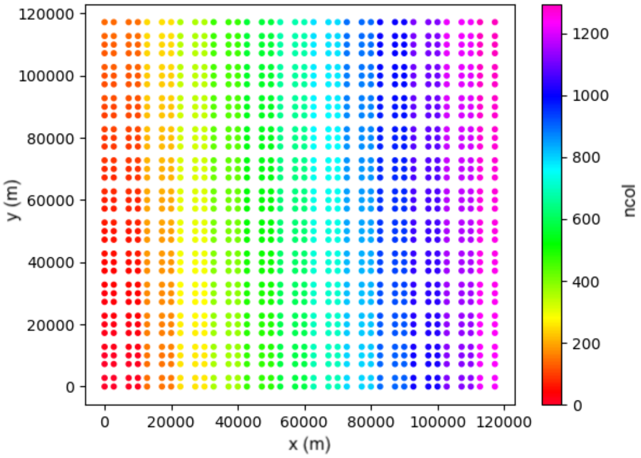

Figure 3.1: Each dot represents the center of a single grid point in SCREAM with a domain size of 120 km × 120 km. The color shows the number of the spatial dimension "ncol" since SCREAM is on a non-uniform, spectral element (not lat-lon) grid.

longwave cloud radiative effects was closest to observations among the schemes used. Here we use a single microphysics scheme (P3) and vary the parameters within the scheme.

The domain size is 120 km × 120 km with a default horizontal grid spacing of about 3.3 km and doubly periodic boundary conditions. The horizontal spacing of the grid points is shown in Figure 3.1. There are 128 vertical pressure levels. There is no Coriolis force or rotation in this setup. We allow the models to spin up for 30 days (initial conditions from the end of a 100-day long run; see Figure 3.2a & b) and then use analysis from the last 30 days of a 90-day simulation period. We use this small domain size as a test bed; here, we can run many simulations with different parameter settings. The model is in radiative-convective equilibrium (RCE) following the RCE_SMALL set up from Wing et al. (2018), meaning that radiative cooling balances the convective heating. The RCE setup (originally a single column model in Manabe & Strickler, 1964) is meant to simulate an idealized tropics with

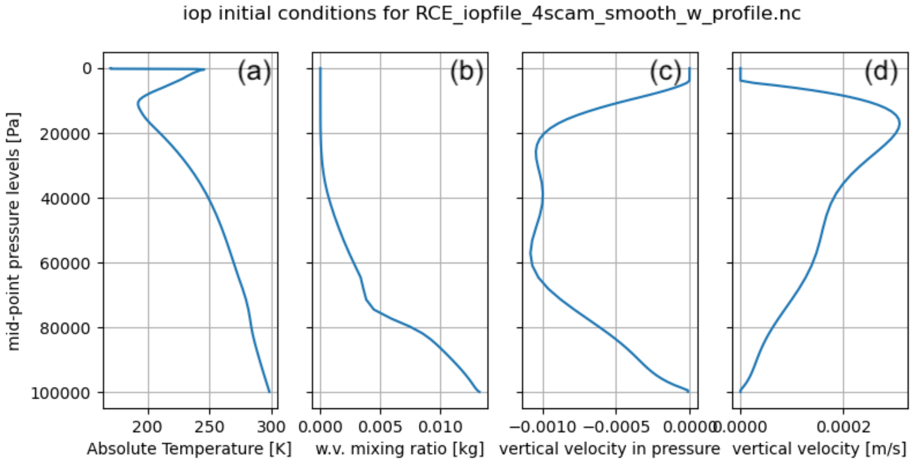

Figure 3.2: The initial conditions used for (a) temperature, (b) water vapor, (c) vertical velocity, ω, in Pa/s, and (d) vertical velocity, w, in m/s as a function of height for the large-scale ascent simulations. For simulations without large-scale ascent, the large-scale vertical velocity is 0 everywhere.

homogeneous sea surface temperature, no rotation, no mean pressure gradient, and no mean flow. Unlike in larger domains, simulations in small domains are less likely to experience convective self-aggregation (Bretherton et al., 2005), providing a more stable mean state in which to evaluate the impact of microphysical process changes.

3.2.2 Sensitivity Study Setup

Within the model framework described above (section 3.2), we update parameters related to ice processes within cirrus clouds to perform a parameter sensitivity study of ice microphysics in SCREAM. We start by adjusting the sedimentation and vapor deposition rates of ice. These two variables are important for ice cloud lifetime and optical properties as discussed in sections 3.1.1 and 3.1.2. These variables are halved and doubled in separate runs. For the first experiment, these changes are applied to all ice in the simulation, but in the second experiment they are only applied to small ice which would be most likely to make up cirrus clouds and are within the range of values we might observe in cirrus. Small ice crystals are also important for cirrus cloud radiation, which depends on the ice crystal size and number (Jensen et al., 2009). We consider small ice to be anything with an ice mass radius less than 25μm. When these changes are applied only to small ice, large ice is left unchanged ($\geq 35\mu$m), and ice with a mass radius between $25 - 35\mu$m is left to linear interpolation. A note on the language used to describe these simulations: we refer to "small ice" as having an ice mass radius of less than 25μm, "large ice" as greater than 35μm, and "all ice" refers to simulations that double and half the microphysical process rates regardless of ice mass radius (i.e., ice of all ice mass radii).

Additionally, in a separate sensitivity study, we update the ice nucleation scheme to permit supersaturation with respect to ice and a more physically realistic nucleation of ice that allows for homogeneous and heterogeneous competition in freezing following Liu and Penner (2005).

Since large-scale circulations may contribute to the formation of in situ cirrus, especially in the TTL, we add a slow mean ascent to the entire domain that mimics the effect of the Brewer-Dobson/Hadley cell/Walker circulations, similar to what we would see in the tropical western Pacific region following Lin et al. (2013) and Blossey et al. (2010). The mean vertical velocity profile imposed is shown in Figure 3.2d.

Finally, we expand our sensitivity study to include varying SSTs. We look at both increasing and decreasing the SST by 4 K to see if the result is symmetric. Table 3.1 summarizes the simulation setups used for this study.

3.3 Results

3.3.1 Ice sedimentation rate

As discussed previously in section 3.1, one of the parameters important for simulations of cirrus clouds is ice sedimentation. Ice sedimentation rate depends on the fall speed of ice, which itself depends on the ice habit and particle size distribution assumptions. Figure 3.3 shows the mean profiles of variables related to ice for the last 30 days of

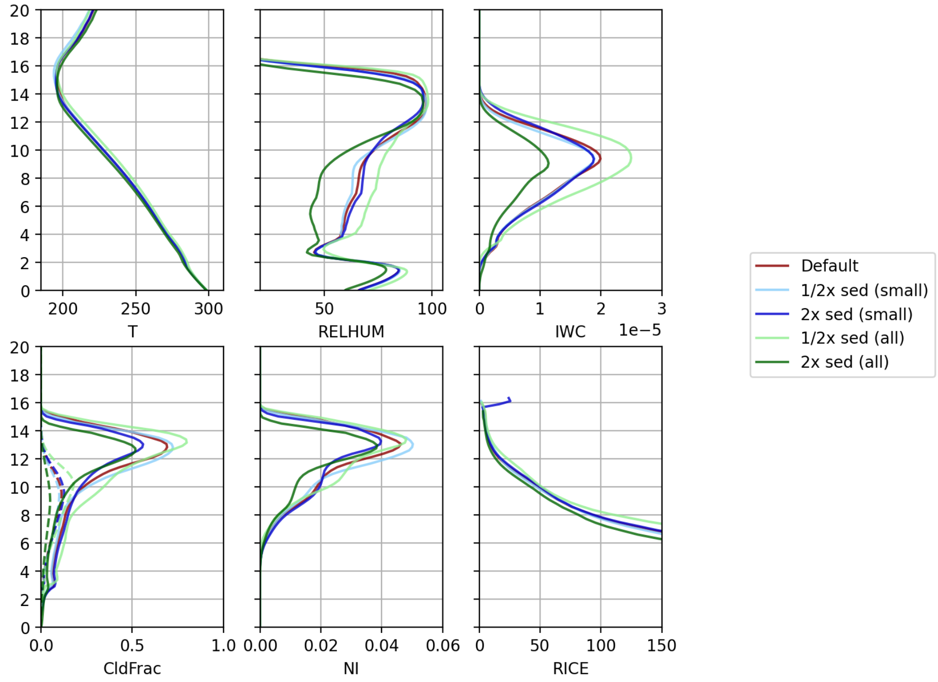

Figure 3.3: (a) temperature in K, (b) relative humidity, (c) ice water content in g/m^3, (d) cloud fraction for deep convective clouds (IWP$>$ 0.01 g/kg) and cirrus ($1e-5 <$IWC$< 1e-3$ g/kg), (e) ice number (NI) in #/kg air, and (f) ice mass radius (RICE) in μm averaged over the last 30 days of each simulation comparing halving and doubling the sedimentation rate of the default run (dark red) for large and small ice (green and blue, respectively).

Table 3.1: Caption

Run name	Description
default	Default settings for P3 in SCREAM
half_sed_all	Sedimentation rate for all ice is halved
2x_sed_all	Sedimentation rate for all ice is doubled
half_dep_all	Vapor deposition rate for all ice is halved
2x_dep_all	Vapor deposition rate for all ice is doubled
half_sed_small	Sedimentation rate for small ice ($< 25\mu$m) is halved
2x_sed_small	Sedimentation rate for small ice ($< 25\mu$m) is doubled
half_dep_small	Vapor deposition rate for small ice ($< 25\mu$m) is halved
2x_dep_small	Vapor deposition rate for small ice ($< 25\mu$m) is doubled
new ice_nuc	Ice nucleation scheme is updated to Liu and Penner (2005)
LS_ascent	Mean large scale ascent is added to the domain
+4K SST	The SST is increased to 304K
-4K SST	The SST is decreased to 296K

the default (red) simulation, those in which the sedimentation of all ice is changes, half_sed_all (light green), 2x_sed_all (dark green), and those in which the sedimentation of only small ice is changes, half_sed_small (light blue), and 2x_sed_small (dark blue).

The largest changes occur in when we half or double the sedimentation rate for all ice compared to the default; most of this change is happening due to the impact of ice sedimentation on deep convective clouds. When we double the sedimentation, we see much less ice throughout the troposphere and fewer clouds (Figure 3.3c & d). The ice mass radius also significantly decreases but the ice number concentration only decreases slightly (Figure 3.3e & f). Changing the ice sedimentation rates of small ice has a relatively small impact on the overall cloud structure. Thus, it is mostly large ice that is changing in the 2x_sed_all and half_sed_all simulations; this makes intuitive sense as the fall speed of larger ice particles is larger and that is exaggerated when we double the sedimentation rates. The relative humidity also decreases in the mid-troposphere when we double sedimentation rates of all ice; further discouraging cloud formation and maybe even sublimating the cloud and inhibiting deep convection.

The converse also applies; when halving the sedimentation rate of all ice (half_sed_all), there is an increase in ice mass (in IWC) and ice mass radius (in RICE) as seen in Figure 3.3c & f (light green) due to the slower descent of ice. Not surprisingly, the cloud fraction increases (especially below the anvil outflow) where the anvil is slowly sedimenting (around 10 km; Figure 3.3d).

However, when we halve the sedimentation rate of small ice, the ice water content and ice mass radius decrease while the ice number concentration increases around $10 - 12$ km in altitude due to the slow descent of ice. In other words, the small ice falls even slower so we see an increase in the ice number in the upper troposphere despite the loss of ice mass. Doubling or halving the sedimentation rate for small ice decreases or increases the anvil cloud fraction, respectively, but has little impact below 10 km (Figure 3.3d green).

3.3.2 Vapor despositional rate

Halving the vapor deposition for small ice implies that the ice crystals grow in size more slowly so there is less competition for available water vapor, which allows more ice particles of smaller ice mass radius to persist longer than they normally would because they sediment slower than their larger counterparts. We see a slight increase in the ice water content in the upper troposphere, so more cirrus are formed in this scenario.

Doubling the vapor deposition for small ice means that ice crystals grow larger faster (and fall out faster than smaller ice); however, some grow until they exceed the threshold for small ice and then growth by deposition returns to normal. The ice number decreases but the total ice mass remains steady since large ice is unaffected.

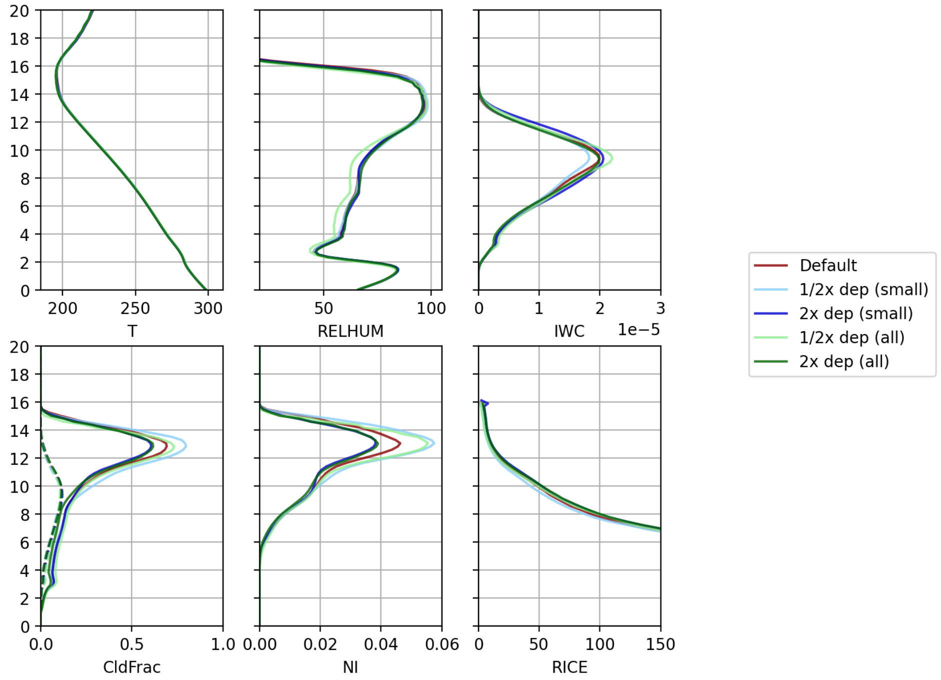

Figure 3.4: Same as Figure 3.3 but for halving and doubling the vapor depositional rate of the default run (dark red) for all and small ice (green and blue, respectively). We focus on the upper troposphere since that is where most of the changes occur (10 – 20 km).

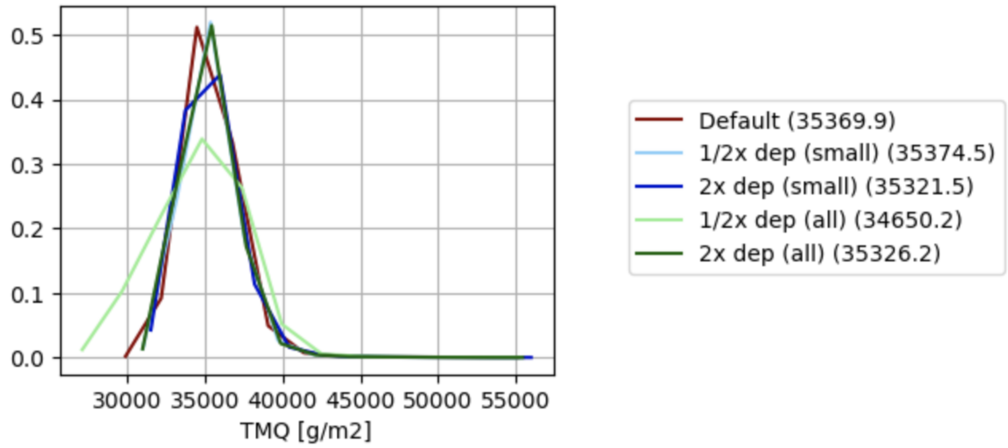

Figure 3.5: Histogram of total column moisture (precipitable water) for each simulation of doubling and halving deposition rate for small ice (blue) and all ice (green) simulations.

This story is complicated by the growth of small ice into large ice that has a normal vapor deposition rate.

When we halve the deposition rate of all ice, we get more variance in the column-integrated water vapor as seen in Figure 3.5. Some columns are much drier while others are extra moist compared to the default case. When the vapor takes longer to deposit onto the ice crystals, the column may be slightly more moist than it would have been if the deposition rate was unchanged. Also due to the slower deposition rate, the ice crystals have more time to sediment out before they have grown as large as they would have, which could impact the amount of water vapor in the grid box. Alternatively, the slower vapor deposition could mean that more ice crystals are competing for the same amount of water vapor, which then dries out the atmosphere.

Vapor deposition is a secondary process for large ice compared to sedimentation; the impacts of vapor deposition on clouds is small compared to sedimentation for all ice. However, in the small ice simulatons, vapor deposition is a primary process; the changes to vapor deposition rate are on par with that of sedimentation when considering only small ice. Changing vapor depositional rates for all ice is similar to that of small ice, so mostly, vapor deposition impacts small ice. When vapor deposition decreases, there is less competition for available water vapor so more ice particles can exist in a grid box; moreover, there are less particles grow into large ice that sediment quickly since the ice growth is slow.

3.3.3 Large-scale ascent

The presence of slow ascent, peaking at the base of the TTL, significantly impacts the amount of thin cirrus in the simulation. This slow ascent increases the cloud fraction in the TTL and simulates clouds in the upper TTL where there were none before. From the adiabatic cooling of the rising air, more clouds are formed when large-scale ascent is included in the model.

The presence of large-scale ascent (LS ascent) does not change convection significantly, but the thin, in-situ TTL cirrus clouds are now much more frequent (Figure 3.6d). The cold-point tropopause has risen and gotten colder due to the presence of LS ascent. This also increases the relative humidity in the TTL (Figure 3.6a & b). The ice number concentration has also increased, so we see a lot of thin cirrus with high number concentrations and small ice mass radius (Figure 3.6e & f). When we halve the imposed mean ascent in the model (Half ascent; Figure 3.6 pink), this shows that any amount of large-scale ascent (however small) will still increase the cloud fraction in the TTL, through impacting the temperature profile and raising the relative humidity in near the cold point tropopause, but the decrease in IWC shows that the impact is not as strong the full LS ascent.

We confirm the clouds in the large-scale ascent simulation are mostly small ice with high number concentration by looking at the joint histogram of ice number concentration and ice mass radius in Figure 3.7.

Halving the mean ascent imposed in the simulations significantly increases the time to reach equilibrium. After 90 days though, the simulations end up with similar

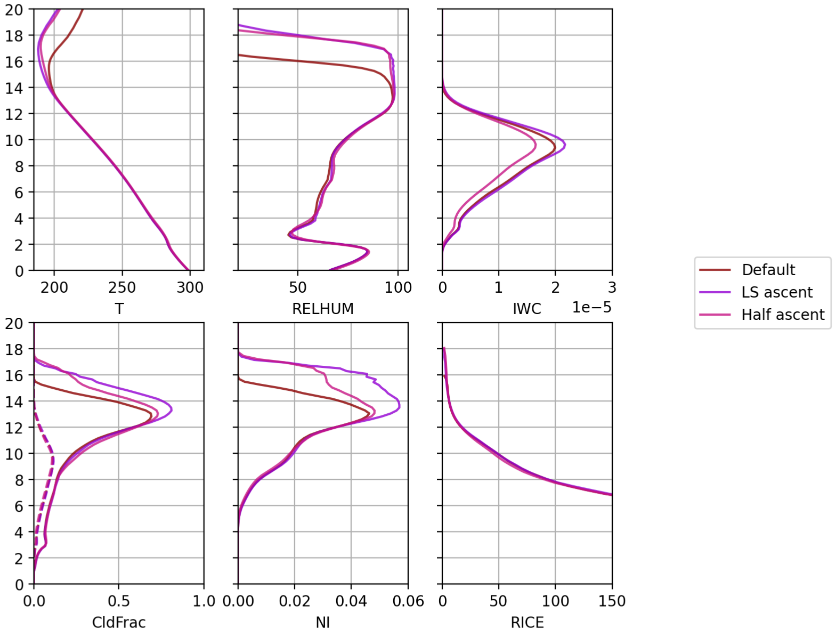

Figure 3.6: Same as Figure 3.3 but for large-scale ascent (purple) and half the large-scale ascent (pink).

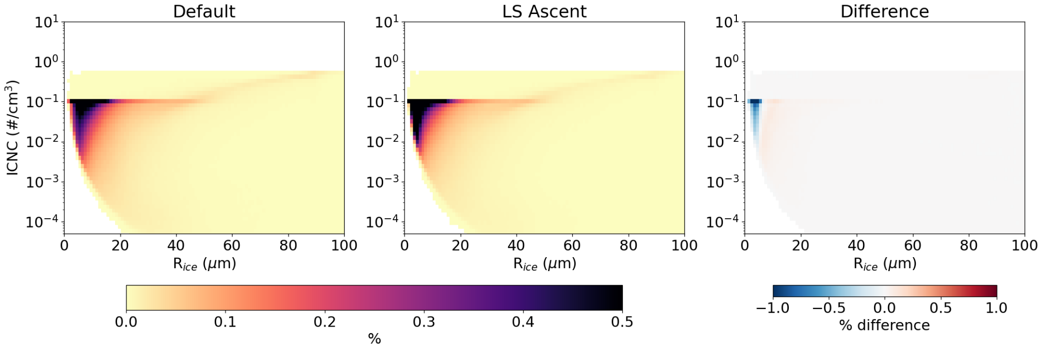

Figure 3.7: The 2D histogram of ice crystal number concentration (ICNC) and ice mass radius (R$_{ice}$)for the (a) default simulation, (b) large-scale ascent simulation, and (c) the difference between the two (a)−(b). The blue colors in (c) signify more grid boxes in the large-scale ascent run had those values of ICNC and R$_{ice}$, and vice versa for red colors.

temperature and relative humidity profiles as seen in Figure 3.6a & b.

3.3.4 Updated ice nucleation scheme

We update the default ice nucleation scheme in SCREAM from a simple mixed phase relationship following Cooper (1986) to a more physical scheme for cirrus clouds following Gasparini et al. (in prep.), which modifies the LP2005 scheme and implements cirrus depositional freezing from Möhler et al. (2006). The implementation in SCREAM was based on that in SAM. The two models both use P3 microphysics but with different versions. The models also differ in their dynamical cores, which may impact interactions with cloud processes, yet we get qualitatively similar results in the two models as discussed later.

Figure 3.9 (left) shows the pathway for ice nucleation in the default setting of SCREAM's P3 microphysics. Simply there are two flags that are hard-coded into the microphysics scheme and decide whether or not to use the prescribed cloud condensation nuclei (CCN) and if so whether to predict or prescribe the number concentration from the aerosol scheme. In this set up most ice is nucleated via deposition and

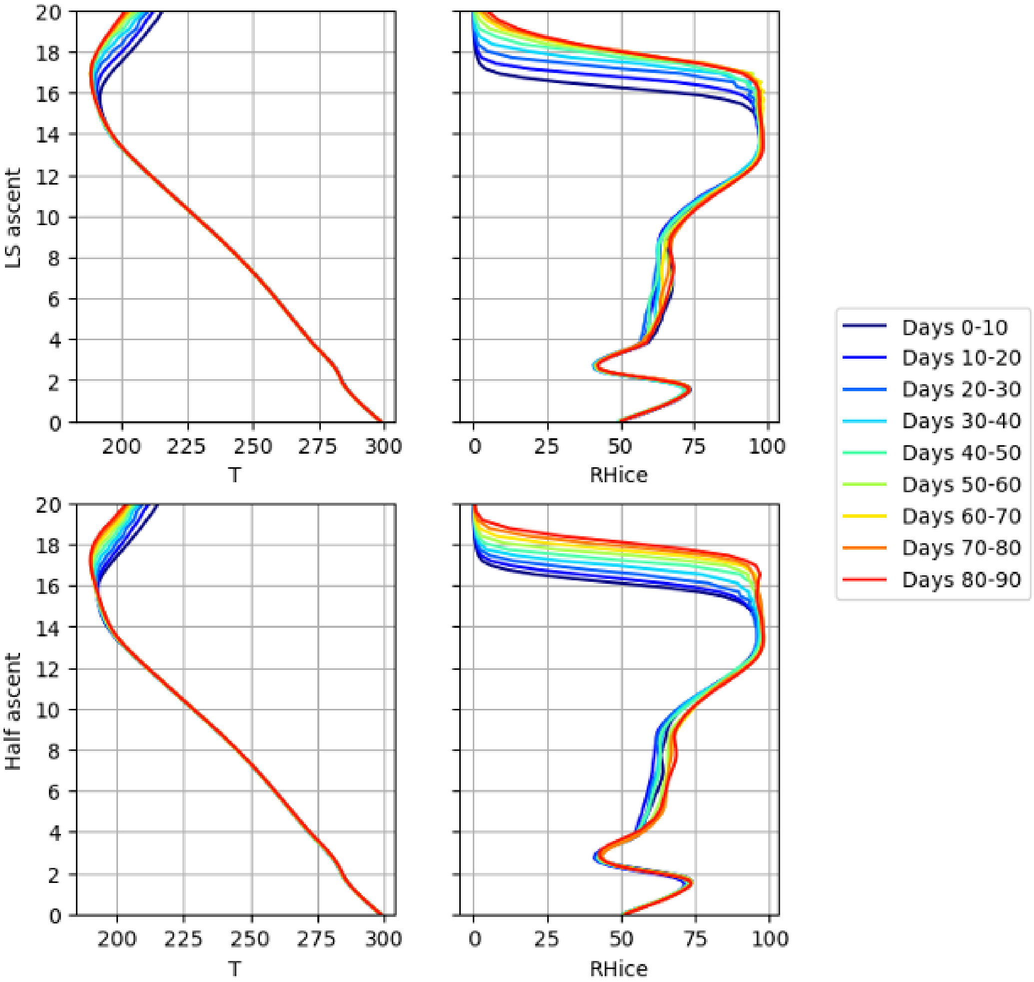

Figure 3.8: The temperature and relative humidity profiles are plotted as ten-day means over the entire 90-day period for the large-scale ascent run (top) and the half ascent (bottom).

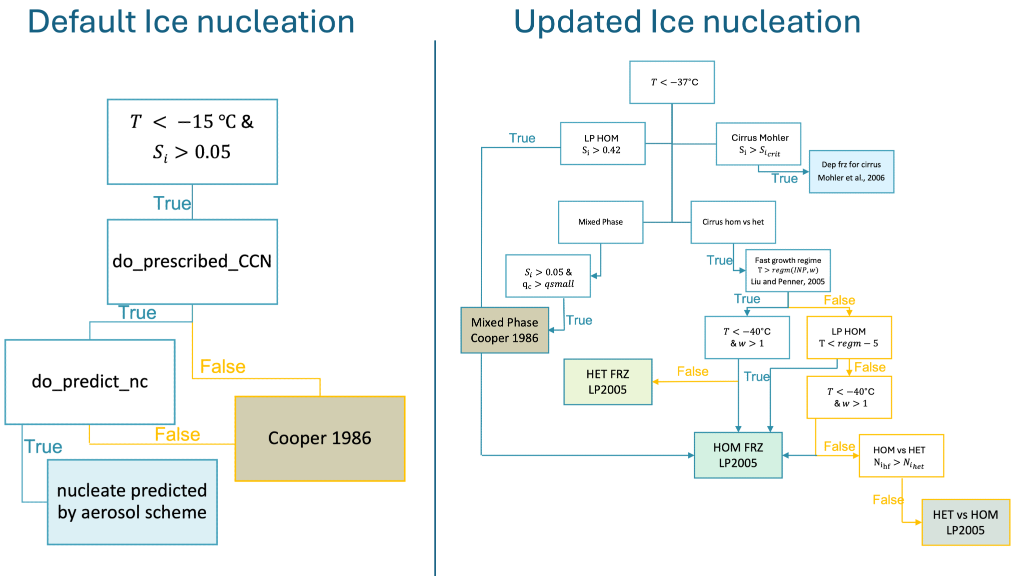

Figure 3.9: Schematic of the two ice nucleation schemes used: standard or default scheme and the new ice nucleation scheme following LP2005.

condensation following Cooper (1986). For more information on ice nucleation see Morrison and Milbrandt (2015, Appendix C).

Some significant updates in the ice nucleation scheme are the updating the homogeneous freezing (LP2005), adding homogeneous and heterogeneous freezing competition (LP2005), and cirrus-specific nucleation (Möhler et al., 2006). The mixed phase nucleation still uses Cooper (1986). We also raised the artificial limit on the ice number concentration as shown in Figure 3.10. This allows a more physical growth and decay of cloud ice without the artificial upper limit. For heterogeneous ice nucleation, we prescribe an a set value for ice nucleating particles (INP), which is based on simulated upper tropospheric (200 hPa) values of dust in Tropical Western Pacific for ECHAM-HAM GCM simulations (Gasparini et al., in prep.). Hawker et al. (2021) showed that just changing the INP used (and using an interactive scheme) can introduce large uncertainties. The pathways for ice nucleation in the updated scheme are shown on the right-hand side of Figure 3.9. The updates add to the complexity of the

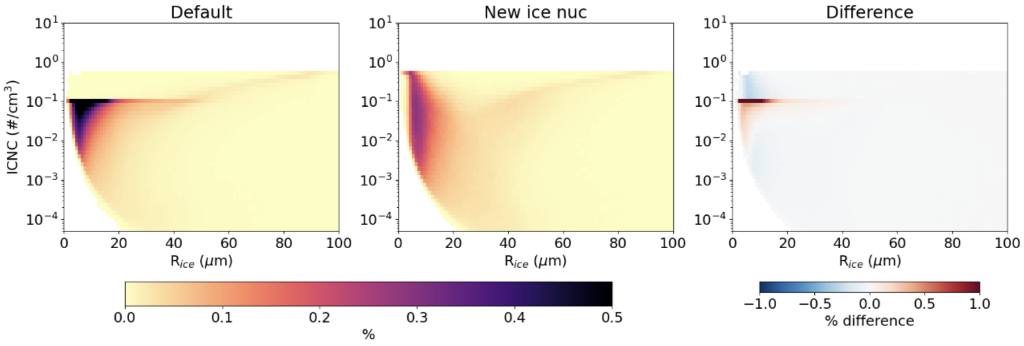

Figure 3.10: Same as Figure 3.7 but for the new ice nucleation scheme. The difference is computed as "Default" minus "New ice nucleation". Note the artificial limit around 10^{-1} #/cm^3 is removed and the distribution of ICNC in the new ice nucleation scheme is much smoother.

ice nucleation scheme having four user-defined flags for nucleation instead of two and adding more realistic treatment of ice formation in cold temperatures ($T_{air} < -35°\text{C}$). The changes were made to improve ice nucleation at cirrus-like temperatures using updated measurements and formulas.

The changes to the mean vertical structure of clouds and the thermodynamics are similar to the default simulation as shown in Figure 3.11a–f. The changes are mostly in the upper TTL with increased relative humidity and cooler temperature in the stratosphere. The new ice nucleation scheme allows more supersaturation, which would allow more cirrus to form. The ice mass radii are larger throughout the troposphere using the updated ice nucleation scheme. The larger ice mass means the ice sediments more quickly, which could explain the increased cloud fraction below the anvil cloud fraction peak (around 10–12 km).

The cloud structure does not change dramatically using the updated ice nucleation scheme from LP2005 but the microphysical properties of the ice clouds are slightly larger in ice mass radius, geometrically thicker, and optically thinner. Theses seemingly small changes in ice nucleation, there is slightly less precipitation, higher PW, and an IWP histogram shifted to smaller values in the updated ice nucleation sim-

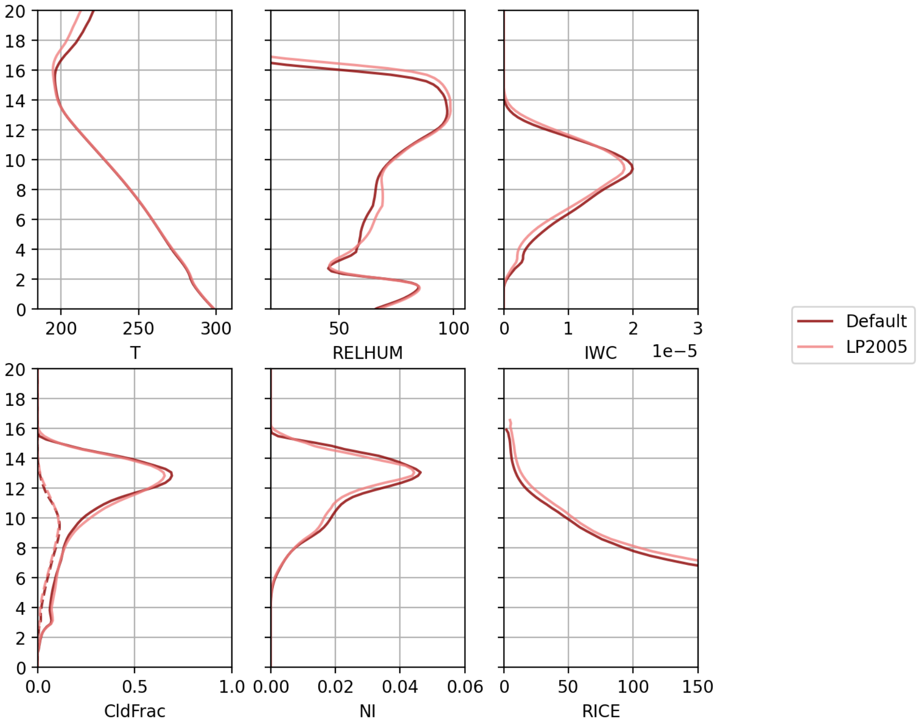

Figure 3.11: Same as 3.3 but for the updated ice nucleation scheme (pink) and the default (maroon).

ulation (not shown). The SW impacts from these changes are smaller than the LW cloud radiative effect (CRE) changes since these impacts are mostly related to thin cirrus clouds (see Figure 3.15a).

3.3.5 Impact of SSTs

The default sea surface temperature (SST) is 300 K uniform over the domain for the entire simulation period. We ran one simulation increasing the SST by 4 K and one decreasing by 4 K to see how changing the SST might impact cirrus clouds and if the response is linear or has differs whether cooling or warming the SST. The +4 K SST emulates a warmer climate under global warming similar to the simulations done in RCEMIP (Radiative-convective equilibrium model intercomparison project; Wing et al., 2018).

Figure 3.12 shows the mean profiles over the last 30 days of each simulation with the SSTs ranging from 296 K to 304 K. Despite a relative humidity with a similar shape (just higher), the cloud fraction is reduced (Figure 3.12b & d). Both the increase in the height of the anvil cloud peak and a decrease in the cloud fraction are consistent with results from GCMs and CRMs (Wing et al., 2020).

The increased SST allows the atmosphere to hold more water due to the warmer temperatures throughout the troposphere following Clausius-Clapeyron (see Figure 3.13b). Since the emission temperature of the water vapor is warmer than at the same level in a cooler run, the OLR increases in warmer runs; we see the OLR increases by +10 W/m2 in the warmed SST run compared to the default and about +16 W/m2 compared to the cooled SST run (see Figure 3.15b). The outgoing SW (SWU) radiation changes by ±5 W/m2; the warmed SST reflects less solar radiation back to space compared to the default due to the change in cloud properties (increased R_{ice}, decreased N_i, lower mean IWC) and decreased cloud. Sokol et al. (2024) found a disproportionate decrease in the thick anvil clouds with warming, leading to thinner and less reflective anvils. We see a slight decrease in the thick anvil clouds (IWP

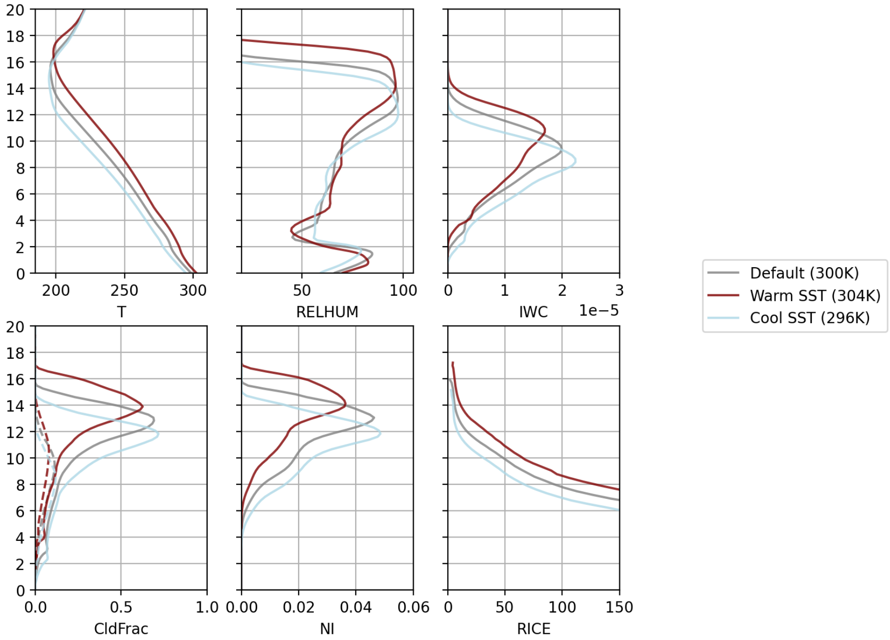

Figure 3.12: Same as Figure 3.6 but for increasing and decreasing SST by 4 K.

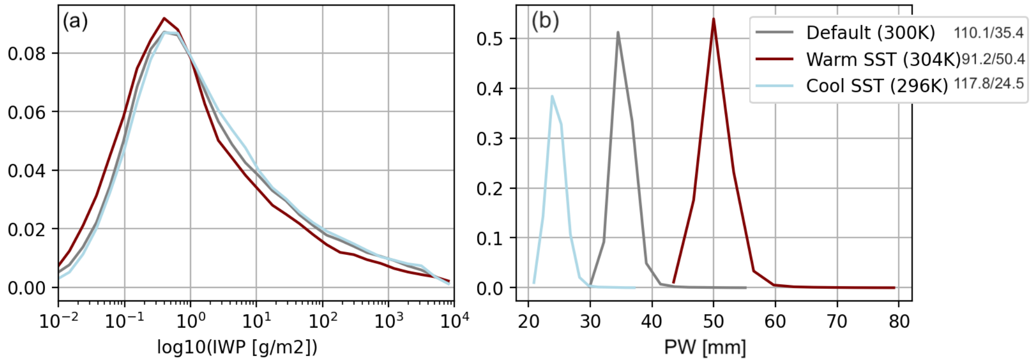

Figure 3.13: (a) ice water path (IWP) and (b) precipitable water (PW) histograms for the default (gray) and ±4 K SST (red and blue). The legend lists the mean values of (a) and (b) respectively.

$>$ 1 g/m2) and a slight increase in thin clouds (IWP $<$ 1 g/m2) in the warmed SST simulation. The effect for cooler SSTs is muted comparatively. The mean values of IWP decrease with increasing SSTs (see first number in legend in Figure 3.13).

The mean column precipitatable water (PW; second number in legend in Figure 3.13) for the default simulation (35.4 mm) is around the 25th percentile compared to other small domain CRMs in RCEMIP (Wing et al., 2020), so a bit on the dry side but well within the model spread (27–48 mm).

Precipitable water variance is similar to the column relative humidity variance, which was introduced in Wing and Cronin (2016) as a metric for convective organization. We start to see self-organized convection in the 304 K SST run as shown in Figure 3.14, which does not occur in the default or cooled SST runs. The convection has developed some spontaneous convective organization (indicated by increased variance) into some very dry columns and some very moist columns around days $45 - 70$, then goes back to a disorganized state. The peak in the precipitable water variance is around 80 kg/m^2, which is about 30% less than the 300K SST large domain simulation which reached about 120 kg/m^2 precipitable water variance and

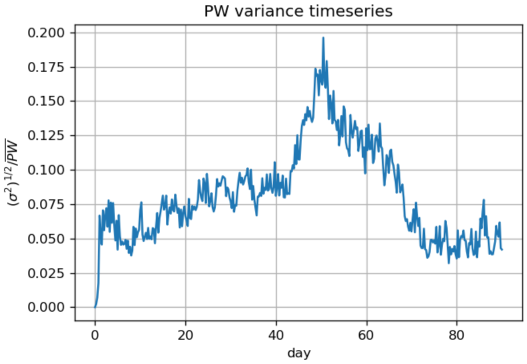

Figure 3.14: A time series of the precipitable water spatial variance. The higher values signify more convective organization.

60% less variance than the 304K SST large domain simulation in Chapter 4.3.2. An increase in convective aggregation is known to cause a decrease in the anvil cloud fraction (Wing et al., 2020), which may also be driving the decrease in anvil cloud fraction seen here since our 304 K run had some aggregation within the last 30 days of the simulation period. There were a few models in the RCEMIP simulations that began to have organized convection in the RCE_SMALL domain with increased SSTs (in that case 305 K) (Wing et al., 2020), which they concluded meant that SSTs have an impact on convective organization.

3.3.6 Summary of sensitivity study

The results of the sensitivity study discussed in this chapter can be summarized by their LW and SW radiative impact at the top-of-atmosphere (TOA). The mean LW and SW cloud (Fig. 3.15a) and all-sky (Fig. 3.15b) radiative effects highlight the role microphysics, large-scale ascent, and changing SSTs on clouds and radiation. The largest impact on TOA radiation is from the ice sedimentation sensitivity simulations for all ice ($\pm 15 and 10 W/m^2$ LW and SW CRE, respectively; Fig. 4.14). Halving and doubling ice sedimentation increased and decreased the IWC significantly and im-

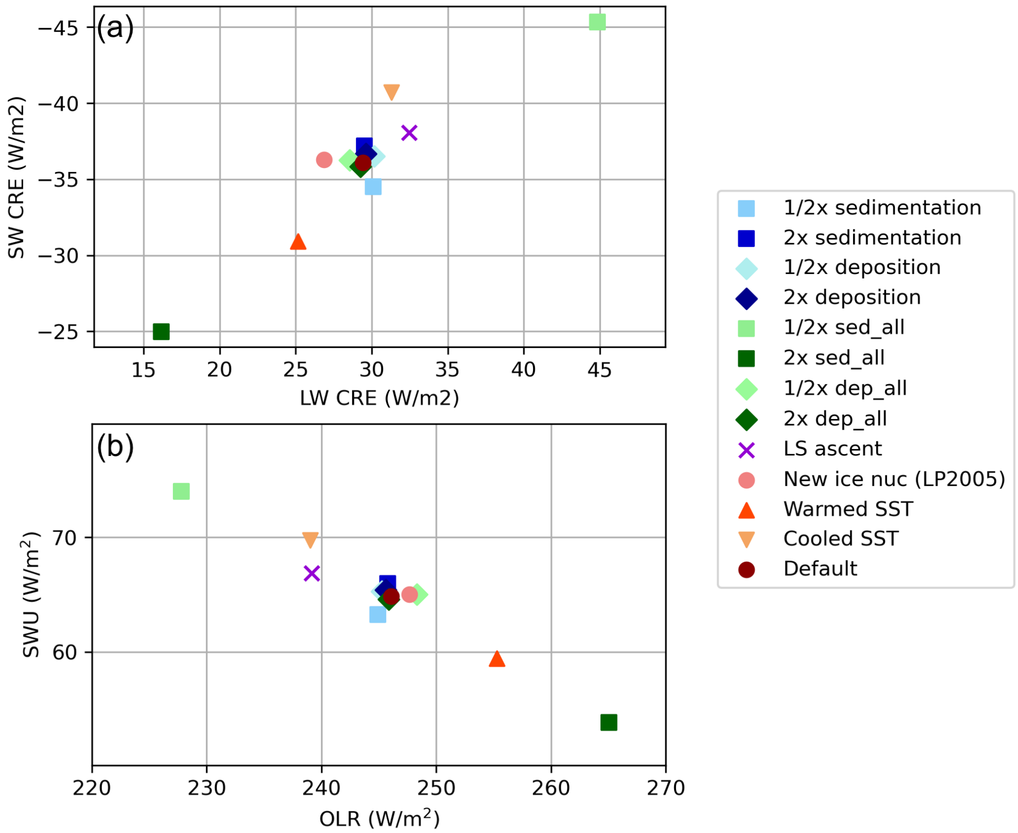

Figure 3.15: The spatiotemporal mean of (a) LW and SW cloud radiative effect (CRE) and (b) OLR and reflected SW radiation at TOA are plotted from the last 30 days of each simulation. The small ice simulations are squares, the large ice simulations are diamonds with the increased or decreased sedimentation rate in blue and deposition in green, the large-scale ascent is an ×, the new ice nucleation, and the default runs are circles, and the different SST simulations are triangles. Most small ice and new ice nucleation simulations are clustered around the default simulation (i.e., small changes in TOA radiation).

pacted deep convective clouds, which strongly impacts the TOA radiation. Increasing and decreasing the SST by 4 K also had a large impact on the TOA radiative fluxes. Increasing SST (and thereby water vapor) has a strong clear-sky radiative impact, so looking at the LW and SW CRE reveals that the cloud impact is also significant in warmed and cooled SST simulations. There is a stronger weakening of the CRE in the warmed simulation compared to the strengthening of the CRE in the cooled simulation. The LS ascent simulation was interesting in that the relative humidity increased in height as much as warming the SST by 4 K but decreased the OLR by as much as the cooled SST simulation. The LW CRE is stronger in the large-scale ascent than the cooler SST simulation. The LS ascent simulation has more thin TTL cirrus that have a strong warming effect.

While ice sedimentation for all ice, changing the SSTs, and adding LS ascent have the greatest TOA radiative impacts, the other simulations also impact the TOA radiation less comparatively but still significant when considering the climate sensitivity and that we are using an idealized model setup. The sensitivity for small ice was chosen since it is representative of uncertainties in measurement and knowledge of ice process rates, and represent the variability from cirrus-specific processes. The sedimentation of small ice and vapor deposition sensitivity simulations all cluster around the default simulation within ± 5 W/m^2 in the all-sky conditions. Ice sedimentation of small ice has a stronger SW than LW CRE. Doubling the sedimentation of small ice reduces the cloud fraction and N_i, which would cause the clouds to be less frequent and less reflective, and vice versa. Changing the deposition rate for all ice and small ice both have a small impact on TOA radiation since the changes are felt most in thin cirrus clouds. The impact of halving deposition of small ice is to weaken the LW CRE while halving all ice deposition strengthens the LW CRE. Halving the deposition rate of all ice causes the mean state to be drier which has a clear-sky radiative impact, so the deposition rate seems larger in the all-sky compared to the CRE. The updated ice nucleation simulation has a similar OLR change as halving the deposition of all ice, yet a strong LW CRE so most of the changes from updating the ice nucleation impacts the clouds mostly (though it does have a slight moistening effect as well). There is some offsetting impacts with deposition simulations; notably, doubling the deposition of small ice increasing the cloud ice content but decreasing the cloud fraction.

The sedimentation rate is important for larger ice; however, vapor deposition is significant in determining the characteristics of small ice relevant for cirrus processes. The uncertainty of cirrus may cascade into larger errors in the simulations of future climates (i.e., small ice simulations which aimed to capture realistic spread due to cirrus impacts TOA radiation up to 20% of the impact from changing SSTs alone). Changing the SST has a linear relationship around the default 300 K simulation where the TOA radiation seems to be in balance between LW and SW (i.e., decreasing the OLR means an increase in the reflected SW radiation, SWU). This balance holds for the sensitivity studies, the all ice sedimentation is close to the same slope as changing the SSTs.

Next, it would be useful to understand the role of convective aggregation and deep convection on cirrus clouds. How much cirrus is formed directly via convective detrainment and how much cirrus is formed in-situ, or far from convection? How do cirrus change in a changing climate? We saw a preview of how the model predicts anvil to change, which was in line with previous studies; however, how do TTL cirrus change with warming? How do in-situ formed cirrus change with warming and is it significant to the climate sensitivity and feedback?

Chapter 4

TROPICAL CIRRUS IN SIMULATIONS OF ORGANIZED CONVECTION IN RCE

4.1 Introduction

The work in this chapter builds on Chapter 3, expanding some of the small domain simulations to a more realistic tropical channel large domain. The large domain allows convective self-aggregation to occur (Wing & Cronin, 2016; Cronin & Wing, 2017). Throughout this thesis, I will refer to *self-aggregation* or *self-organization* all as *convective organization* or simply *organized convection.* We use three simulations setups from the previous chapter to create a set of simulations using SCREAM to explore the role of microphysics on cirrus in large domains with organized convection: (1) default, (2) large-scale ascent, and (3) new ice nucleation.

Passive tracers were added to these simulations to diagnose the origin of cirrus and the role of convection in their lifecycle (described in Ch. 4.2.2). First, we break down the cirrus origins in the default simulation then we add in the other simulations, which we found important in the small domain sensitivity study (Ch. 3). We see if changing the microphysics can impact the tropical mean values of OLR comparable to the DYAMOND model spread (Ch. 2).

4.2 Methods

4.2.1 Model setup

The large domain is 5120 km ×320 km in the horizontal with 3.3 km grid spacing (see Figure 4.1). There are 128 vertical levels, uniform SST, and radiative-convective equilibrium just as in the small domain setup in Chapter 3. The large domain allows

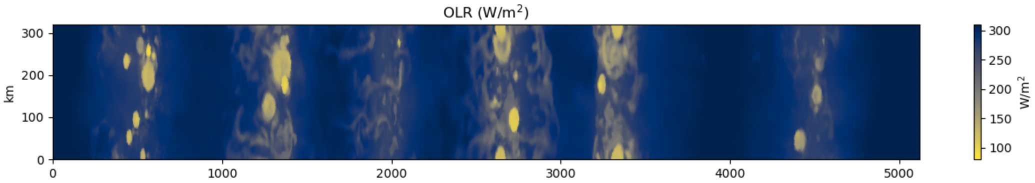

Figure 4.1: A snapshot of OLR (W/m^2) from the large domain simulation. The domain is shown in kilometers (5120 km ×320 km), a "bowling alley" or channel domain set up. The convection aggregates and organizes into patches with active convection and low OLR, separated by drier regions with larger OLR. A movie of OLR can be found here: `https://youtu.be/AHQvo81dcqQ`.

Table 4.1: The model setup for the large domain SCREAM simulations

Run name	Description
Default_300K	Default settings for P3 in SCREAM with a uniform 300 K SST
LPFRZ_300K	Ice nucleation scheme is updated to Liu and Penner (2005)
LSascent_300K	Mean large-scale ascent is added to the domain
Default_304K	The SST is increased to 304K with default settings
LPFRZ_304K	Same as LPFRZ_300K but with 304K SST
LSascent_304K	Same as LSascent_300K but with 304K SST

convection to self-aggregate, or organize, into regions of moist convection and regions of dry descent (Bretherton et al., 2005; Wing et al., 2020).

These large domain simulations are initialized using the temperature profiles from the end of a 100-day small domain simulation with the same setup (default, large-scale ascent, +4 K SST, etc. from Chapter 3.2.1). The current climate simulations are prescribed uniform SST of 300K while the +4K "future climate" simulation are prescribed an SST of 304K. This is similar to the RCE model intercomparison project (RCEMIP), which uses 305K SSTs for their warmed climate (Wing et al., 2017).

4.2.2 Passive tracers for nucleation and convection

Passive tracers were added to the microphysics scheme to track the time since nucleation and convection separately as well as vertical velocity and ice number concentration at nucleation. The tracers advect with the mean flow.

The convective tracer is initialized to 1 when the grid box is in a strong cloudy updraft (i.e., $q_i > $ 1e-5 kg/kg and $\omega \leq -0.1$ Pa/s). This threshold was taken from the strongest 20% of vertical velocity in the small domain simulations (this is the strongest 40% of updrafts). For each timestep that the grid box is not in a strong cloudy updraft, the tracer decays exponentially. The nucleation tracer is also initialized to 1 when the grid box experiences fresh nucleation (i.e., the nucleation tendency from the ice nucleation scheme is positive). For each timestep that the grid box does not experience fresh nucleation, the tracer decays exponentially. For this analysis the tracers are converted to hours, τ_{conv} and τ_{nuc}, time since convection and nucleation respectively. In addition to the tracers for convection and nucleation, I added two more tracers to track the ice number concentration and vertical velocity when nucleation occurs. These tracers decay at the same rate as the nucleation tracers so we can approximately reconstruct these variables at the time of nucleation.

We define in-situ cirrus as clouds with a temperature, $T < -60$°C (213.15K) and $\tau_{conv} > 5$ hrs. Our results are somewhat sensitive to this threshold but it seems to capture a substantial amount thin cirrus in the upper troposphere. Our definition of strong cloudy updraft is generous and so includes many anvil recently detrained from deep convective cores. We consider anvil clouds as detrained from a strong cloudy updraft within the last two hours. This includes convective cores and recently detrained anvil and cirrus. We contrast these two types of clouds (in-situ and anvil clouds) throughout the rest of this chapter.

1. in-situ cirrus : $\tau_{nuc} < (\tau_{conv} - 5 \text{ hrs})$ & $T < -60°\text{C}$

2. anvil clouds : $\tau_{conv} < 2$ hrs

To get enough grid points to compute statistics, we define in-situ generously and may include some aged anvil instead of solely remote cirrus. Regardless of the definition of in-situ cirrus here, we will still be including some cirrus that is attached to convection. We added two additional tracers to provide insight about nucleation by reconstructing the vertical velocity, ω_{nuc}, and ice number concentration $N_{i_{nuc}}$ at nucleation.

The code for this is on my GitHub repository for SCREAM (`github.com/smturbev/scream`). See the file cldera_passive_tracers.F90 for the implementation of the tracers into SCREAM.

4.2.3 Quantities explained

The mean ice mass radius, R_{ice} is calculated following Krämer et al. (2009):

$$R_{ice} = (q_i \frac{3}{4} \pi \rho N_i)^{1/3} \tag{4.1}$$

where q_i is the cloud ice mixing ratio, ρ is the density of air, N_i is the ice number concentration.

4.3 Results

I present the results of the large domain simulations described in Table 4.1. The default simulation is the "out of the box" setup of SCREAM using P3 microphysics. The ice nucleation is Cooper (1986) for mixed-phase condensation and deposition freezing that is extrapolated to extremely cold cirrus temperatures, which is a known simplification as described in Chapter 3.2.1. Passive tracers were added to SCREAM as described in the methods section (Ch. 4.2) that track time since convection and nucleation separately. I use these two tracers together to determine the presence of in-situ cirrus and the role of convection in cirrus formation.

First, I show the degree of convective organization in each simulation and its impact on the background state of the model. From snapshots of the tracers for convection and nucleation, we see that nucleation occurs near and far from convection and that cirrus clouds experience fresh nucleation throughout their life cycles. We define in-situ formation as cirrus clouds with nucleation that happens more than 5 hours outside of a strong cloudy updraft (i.e., in-situ is $\tau_{nuc} < \tau_{conv} - 5\text{hrs}$) . We defined anvil clouds to be within two hours of strong cloudy updraft (i.e., anvil is $\tau_{conv} < 2\text{hrs}$). We compare the spatial and vertical distribution of in-situ cirrus in each of the different simulations and investigate how they change with warming. Including large-scale slow mean ascent in these simulations greatly increases the thin cirrus in the TTL. How much of those TTL cirrus are still related to convection? Also how does convective organization impact TTL or in-situ cirrus?

4.3.1 The Default Simulation

Figure 4.2 shows the temperature warms slightly compared to the initial condition, which is the equilibrium state of the small domain simulation. This is true for the other simulations listed in Table 4.1 as well (not shown). This is consistent with Bretherton et al. (2005, Fig. 4), which links the warmer mean state with the change in moist static energy between the lower and upper troposphere in moist versus dry columns. The organized convection leads to a separation of moist columns and the dry columns which are drier than in a disorganized state. On average, there is lower moisture to net drier and warmer with convective organization in the simulations, which is consistent with results using other RCE models (Wing & Cronin, 2016). Convection in the large domain simulation presented here shows strong evidence of spontaneous organization.

There are several different metrics to quantify convective organization; here, I chose to use the spatial variance of precipitable water which is similar to column relative humidity (e.g., Wing et al., 2020; Bretherton et al., 2005). Precipitable water

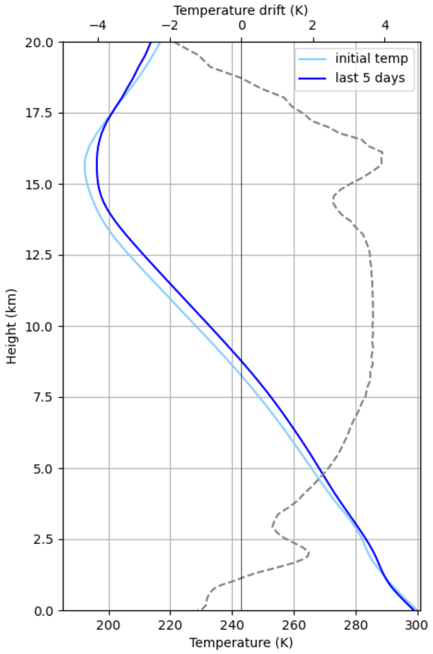

Figure 4.2: The temperature drift is shown in the gray dashed line (top axis), which is the difference between the initial temperature (light blue) and the ending temperature (dark blue), which is the average temperature over the last 5 days (bottom axis). The simulation is 50 days long. The temperature drift (end-beginning) is the dashed gray line, which corresponds to the top axis.

(PW) is the column-integrated water vapor path. The mean value of PW is listed in the legend of Figure 4.3 which is 7 kg/m^2 drier than the small domain default simulation. Most of the RCEMIP models also simulated a drier mean state in the large domain simulation with more precipitation; the difference between the large and small domain mean state is inferred to be from organized convection (Wing et al., 2020). When convective organization occurs, the columns organize into moist and dry columns; thus, the spatial variance of precipitable water increases. Over the first 30 days, the convection begins to organize (Figure 4.3). The convective organization peaks around the 40th day of the simulation and seems to be in equilibrium. The next

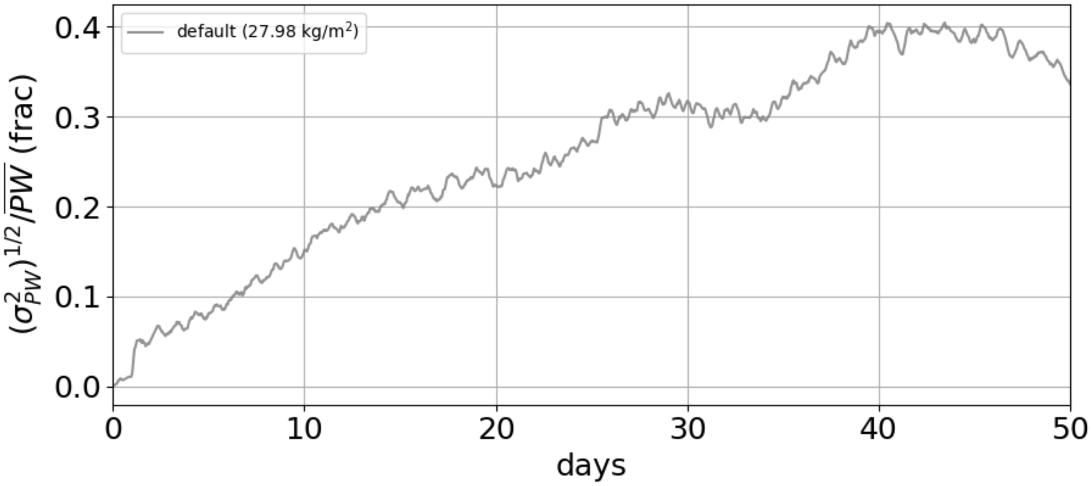

Figure 4.3: The normalized square root of variance of precipitable water for the default_300K large domain simulation.

three figures (Figures 4.4–4.6) take snapshots from days 10, 20, and 40 of the default large domain simulation ranging from disorganized at day 10 to highly organized convection at day 40.

Figure 4.4 shows precipitable water (PW), OLR, IWP, and time since nucleation for different ranges of time since convection from anvil cloud ($<$ 2 hrs), aged anvil ($2-5$ hrs), in-situ ($5-50$) and remote ($>$ 50 hrs) from day 10. Figure 4.4g shows the cloud layer mean value of the nucleation tracer, τ_{nuc}, for each column when it has been over two days since a strong cloud updraft ($\tau_{conv} >$ 50hrs). It is evident that nucleation is happening near and far from convection. As convection organizes (Figure 4.6), it seems that remote cirrus ($\tau_{conv} >$ 50 hrs) covers a larger area than when convection is disorganized; it may be an artifact of the increased distance between convective areas with organization that allows more grid cells to survive more than 2 days without encountering a fresh convective updraft.

Even though we get more remote cirrus with organized convection, it is still rare, possibly, because convection occurs so frequently in the domain that no column is too far from convection. In this setup, it is also rare that a column is further than

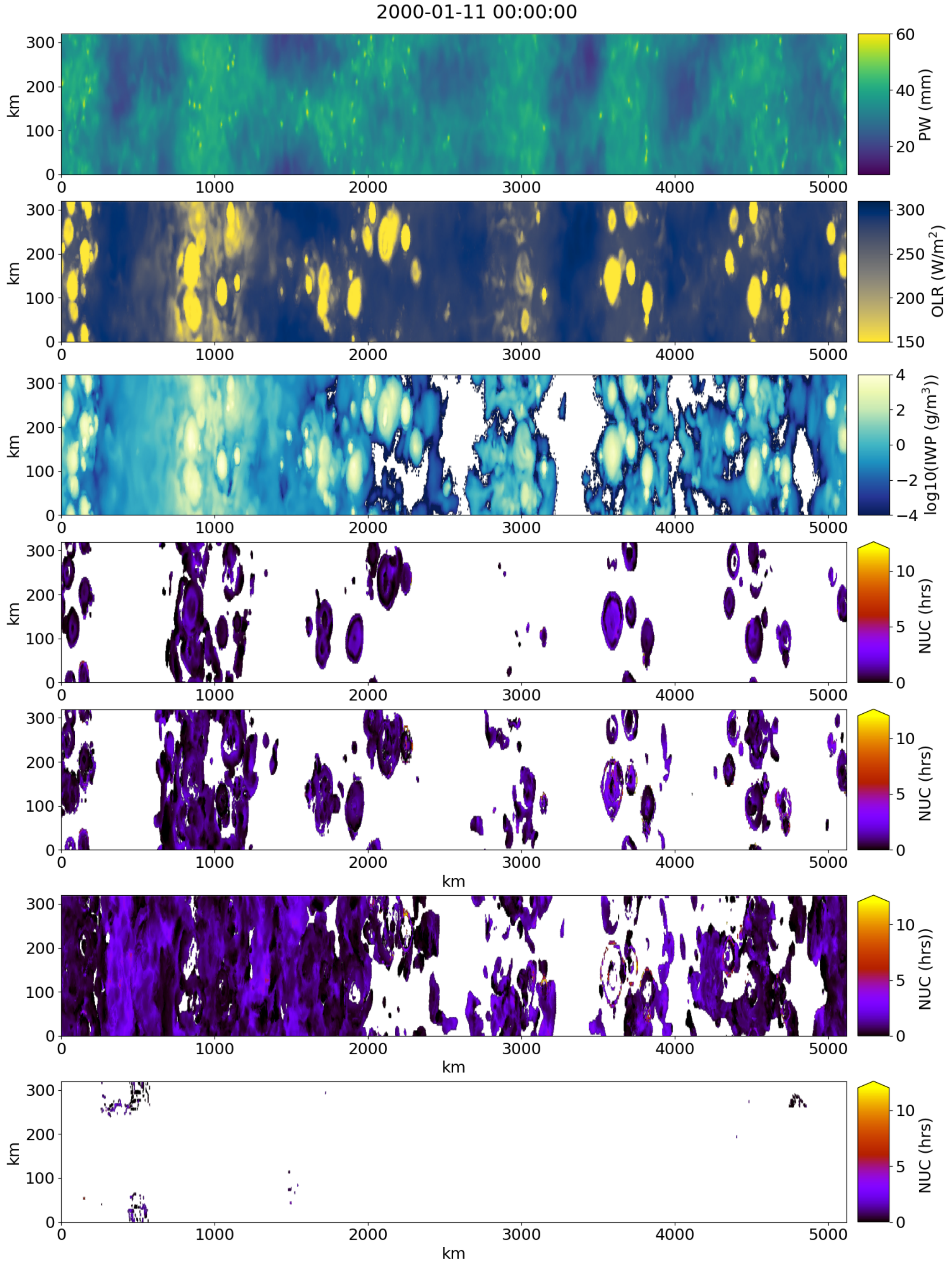

Figure 4.4: Snapshot on day 10 of the simulation showing the precipitable water (PW), OLR, IWP, layer-mean time since nucleation near fresh convection (time since convection is less than 2 hours), 2-5 hrs from convection, 5-50 hrs from convection and far from convection ($>$ 50 hrs). Convection is relatively disorganized during this time.

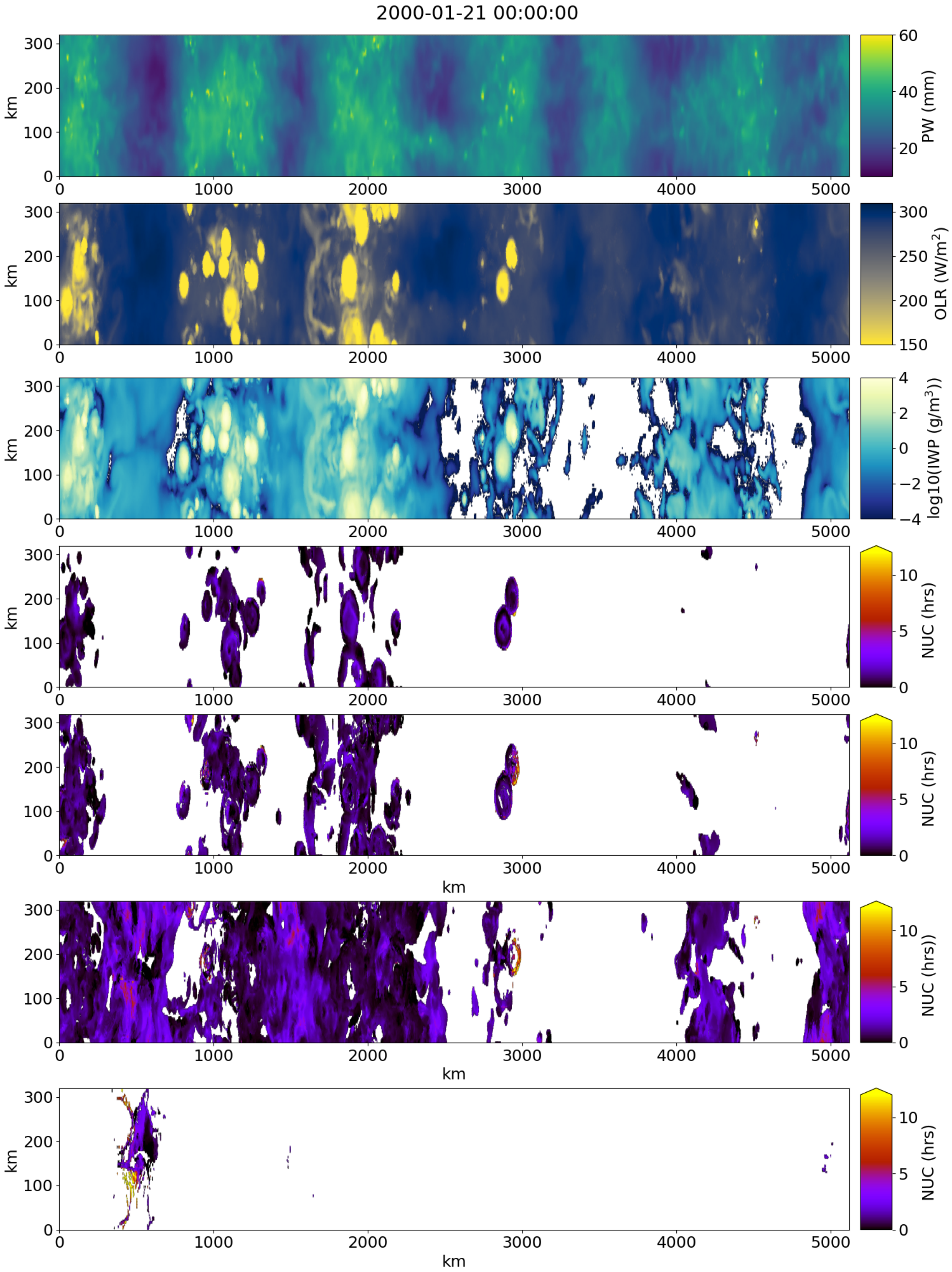

Figure 4.5: Same as Figure 4.4 but for day 20. Convection is beginning to organize at this time.

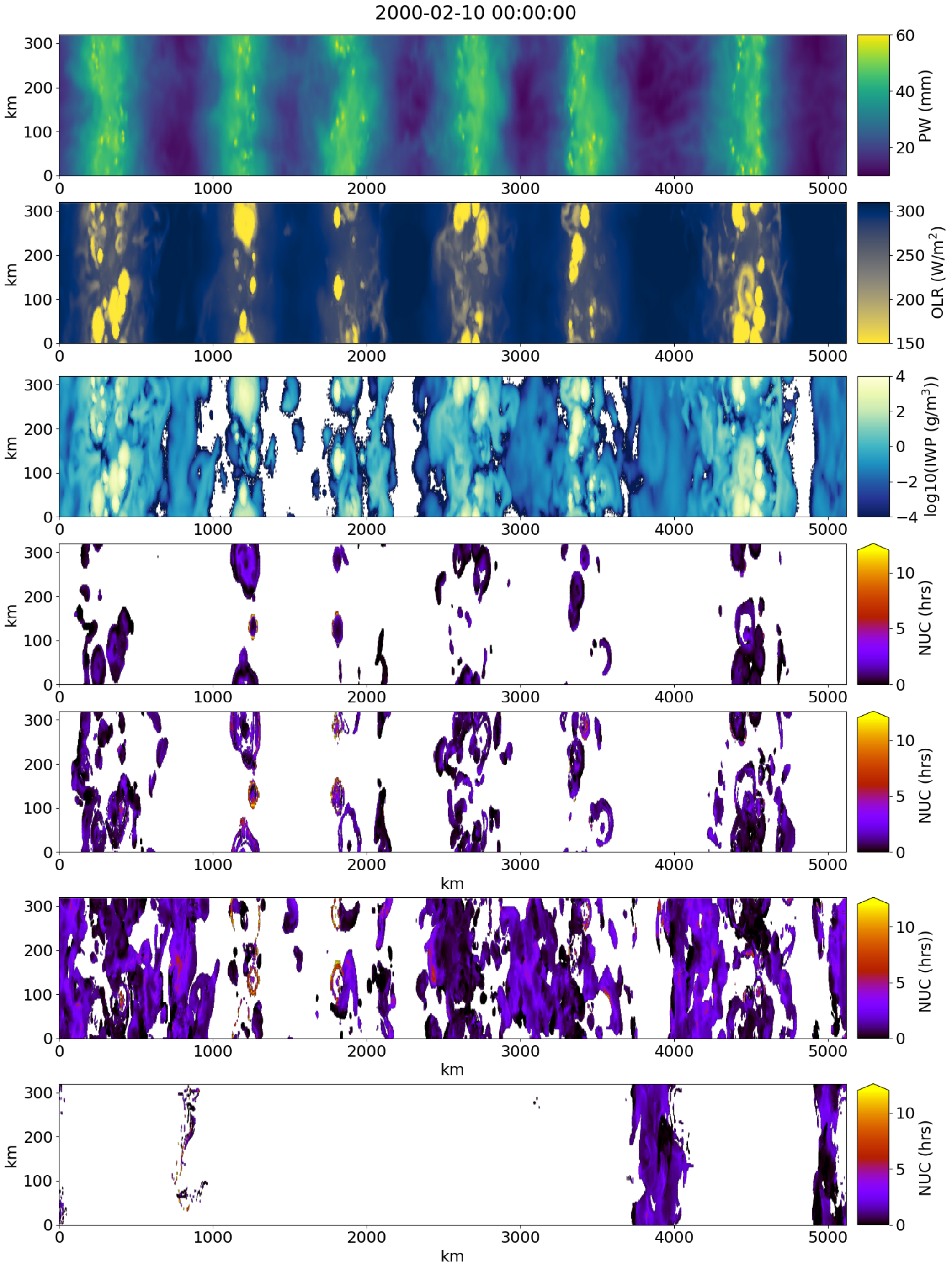

Figure 4.6: Same as Figure 4.4 but for day 40. Convection is highly organized by this time.

500 km from convection. Tropical cirrus have been observed to advect $600 - 1000$ km in their lifecycle (Luo & Rossow, 2004), in which time the cirrus in our simulations might enter another active zone of convection and may experience the impact of fresh convection.

4.3.2 Cirrus cloud origin

As a case study, we look at an instantaneous vertical cross-section in Figure 4.7 to get an idea of what these tracers look like in space. The cross section is at $y = 0$ km, the periodic boundary conditions mean that the chosen y value is insignificant, we should still see about 6 areas of active convection across the x direction. Figure 4.7, around $x = 3000$ km, shows TTL cirrus over 40 hours from convection at an altitude of 15 km, which has recently nucleated ice ($\tau_{nuc} < 2$ hrs). There are a few other examples of TTL cirrus that are distant from convection but freshly nucleated in this snapshot alone. This snapshot is typical of the highly organized state in this simulation, so these results may be generalized. Taking this case study as an example, we use statistics over the last 30 days of the simulation to quantify the amount of in-situ cirrus and the role of deep convection. Without fresh nucleation, these TTL cirrus would likely sediment out of the TTL within 5.5 hrs, if we assumed a slow fall speed of an aggregate ice crystal to be 20 cm/, which is on the slow end of ice crystals in cirrus (Lamraoui et al., 2023).

Following Sassen et al. (2009), we show the cirrus cloud fraction next to the mean ice water path (IWP; Figure 4.8). Our results are similar to those of (Sassen et al., 2009) and the DYAMOND 2 results in Chapter 2.3.3 where we saw that the DYAMOND models simulate thin TTL cirrus, SCREAM has in-situ cirrus near to and surrounding convection and anvil.

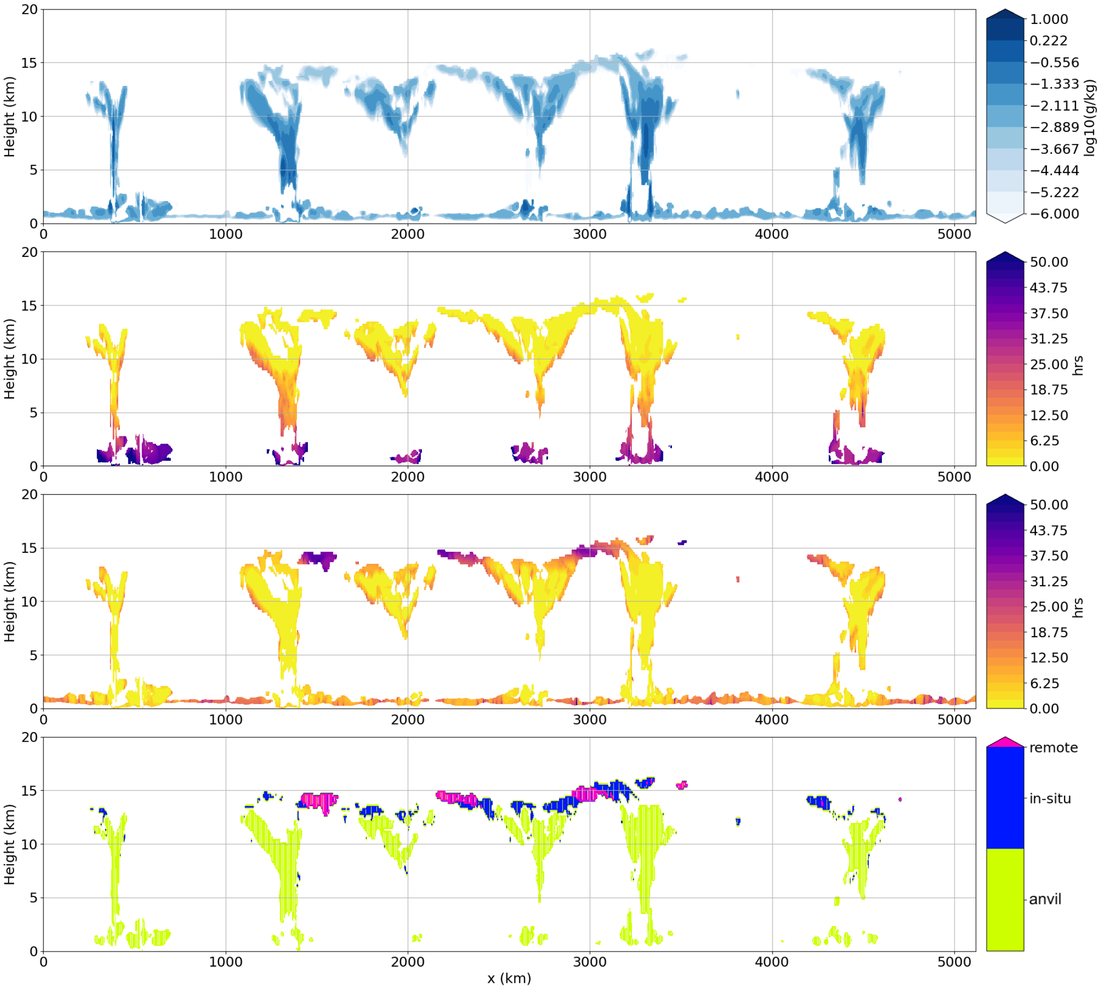

Figure 4.7: (a) cloud ice and liquid mixing ratios (log10(g/kg)); (b) time since nucleation (hrs); (c) time since convection (hrs); (d) cloud type flag (anvil, in-situ, or remote cirrus). This snapshot is near the end of the simulation period, where convection is highly organized.

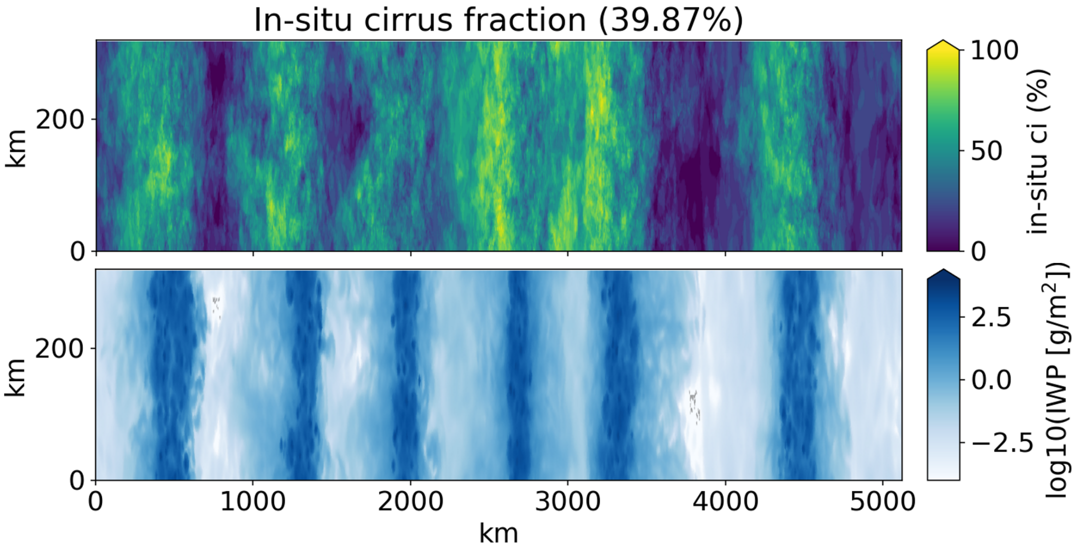

Figure 4.8: Cloud cover of in-situ cirrus (top) and mean IWP (log10(g/m^2) (bottom) for the default simulation. The spatial pattern of cirrus is spread out from the regions of deep convection with high IWP.

4.3.3 Microphysical properties of in-situ and convective origin cirrus

The lifecycle of a convective system begins with a strong updraft bringing hydrometeors and water vapor into the upper troposphere where the ice tends to be large (high R_{ice}) and numerous (high ICNC) as seen in Figure 4.9a. As soon as we are outside of the convective updraft, we can get fresh nucleation that typically has a smaller R_{ice} but high ICNC (peak in the histograms in Figure 4.9b–e is around 0.1 cm^3). When we are far from convection (Figure 4.9f), the remote cirrus are infrequent and do not have R_{ice} larger than 35 μm. Coincidentally, this was the threshold used for "large" ice in the sensitivity studies changing the vapor deposition and sedimentation rates in Chapter 3.2 but confirms that cirrus clouds, especially in-situ origin cirrus typically have a mean $R_{ice} < 25\mu$m. The peak in the distributions in Figure 4.9b–e is likely caused by the artificial upper limit on ICNC in the microphysics scheme for ice as noted in Atlas et al. (2024) and Gasparini et al. (in prep.).

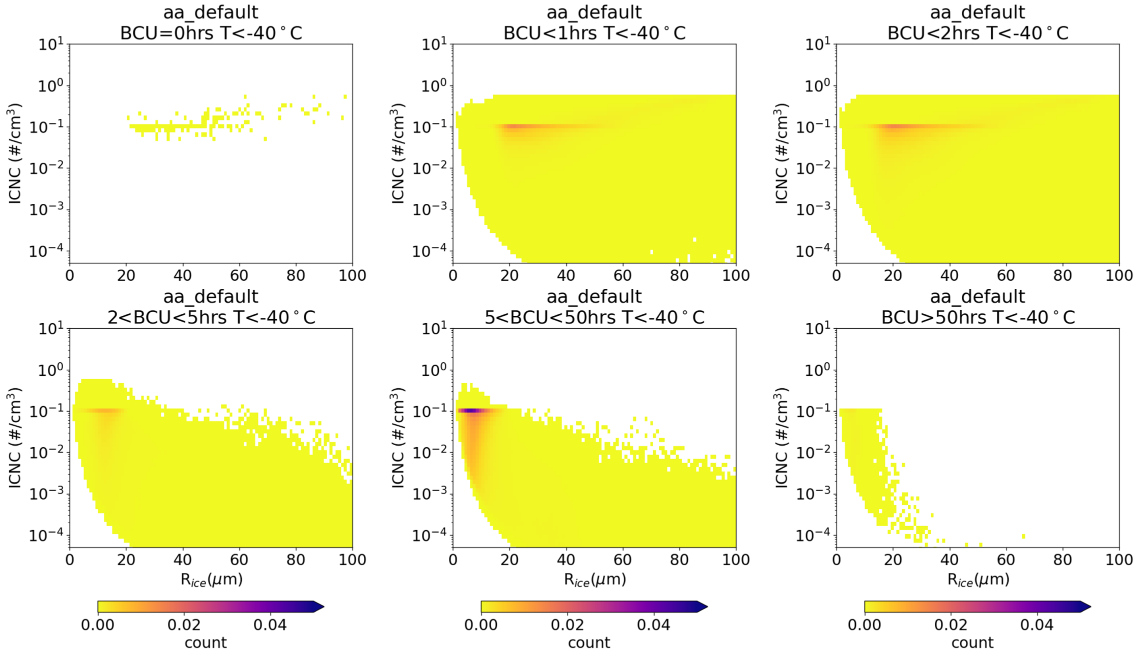

Figure 4.9: The joint histogram of ice mass radius (R_{ice}) and ice crystal number concentration (ICNC) for upper tropospheric clouds ($T < -40°C$) for different ranges of time since convection. (a) in convection, (b) less than one hour since convection (c) less than two hours since convection, (d) 2–5 hours since convection (e) 5–50 hours since convection, and (f) more than 50 hours since convection. (b) and (c) are likely anvil cirrus, while (e) and (f) are more likely to be in-situ cirrus, detached from convection.

The time since nucleation also varies in this microphysical space of R_{ice} and ICNC. Typically, nucleation occurs and populates the grid box with many new ice crystals, approaching the artificial limit near 0.1 cm^{-3}. The average time since nucleation at that limit is less than an hour. Aged cirrus have a smaller ICNC but hit a sweet spot of R_{ice} around 40 μm. This may be the R_{ice} value where the crystals sediment slowly but are still large enough to constitute a cloud (much smaller and the cloud likely dissipates or is too disperse to be considered a cloudy grid box).

The combination of the passive tracers for time since nucleation and time since convection reveal new insights into the origin of cirrus and properties of clouds from

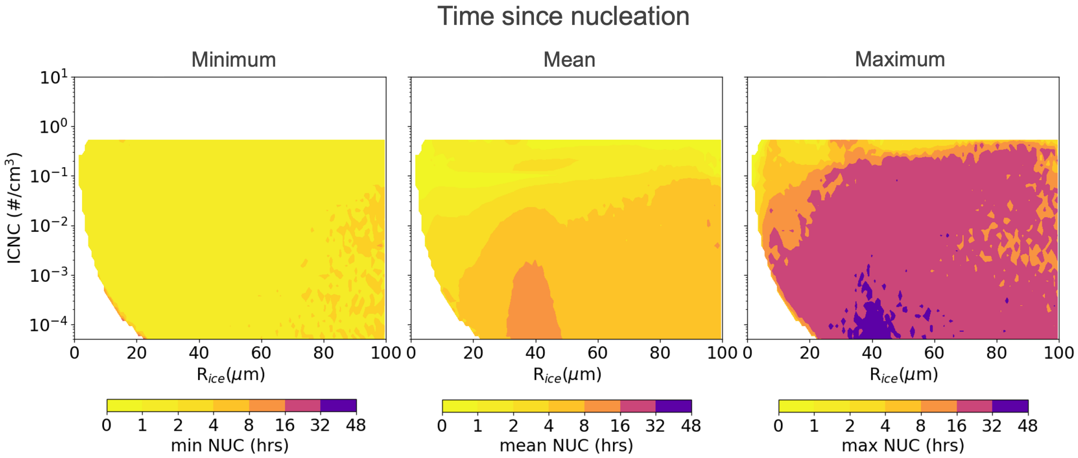

Figure 4.10: For a given ice mass radius (Rice) and ice crystal number concentration (ICNC), the time since nucleation is plotted as the minimum (freshest nucleation), mean nucleation, and maximum (oldest nucleation) for the default simulation for upper tropospheric values only (i.e., $T < -40°C$).

the macro- to the microscale. The typical cirrus cloud appears to be connected to convection as aged anvil, rarely getting remote cirrus clouds that are separate from the convective anvil. Yet long lifetime of cirrus away from convection emphasizes the need for mechanisms to maintain these cirrus clouds, likely internal cloud circulations and cirrus lofting (e.g., T. Dinh et al., 2012, 2014). These cirrus have different microphysical properties than cirrus near convection.

4.4 *Cirrus changes with large-scale ascent and warmed SSTs*

4.4.1 Convective organization

In the RCEMIP simulations, about half increase convective organization with warming (Wing et al., 2020). The SCREAM model retains similar levels of convective organization when we used a normalized metric. Normalizing the variance of PW accounts for the higher amount of column water vapor, the convective organization is similar across all of the simulations, regardless of SST (Figure 4.11). The mean

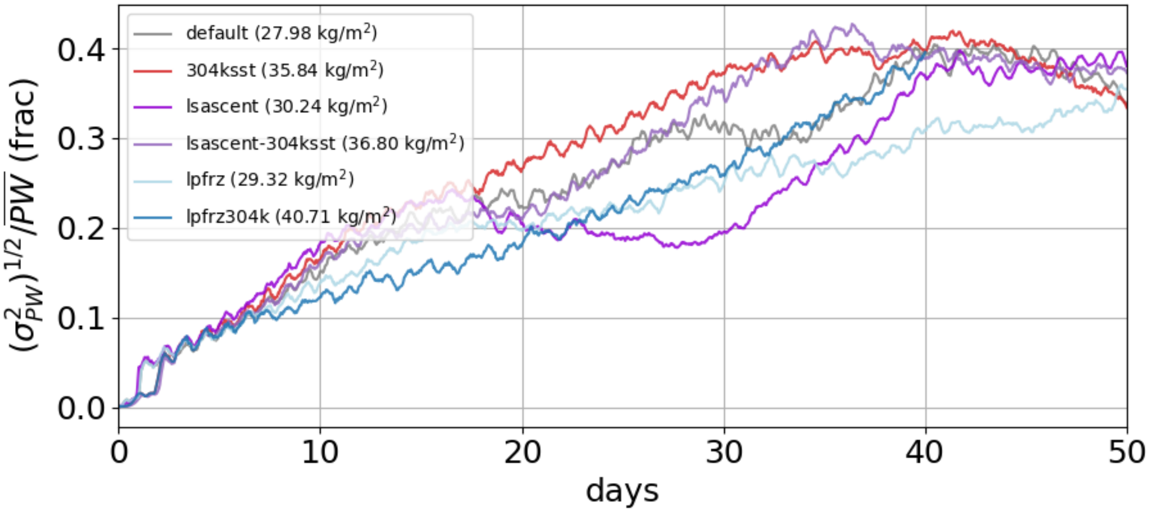

Figure 4.11: Same as Figure 4.3, but for the default (gray), default with +4K SST (red), large-scale ascent (dark purple), large-scale ascent with +4K SST (light purple), and the new LPFRZ ice nucleation 300K SST (light blue). The average PW from days 30–50 is listed in the legend for each simulation.

values of PW from days 30–50 are listed in the legend in Figure 4.11. There is an increase in PW (column-integrated water vapor) in the +4K SST simulations by about $7 - 11$ kg/m^2 ($5 - 10\%$/K). The updated ice nucleation scheme (LPFRZ) increases the moisture of the simulation significantly, especially in the +4K SST simulation (LPFRZ_304K) as listed in the legend of Figure 4.3.

Interestingly, the large-scale ascent 300K simulation and the updated ice nucleation scheme (LPFRZ) both are slightly more moist (higher mean PW listed in the legend in Figure 4.11), than the default simulation, and delayed growth of normalized PW variance relative to default. Both have convective organization with two to three convectively active regions (one large region dominating the domain) compared to the five or six smaller convective regions in the default simulations at 300K SST. The change to microphysics is driving the change to in the dynamics in the model. More work needs to be done to figure out why convection organizes differently with different model setups and if this is behavior is repeatable or predictable. All of the +4K SST

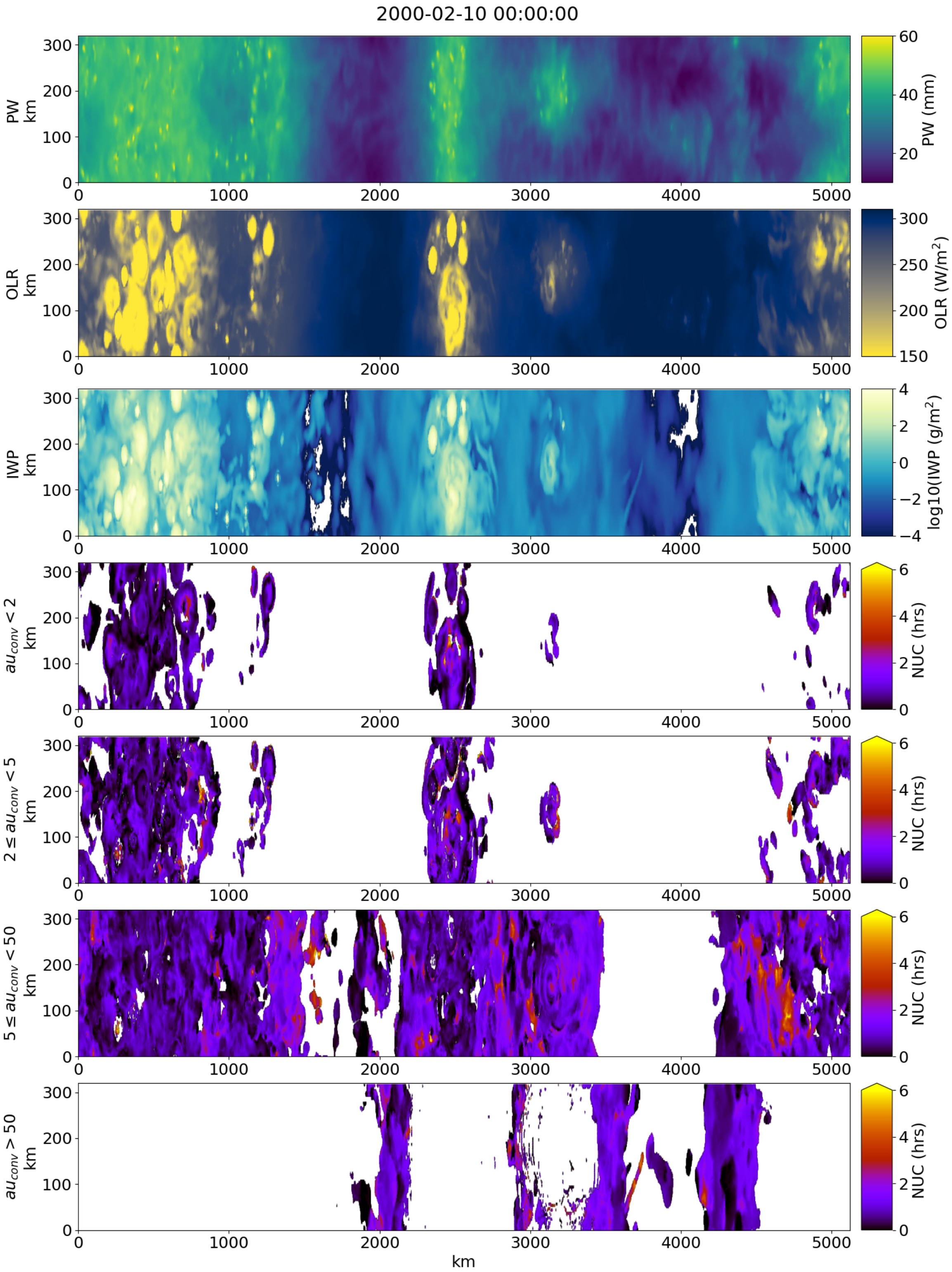

Figure 4.12: Same as Figure 4.6 but for the large-scale ascent simulation at 300K SST (LSascent_300K). Day 40 here is a highly organized state of convection with two main regions of active convection.

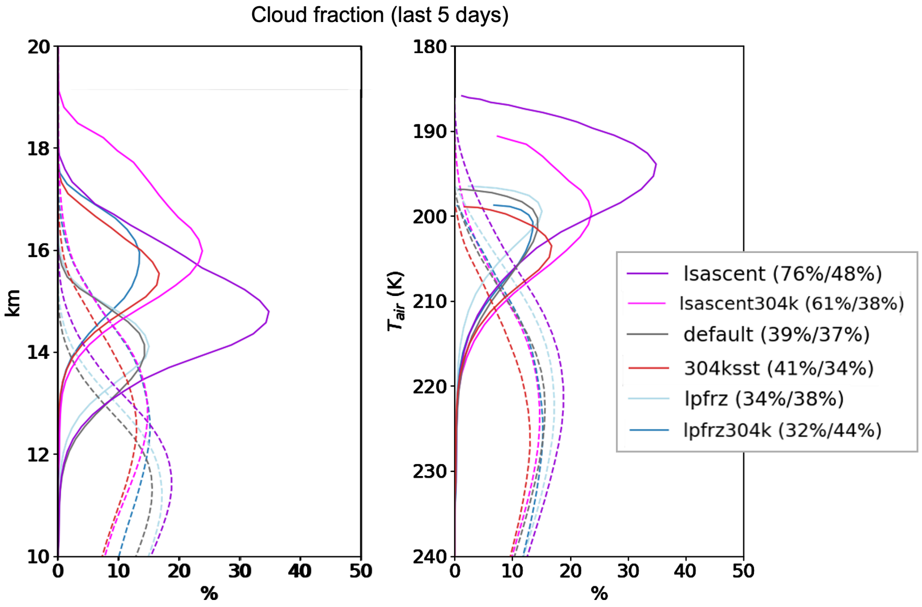

Figure 4.13: In-situ cirrus cloud fraction ($\tau_{conv} > 5$ hrs) is plotted as the solid lines and the anvil cloud fraction ($\tau_{conv} < 2$ hrs) is plotted as the dashed line for both (a) height in km and (b) potential temperature in K.

simulations have five to six convectively active zones and faster growth of normalized PW variance than their 300 K counterparts. Figure 4.12 shows a snapshot from day 40 (a highly organized state) of LSascent_300K. The convection is mainly clustered between $x = 0$ and 1000 km with a smaller secondary region of active convection around $x = 2500$ km. More remote cirrus form in this simulation, which may be an artifact of this highly clustered convection with a larger subsidence region of drier, convection-free columns.

4.4.2 Increasing SSTs

As we saw in Chapter 3.3.5 with the small domain simulations, the anvil cloud fraction decreased in magnitude and increased in height with increased SSTs. Figure 4.13 shows the fraction of anvil clouds ($\tau_{conv} < 2$) and in-situ cirrus ($\tau_{nuc} < \tau_{conv} - 5$) in each simulation. For all three simulation setups, there is a clear decrease in the anvil cloud peak (dashed lines in Fig. 4.13) from the 300K to 304K SST simulations. We also see a rise in the altitude for the +4K SST simulations (Fig. 4.13a) though the temperature stays roughly the equal (Fig. 4.13b).

The increase in anvil clouds by imposing a slow mean large-scale ascent (10%) is smaller for the +4K SST simulations and there is a corresponding decrease in the in-situ cirrus fraction (15%) as shown in Figure 4.13 (cloud cover listed in the legend). This could also be an artifact of the large-scale ascent being maximized at 14 km so with the +4K SSTs the cirrus fraction in the default is already above that, leading to a less obvious increase in thin TTL cirrus in the large-scale +4K SST simulation; however, we still see in-situ cirrus occurring much higher in altitude in the large-scale ascent +4K SST simulation than any other simulation.

In the default setup, in-situ cirrus increase but in the LSascent and LPFRZ simulations, cirrus decrease with warming. The different characteristic of organized convection in the setups at 300K SST may play a role in these results. We could verify the equilibrium of the models by extending the simulations for another 40 days or so. In-situ cirrus cloud fraction peak rises in altitude and warms in absolute temperature with warming (Fig. 4.13a & b). The warming is likely a result of the overall warming of the temperature profile in the +4K simulations $2-4$K (not shown). The change in magnitude of the in-situ cirrus cloud fraction peak is uncertain; it decreases in two simulation setups and slightly increases in the default simulation.

4.4.3 TOA radiative fluxes

Figure 4.14 nicely summarizes the different simulations as they impact the LW and SW radiative fluxes as a result of cloud radiative effect from changing cirrus-related processes and the impact from SSTs. Both the changes to cloud cover and vertical structure of cirrus impact the CRE while cloud cover, SSTs and cloud-top height impact the all sky radiative fluxes (OLR vs reflected SW).

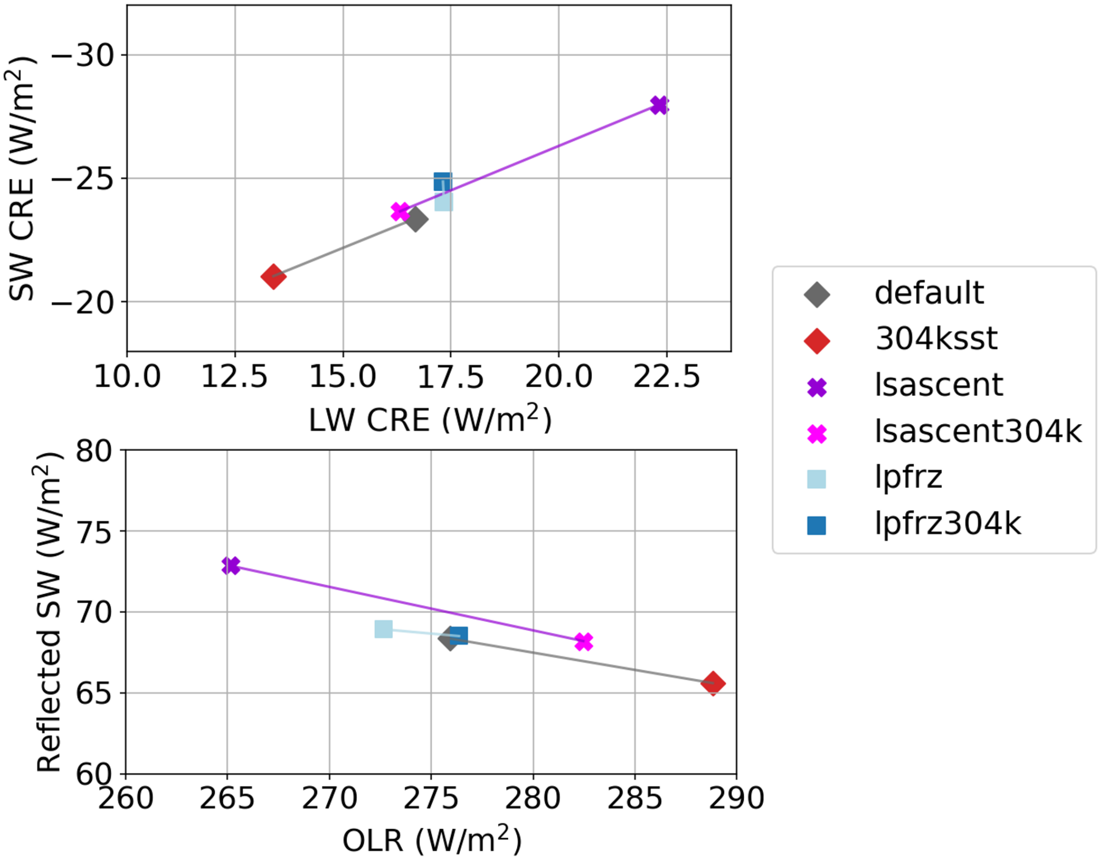

Figure 4.14: Mean values of (a) LW and SW CRE and (b) LW (OLR) and SW (reflected SW) upward radiation at TOA from days 30 − 50 of each simulation. The default setups are plotted as diamonds for the 300K (gray) and 304K (red) SST simulations. Large-scale ascent was imposed for both SSTs (purple and magenta ×). The updated ice nucleation schemes was implemented for both SSTs (light and dark blue squares). A line connects simulations with same setup but different SSTs.

By changing the ice nucleation scheme and imposing LS ascent, we are changing the ice cloud properties so it makes sense that we see the largest impact in the LW radiation; the mean OLR from days $30-50$ ranges from 265 W/m^2 in LSascent_300K to 288 W/m^2 in Default_304K. The OLR is highest in the +4K SST simulations due to the warmer SSTs and more water vapor in the column. The addition of large-scale ascent decreases the OLR and increases the reflected SW in both 300 and 304K SST simulations because of the increased cloud-top height and cloud cover. Adding LS ascent strengthened the CRE by as much as reducing the SST by 4K (Fig. 4.14a). The OLR only slightly increases for the updated ice nucleation scheme (from LPFRZ to LPFRZ_304K) despite the same change to SST and water vapor as in the other two simulation setups.

The amount of reflected SW radiation at TOA changes slightly between runs from 66 W/m^2 in Default_304K to 73 W/m^2 in LSascent_300K. The slight decrease of reflected SW radiation with warming comes from the change in reflectivity of the clouds, signifying that the anvil cirrus clouds may thin as in Sokol et al. (2024). It seems like the different characteristics of convective organization do not seem to impact the reflected SW radiation much.

Even using the tracers for time since convection and nucleation, it is sometimes difficult to distinguish the line between in-situ and convective cirrus yet this provides a good start to understanding the role of convection and persistence of in-situ cirrus. Convection undoubtedly plays a major role whether directly (via hydrometeor injection into the TTL or cirrus outflow) or indirectly (through its supply of water vapor to the upper troposphere and its influence on gravity waves).

Chapter 5

CONCLUSIONS

5.1 Summary

This dissertation aims to improve understanding of tropical cirrus clouds in storm-resolving (convection-permitting) models. This is among the first studies to analyze the spatial coverage and vertical distribution of thin upper-tropospheric cirrus clouds in this new class of global models. These cirrus clouds have important impacts on radiative fluxes at the top of atmosphere and water vapor entering the stratosphere through the tropics (Fueglistaler et al., 2009). We focus on the tropical western pacific region, which is known to have a neutral cloud radiative impact because of the small but persistent LW warming from cirrus clouds that counteract the strong SW cooling from convection (Wall & Hartmann, 2018). This dissertation answers three main questions: 1) how well are cirrus represented in GSRMs?, 2) how much does ice microphysics matter for cirrus clouds?, and 3) what are the cirrus cloud origins and lifecycle in simulations with convective organization?

1. We are able to say with confidence that GSRMs are able to simulate thin tropical cirrus clouds reasonably well; however, most models under-represented cirrus cloud coverage. TTL cirrus vary in altitude and apparent connection to convection, but all had small IWC values, which are consistent with in-situ formation according to the microphysics guide in Krämer et al. (2020). Differences in TTL cirrus are likely driven by different ice microphysics; however, dynamical and microphysical effects across the DYAMOND models could not be separated.

2. In order to parse out the role of microphysics from dynamics, we perform a

single model microphysics sensitivity study. Using a single model with a small domain keeps the dynamics consistent. This idealized small domain RCE model setup allows us to investigate the impact of ice microphysics on cirrus clouds in Chapter 3. Ice sedimentation had the strongest impact on anvil and cirrus clouds, but large-scale ascent had the largest impact on cirrus (without impacting convective clouds as much). Updating the ice nucleation changed the cloud properties, tending to form cirrus that are slightly optically thinner and at slightly colder temperatures.

3. In Chapter 4 we explored the role of convective organization, along with increasing the SST by 4K for three setups: the default, updated ice nucleation, and large-scale ascent. We found no clear relationship between in-situ cirrus and SST. It may have been complicated by the different patterns of convective organization in the model setups in two of the 300K SST simulations (new ice nucleation and large-scale ascent). The amount of in-situ cirrus ranged from 32% to 76% across different simulations and was largest in the 300K large-scale ascent simulation. The in-situ cirrus vertical cloud fraction peak increased in altitude and temperature with warming, but the change to in-situ cirrus cloud cover was uncertain.

5.2 Discussion

Throughout this dissertation, I find that seemingly small changes to cirrus cloud processes can have large-scale impacts. The mean model radiative fluxes, the vertical structure, precipitation, moisture, and convective organization all have a large model spread whether among different GSRMs in DYAMOND or a sensitivity study using SCREAM. The results presented in this dissertation are part of a growing body of work that emphasizes the importance of cirrus and ice processes in models (e.g., Ackerman et al., 1988; Jensen et al., 1996; T. Dinh et al., 2014; Feofilov & Stubenrauch, 2019; Baran et al., 2016; Gasparini et al., 2023; Kärcher, 2022; Atlas et al., 2024). As models improve by reducing their spatial resolutions down to kilometer scales, we need to update our ice microphysics as well and include more physically-based and improved treatment of processes important to tropical cirrus. Even though the cloud microphysics problem still refuses to die (Randall et al., 2003), we can make certain strides towards improving simulations of tropical cirrus by diagnosing model biases in intercomparisons, quantifying the uncertainty of microphysical parameters and cirrus-related processes, and implementing passive tracers to quantify the prevalence of in-situ cirrus in simulations, as we have done in this dissertation.

In-situ cirrus clouds, while theoretically independent from convection, may depend on convection for the initial formation of cirrus clouds (as outflow), injection of water vapor, and convectively-generated gravity waves, which depend on the model dynamics and setup. While many individual cirrus clouds originate from convection or appear to be connected to convection as extended anvils, new ice nucleation occurs outside of convection, allowing cirrus to persist for more than two days after detrainment from a convective updraft. This new nucleation could occur from updrafts outside of convection (so the tracer τ_{conv} is not reset). These updrafts could also be initiated by in-cloud radiation; LW radiation heats the cloud bottom and cooling at the cloud top causes internal circulations that could lead to cirrus maintenance (Gu & Liou, 2000; T. P. Dinh et al., 2010; Hartmann et al., 2018; Sokol & Hartmann, 2020). The cloud heating locally is significant for thin TTL cirrus which impact the TTL temperature structure (Fu et al., 2018; Yang et al., 2010).

Cirrus clouds are important to get right in simulations of the atmosphere in order to reduce the uncertainty associated with high clouds (Sherwood et al., 2020). As we saw throughout this dissertation, large variability in TOA radiative fluxes from small changes to cirrus-related processes has shown that improving ice and cirrus clouds representation are essential to improving simulations of the current climate. Comparison and sensitivity studies using these high-resolution models reveal insights into the physics that drives cirrus cloud formation and life cycle.

High-resolution models promise to be a very useful tool to improve our knowledge of cirrus clouds processes, especially TTL cirrus, due to the difficulty of directly observing their properties with high spatiotemporal resolution to track the lifecycle and vertical structure of clouds like we can in high-resolution global and regional models. As GSRMs move toward emulating future climates, reducing model spread is important and targeting ice microphysics (especially in the tropics) should be a priority for modelling centers moving forward. This dissertation highlights some of the challenges in using high-resolution models and areas for improvement so they can be even better for future work. It is imperative that more analyses, comparisons, and diagnoses of model biases like this dissertation are done to reduce uncertainties in current climate simulations.

5.3 Future directions

5.3.1 Convective organization

One of the most interesting next steps for this work would be to dive into the convective organization in the large-domain SCREAM simulations. Chapter 4 showed that changing the ice nucleation and adding large-scale ascent changed the structure of convective organization. There were larger clusters of convection with more space in-between the convectively active bands as well. SCREAM is known to have “popcorn” convection, which tends to favor more isolated towers of convection, but when convection organized differently it seemed like the “popcorn” convection shifted towards more clustered convection with less isolated deep convective cores. First, we could run the large domain simulations longer than 50 days to see if the LSascent_300K and LPFRZ_300K eventually organize into $5-6$ convectively active zones or if they are in equilibrium when organized into one large convective area with smaller secondary zones. It would also be insightful to run more sensitivity runs to see if the different structure of convective organization is repeatable and how much of a perturbation is needed to change the structure of convective organization.

5.3.2 Ice nucleation

There are several different configurations of the updated nucleation scheme we could use. The version used in this dissertation implemented the LP2005 homogeneous freezing and homogeneous-heterogeneous competition. We could turn on the implementation of cirrus depositional freezing from Möhler et al. (2006). We also added options to remove all artificial limits, which set the maximum value of allowable ice number from different types of nucleation. We added another option to turn off heterogeneous freezing which would illuminate the role of heterogeneous vs homogeneous freezing in the TTL. Furthermore it would be useful in future simulations to add the ice nucleation scheme from Kärcher (2022) as an option, which is a more updated and physically-based ice nucleation scheme. If we add these to our sensitivity study, we could get more variability from ice microphysics all from equally likely, or realistic, scenarios in these simulations of current and future climates.

5.3.3 Tracers

There is also so much more we could do with the passive tracers since this dissertation did not really dive into the secondary tracers for nucleation, which tracked ice crystal number concentrations and vertical velocity. We could also add output that tracks the fraction of ice within a grid box arising from different formation mechanisms, such as homogeneous versus heterogeneous freezing, condensation, etc. This would reveal which freezing mechanisms are dominant throughout the cirrus lifecycle and further distinguish in-situ cirrus from convective-origin.

References

Ackerman, T., Liou, K., Valero, F., & Pfister, L. (1988). Heating rates in tropical anvil. *Journal of Atmospheric Sciences*, *45*(10), 1606–1623.

Adams-Selin, R., Van Den Heever, S., & Johnson, R. (2013). Impact of graupel parameterization schemes on idealized bow echo simulations. *Monthly Weather Review*, *141*(4), 1241–1262. doi: 10.1175/MWR-D-12-00064.1

Albern, N., Voigt, A., Buehler, S. A., & Grützun, V. (2018). Robust and Nonrobust Impacts of Atmospheric Cloud-Radiative Interactions on the Tropical Circulation and Its Response to Surface Warming. *Geophysical Research Letters*, *45*(16), 8577–8585. doi: 10.1029/2018GL079599

Atlas, R. L., Bretherton, C. S., Sokol, A. B., Blossey, P. N., & Khairoutdinov, M. F. (2024). Tropical Cirrus Are Highly Sensitive to Ice Microphysics Within a Nudged Global Storm-Resolving Model. *Geophysical Research Letters*, *51*(1). doi: 10.1029/2023GL105868

Baldauf, M., Seifert, A., Förstner, J., Majewski, D., Raschendorfer, M., & Reinhardt, T. (2011). Operational Convective-Scale Numerical Weather Prediction with the COSMO Model: Description and Sensitivities. *Monthly Weather Review*, *139*(12), 3887–3905. doi: 10.1175/MWR-D-10-05013.1

Bao, J.-W., Michelson, S. A., & Grell, E. D. (2019). Microphysical process comparison of three microphysics parameterization schemes in the wrf model for an idealized squall-line case study. *Monthly Weather Review*, *147*(9), 3093 - 3120. doi: 10.1175/MWR-D-18-0249.1

Baran, A. J., Hill, P., Walters, D., Hardiman, S. C., Furtado, K., Field, P. R., & Manners, J. (2016). The Impact of Two Coupled Cirrus Microphysics–Radiation Parameterizations on the Temperature and Specific Humidity Biases in the Tropical Tropopause Layer in a Climate Model. *Journal of Climate*, *29*(14), 5299–5316. doi: 10.1175/JCLI-D-15-0821.1

Beer, C. G., Hendricks, J., & Righi, M. (2024). Impacts of ice-nucleating particles on cirrus clouds and radiation derived from global model simulations with made3 in emac. *Atmospheric Chemistry and Physics*, *24*(5), 3217–3240. doi: 10.5194/acp-24-3217-2024

Blossey, P. N., Kuang, Z., & Romps, D. M. (2010). Isotopic composition of water in the tropical tropopause layer in cloud-resolving simulations of an idealized tropical circulation. *Journal of Geophysical Research: Atmospheres*, *115*(D24). doi: 10.1029/2010JD014554

Bolot, M., Harris, L. M., Cheng, K.-Y., Merlis, T. M., Blossey, P. N., Bretherton, C. S., ... Fueglistaler, S. (2023). Kilometer-scale global warming simulations and active sensors reveal changes in tropical deep convection. *Climate and Atmospheric Science*, *6*(1), 1–8. doi: 10.1038/s41612-023-00525-w

Bolvin, D. T., Huffman, G. J., Nelkin, E. J., & Tan, J. (2021). Comparison of Monthly IMERG Precipitation Estimates with PACRAIN Atoll Observations. *Journal of Hydrometeorology*, *22*(7), 1745–1753. doi: 10.1175/JHM-D-20-0202.1

Bretherton, C. S., Blossey, P. N., & Khairoutdinov, M. (2005). An energy-balance analysis of deep convective self-aggregation above uniform sst. *Journal of the Atmospheric Sciences*, *62*(12), 4273–4292. doi: 10.1175/JAS3614.1

Bryan, G. H., & Morrison, H. (2012). Sensitivity of a simulated squall line to horizontal resolution and parameterization of microphysics. *Monthly Weather Review*, *140*. doi: 10.1175/MWR-D-11-00046.1

Caldwell, P. M., Terai, C. R., Hillman, B., Keen, N. D., Bogenschutz, P., Lin, W., ... Zender, C. S. (2021). Convection-Permitting Simulations With the E3SM Global Atmosphere Model. *Journal of Advances in Modeling Earth Systems*, *13*(11). doi: 10.1029/2021MS002544

Cazenave, Q., Ceccaldi, M., Delanoë, J., Pelon, J., Groß, S., & Heymsfield, A. (2019). Evolution of DARDAR-CLOUD ice cloud retrievals: new parameters and impacts on the retrieved microphysical properties. *Atmospheric Measurement*

Techniques, *12*(5), 2819–2835. doi: 10.5194/amt-12-2819-2019

Chae, J. H., & Sherwood, S. C. (2010). Insights into Cloud-Top Height and Dynamics from the Seasonal Cycle of Cloud-Top Heights Observed by MISR in the West Pacific Region. *Journal of the Atmospheric Sciences*, *67*(1), 248–261. doi: 10.1175/2009JAS3099.1

Cooper, W. A. (1986). Ice initiation in natural clouds. In R. R. Braham et al. (Eds.), *Precipitation enhancement—a scientific challenge* (p. 29–32). Boston, MA: American Meteorological Society.

Cronin, T., & Wing, A. (2017). Clouds, circulation, and climate sensitivity in a radiative-convective equilibrium channel model. *Journal of Advances in Modeling Earth Systems*, *9*(8), 2883–2905. doi: 10.1002/2017MS001111

Deng, M., Mace, G. G., Wang, Z., & Lawson, R. P. (2013). Evaluation of Several A-Train Ice Cloud Retrieval Products with In Situ Measurements Collected during the SPARTICUS Campaign. *Journal of Applied Meteorology and Climatology*, *52*(4), 1014–1030. doi: 10.1175/JAMC-D-12-054.1

Dinh, T., Durran, D. R., & Ackerman, T. (2012). Cirrus and water vapor transport in the tropical tropopause layer – part 1: A specific case modeling study. *Atmospheric Chemistry and Physics*, *12*(20), 9799–9815. doi: 10.5194/acp-12-9799-2012

Dinh, T., Fueglistaler, S., Durran, D., & Ackerman, T. (2014). Cirrus and water vapour transport in the tropical tropopause layer – part 2: Roles of ice nucleation and sedimentation, cloud dynamics, and moisture conditions. *Atmospheric Chemistry and Physics*, *14*(22), 12225–12236. doi: 10.5194/acp-14-12225-2014

Dinh, T. P., Durran, D. R., & Ackerman, T. P. (2010). Maintenance of tropical tropopause layer cirrus. *Journal of Geophysical Research: Atmospheres*, *115*(D2). doi: 10.1029/2009JD012735

Doelling, D. R., Loeb, N. G., Keyes, D. F., Nordeen, M. L., Morstad, D., Nguyen, C., … Sun, M. (2013). Geostationary Enhanced Temporal Interpolation for

CERES Flux Products. *Journal of Atmospheric and Oceanic Technology*, *30*(6), 1072–1090. doi: 10.1175/JTECH-D-12-00136.1

Doelling, D. R., Sun, M., Nguyen, L. T., Nordeen, M. L., Haney, C. O., Keyes, D. F., & Mlynczak, P. E. (2016). Advances in Geostationary-Derived Longwave Fluxes for the CERES Synoptic (SYN1deg) Product. *Journal of Atmospheric and Oceanic Technology*, *33*(3), 503–521. doi: 10.1175/JTECH-D-15-0147.1

ECMWF. (2020). *IFS Documentation CY47R1 - Part III: Dynamics and Numerical Procedures* (Technical). doi: 10.21957/u8ssd58

Feng, Z., Leung, L. R., Hardin, J., Terai, C. R., Song, F., & Caldwell, P. (2023). Mesoscale convective systems in dyamond global convection-permitting simulations. *Geophysical Research Letters*, *50*(4), e2022GL102603. doi: 10.1029/2022GL102603

Feofilov, A. G., & Stubenrauch, C. J. (2019). Diurnal variation of high-level clouds from the synergy of airs and iasi space-borne infrared sounders. *Atmospheric Chemistry and Physics*, *19*(22), 13957–13972. doi: 10.5194/acp-19-13957-2019

Fridlind, A. M., Van Diedenhoven, B., Ackerman, A. S., Avramov, A., Mrowiec, A., Morrison, H., … Shupe, M. D. (2012). A fire-ace/sheba case study of mixed-phase arctic boundary layer clouds: Entrainment rate limitations on rapid primary ice nucleation processes. *Journal of the Atmospheric Sciences*, *69*(1), 365–389. doi: 10.1175/JAS-D-11-052.1

Fu, Q., Smith, M., & Yang, Q. (2018). The Impact of Cloud Radiative Effects on the Tropical Tropopause Layer Temperatures. *Atmosphere*, *9*(10), 377. doi: 10.3390/atmos9100377

Fueglistaler, S., Dessler, A. E., Dunkerton, T. J., Folkins, I., Fu, Q., & Mote, P. W. (2009). Tropical tropopause layer. *Reviews of Geophysics*, *47*(1). doi: 10.1029/2008RG000267

Gao, S., Cui, X., Zhou, Y., & Li, X. (2005). Surface rainfall processes as simulated in a cloud-resolving model. *Journal of Geophysical Research: Atmospheres*, *110*(D10). doi: 10.1029/2004JD005467

Garrett, T. J., Dean-Day, J., Liu, C., Barnett, B., Mace, G., Baumgardner, D., ... Minnis, P. (2006). Convective formation of pileus cloud near the tropopause. *Atmospheric Chemistry and Physics*, *6*(5), 1185–1200. doi: 10.5194/acp-6-1185-2006

Gasparini, B., Blossey, P. N., Hartmann, D. L., Lin, G., & Fan, J. (2019). What Drives the Life Cycle of Tropical Anvil Clouds? *Journal of Advances in Modeling Earth Systems*, *11*(8), 2586–2605. doi: 10.1029/2019MS001736

Gasparini, B., Sullivan, S. C., Sokol, A. B., Kärcher, B., Jensen, E., & Hartmann, D. L. (2023). Opinion: Tropical cirrus — From micro-scale processes to climate-scale impacts. *Atmospheric Chemistry and Physics*, *23*(24), 15413–15444. doi: 10.5194/acp-23-15413-2023

Gasparini, B., Voigt, A., Krämer, M., & Blossey, P. N. (in prep.). An improved ice microphysics for studying tropical cirrus evolution. *JAMES*.

Gettelman, A., Liu, X., Barahona, D., Lohmann, U., & Chen, C. (2012). Climate impacts of ice nucleation. *Journal of Geophysical Research: Atmospheres*, *117*(D20). doi: 10.1029/2012JD017950

Gu, Y., & Liou, K. N. (2000). Interactions of radiation, microphysics, and turbulence in the evolution of cirrus clouds. *Journal of the Atmospheric Sciences*, *57*(15), 2463–2479. doi: 10.1175/1520-0469(2000)057¡2463:IORMAT¿2.0.CO;2

Haladay, T., & Stephens, G. (2009). Characteristics of tropical thin cirrus clouds deduced from joint CloudSat and CALIPSO observations. *Journal of Geophysical Research*, *114*. doi: 10.1029/2008JD010675

Harris, L., Chen, X., Putman, W., Zhou, L., & Chen, J.-H. (2021). *A Scientific Description of the GFDL Finite-Volume Cubed-Sphere Dynamical Core* (Tech. Rep.). GFDL Weather and Climate Dynamics Division. doi: 10.25923/6NHS-5897

Harris, L., Zhou, L., Kaltenbaugh, A., Clark, S., Cheng, K.-Y., & Bretherton, C.

(2023). A Global Survey of Rotating Convective Updrafts in the GFDL X-SHiELD 2021 Global Storm Resolving Model. *Journal of Geophysical Research: Atmospheres*, *128*(10). doi: 10.1029/2022JD037823

Hartmann, D. L., & Berry, S. E. (2017). The balanced radiative effect of tropical anvil clouds. *Journal of Geophysical Research: Atmospheres*, *122*(9), 5003–5020. doi: 10.1002/2017JD026460

Hartmann, D. L., Gasparini, B., Berry, S. E., & Blossey, P. N. (2018). The Life Cycle and Net Radiative Effect of Tropical Anvil Clouds. *Journal of Advances in Modeling Earth Systems*, *10*(12), 3012–3029. doi: 10.1029/2018MS001484

Hashino, T., Satoh, M., Hagihara, Y., Kubota, T., Matsui, T., Nasuno, T., & Okamoto, H. (2013). Evaluating cloud microphysics from nicam against cloudsat and calipso. *Journal of Geophysical Research: Atmospheres*, *118*(13), 7273-7292. doi: https://doi.org/10.1002/jgrd.50564

Hawker, R. E., Miltenberger, A. K., Wilkinson, J. M., Hill, A. A., Shipway, B. J., Cui, Z., ... Murray, B. J. (2021). The temperature dependence of ice-nucleating particle concentrations affects the radiative properties of tropical convective cloud systems. *Atmospheric Chemistry and Physics*, *21*(7), 5439–5461. doi: 10.5194/acp-21-5439-2021

Heymsfield, A. J., & Donner, L. J. (1990). A scheme for parameterizing ice-cloud water content in general circulation models. *Journal of Atmospheric Sciences*, *47*(15), 1865 - 1877. doi: 10.1175/1520-0469(1990)047¡1865:ASFPIC¿2.0.CO;2

Highwood, E. J., & Hoskins, B. J. (1998, July). The tropical tropopause. *Quarterly Journal of the Royal Meteorological Society*, *124*(549), 1579–1604. doi: 10.1002/qj.49712454911

Holton, J. R., & Gettelman, A. (2001, July). Horizontal transport and the dehydration of the stratosphere. *Geophysical Research Letters*, *28*(14), 2799–2802. doi: 10.1029/2001GL013148

Hong, S.-Y., Lim, K.-S. S., Kim, J.-H., Lim, J.-O. J., & Dudhia, J. (2009). Sensitivity study of cloud-resolving convective simulations with wrf using two bulk microphysical parameterizations: Ice-phase microphysics versus sedimentation effects. *Journal of Applied Meteorology and Climatology*, *48*, 61–76. doi: 10.1175/2008JAMC1960.1

Huffman, G. J., Bolvin, D. T., Braithwaite, D., Hsu, K.-L., Xie, P., Joyce, R., & Yoo, S.-H. (2015). *NASA global precipitation measurement (GPM) integrated multi-satellite retrievals for GPM (IMERG)* (Vol. 4; Tech. Rep. No. 26). Greenbelt, MD: NASA Goddard Space Flight Center.

Immler, F. (2008). Correlation between equatorial Kelvin waves and the occurrence of extremely thin ice clouds at the tropical tropopause. *Atmos. Chem. Phys.*, *8*(14). doi: 10.5194/acp-8-4019-2008

Jensen. (2004). Transport and freeze-drying in the tropical tropopause layer. *Journal of Geophysical Research*, *109*(D2), D02207. doi: 10.1029/2003JD004022

Jensen, Lawson, P., Baker, B., Pilson, B., Mo, Q., Heymsfield, A. J., … Tanelli, S. (2009). On the importance of small ice crystals in tropical anvil cirrus. *Atmospheric Chemistry and Physics*, *9*(15), 5519–5537. doi: 10.5194/acp-9-5519-2009

Jensen, Toon, O., Selkirk, H., Spinhirne, J., & Schoeberl, M. (1996). On the formation and persistence of subvisible cirrus clouds near the tropical tropopause. *Journal of Geophysical Research: Atmospheres*, *101*(D16), 21361–21375. doi: 10.1029/95JD03575

Jensen, M. P., & Genio, A. D. D. (2006). Factors Limiting Convective Cloud-Top Height at the ARM Nauru Island Climate Research Facility. *Journal of Climate*, *19*(10), 2105–2117. doi: 10.1175/JCLI3722.1

Johnson, R. H., Rickenbach, T. M., Rutledge, S. A., Ciesielski, P. E., & Schubert, W. H. (1999). Trimodal Characteristics of Tropical Convection. *Journal of Climate*, *12*(8), 2397–2418. (Publisher: American Meteorological Society Section: Journal of Climate) doi: 10.1175/1520-0442(1999)012¡2397:TCOTC¿2.0.CO;2

Judt, F., Klocke, D., Rios-Berrios, R., Vanniere, B., Ziemen, F., Auger, L., … Zhou, L. (2021). Tropical cyclones in global storm-resolving models. *Journal of the Meteorological Society of Japan. Ser. II*, *99*(3), 579–602. doi: 10.2151/jmsj.2021-029

Kato, S., Rose, F. G., Rutan, D. A., Thorsen, T. J., Loeb, N. G., Doelling, D. R., … Ham, S.-H. (2018). Surface Irradiances of Edition 4.0 Clouds and the Earth's Radiant Energy System (CERES) Energy Balanced and Filled (EBAF) Data Product. *Journal of Climate*, *31*(11), 4501–4527. doi: 10.1175/JCLI-D-17-0523.1

Kato, S., Rose, F. G., Sun-Mack, S., Miller, W. F., Chen, Y., Rutan, D. A., … Collins, W. D. (2011). Improvements of top-of-atmosphere and surface irradiance computations with CALIPSO-, CloudSat-, and MODIS-derived cloud and aerosol properties. *Journal of Geophysical Research: Atmospheres*, *116*(D19). doi: 10.1029/2011JD016050

Kato, S., Sun-Mack, S., Miller, W. F., Rose, F. G., Chen, Y., Minnis, P., & Wielicki, B. A. (2010). Relationships among cloud occurrence frequency, overlap, and effective thickness derived from CALIPSO and CloudSat merged cloud vertical profiles. *Journal of Geophysical Research: Atmospheres*, *115*(D4). doi: 10.1029/2009JD012277

Khairoutdinov, M. F., Blossey, P. N., & Bretherton, C. S. (2022). Global System for Atmospheric Modeling: Model Description and Preliminary Results. *Journal of Advances in Modeling Earth Systems*, *14*(6). doi: 10.1029/2021MS002968

Klocke, D., Brueck, M., Hohenegger, C., & Stevens, B. (2017). Rediscovery of the doldrums in storm-resolving simulations over the tropical Atlantic. *Nature Geoscience*, *10*(12), 891–896. doi: 10.1038/s41561-017-0005-4

Krämer, M., Rolf, C., Luebke, A., Afchine, A., Spelten, N., Costa, A., … Avallone, L. (2016). A microphysics guide to cirrus clouds – Part 1: Cirrus types. *Atmospheric Chemistry and Physics*, *16*(5), 3463–3483. doi: 10.5194/acp-16-

3463-2016

Krämer, M., Rolf, C., Spelten, N., Afchine, A., Fahey, D., Jensen, E., … Sourdeval, O. (2020). A Microphysics Guide to Cirrus – Part II:Climatologies of Clouds and Humidity fromObservations. *Atmospheric Chemistry and Physics*. doi: 10.5194/acp-20-12569-2020

Krämer, M., Schiller, C., Afchine, A., Bauer, R., Gensch, I., Mangold, A., … Spichtinger, P. (2009). Ice supersaturations and cirrus cloud crystal numbers. *Atmospheric Chemistry and Physics*, *9*(11), 3505–3522. doi: 10.5194/acp-9-3505-2009

Kuang, Z., & Bretherton, C. S. (2004). Convective influence on the heat balance of the tropical tropopause layer: A cloud-resolving model study. *Journal of the Atmospheric Sciences*, *61*(23), 2919–2927. doi: 10.1175/JAS-3306.1

Kubar, T. L., & Hartmann, D. L. (2008). Vertical structure of tropical oceanic convective clouds and its relation to precipitation. *Geophysical Research Letters*, *35*(3). doi: 10.1029/2007GL032811

Kulkarni, G., Fan, J., Comstock, J. M., Liu, X., & Ovchinnikov, M. (2012). Laboratory measurements and model sensitivity studies of dust deposition ice nucleation. *Atmospheric Chemistry and Physics*, *12*(16), 7295–7308. doi: 10.5194/acp-12-7295-2012

Kärcher, B. (2022). A Parameterization of Cirrus Cloud Formation: Revisiting Competing Ice Nucleation. *Journal of Geophysical Research: Atmospheres*, *127*(18). doi: 10.1029/2022JD036907

Lamb, K. D., Harrington, J. Y., Clouser, B. W., Moyer, E. J., Sarkozy, L., Ebert, V., … Saathoff, H. (2023). Re-evaluating cloud chamber constraints on depositional ice growth in cirrus clouds – part 1: Model description and sensitivity tests. *Atmospheric Chemistry and Physics*, *23*(11), 6043–6064. Retrieved from `https://acp.copernicus.org/articles/23/6043/2023/` doi: 10.5194/acp-23-6043-2023

Lamraoui, F., Krämer, M., Afchine, A., Sokol, A. B., Khaykin, S., Pandey, A., & Kuang, Z. (2023). Sensitivity of convectively driven tropical tropopause cirrus properties to ice habits in high-resolution simulations. *Atmospheric Chemistry and Physics*, *23*(4), 2393–2419. doi: 10.5194/acp-23-2393-2023

Lang, T., Naumann, A. K., Stevens, B., & Buehler, S. A. (2021). Tropical free-tropospheric humidity differences and their effect on the clear-sky radiation budget in global storm-resolving models. *Journal of Advances in Modeling Earth Systems*, *13*(11), e2021MS002514. doi: 10.1029/2021MS002514

Lawson, R. P., Woods, S., Jensen, E., Erfani, E., Gurganus, C., Gallagher, M., ... Krämer, M. (2019). A review of ice particle shapes in cirrus formed in situ and in anvils. *Journal of Geophysical Research: Atmospheres*, *124*(17–18), 10049–10090. doi: 10.1029/2018JD030122

Lilly, D. (1988). Cirrus outflow dynamics. *Journal of Atmospheric Sciences*, *45*(10), 1594–1605.

Lin, L., Fu, Q., Zhang, H., Su, J., Yang, Q., & Sun, Z. (2013). Upward mass fluxes in tropical upper troposphere and lower stratosphere derived from radiative transfer calculations. *Journal of Quantitative Spectroscopy and Radiative Transfer*, *117*, 114–122. doi: 10.1016/j.jqsrt.2012.11.016

Liou, K.-N. (1986). Influence of cirrus clouds on weather and climate processes: A global perspective. *Monthly Weather Review*, *114*(6), 1167–1199. doi: 10.1175/1520-0493(1986)114¡1167:IOCCOW¿2.0.CO;2

Liu, X., & Penner, J. E. (2005). Ice nucleation parameterization for global models. *Meteorologische Zeitschrift*, *14*(4), 499–514. doi: 10.1127/0941-2948/2005/0059

Luo, Z., & Rossow, W. B. (2004, December). Characterizing tropical cirrus life cycle, evolution, and interaction with upper-tropospheric water vapor using lagrangian trajectory analysis of satellite observations. *Journal of Climate*, *17*(23), 4541–4563. doi: 10.1175/3222.1

Manabe, S., & Strickler, R. (1964). Thermal equillibrium of the atmosphere with convective adjustment. *Journal of Atmospheric Sciences*, *21*, 361–385. doi: 10.1175/1520-0469(1964)021¡0361:TEOTAW¿2.0.CO;2

Massie, S., Gettelman, A., Randel, W., & Baumgardner, D. (2002). Distribution of tropical cirrus in relation to convection. *Journal of Geophysical Research: Atmospheres*, *107*(D21), AAC 19-1-AAC 19-16. doi: 10.1029/2001JD001293

McCumber, M., Tao, W.-K., Simpson, J., Penc, R., & Soong, S.-T. (1991). Comparison of ice-phase microphysical parameterization schemes using numerical simulations of tropical convection. *Journal of Applied Meteorology and Climatology*, *30*, 985–1004. doi: 10.1175/1520-0450-30.7.985

McFarquhar, G. M., Heymsfield, A. J., Spinhirne, J., & Hart, B. (2000). Thin and Subvisual Tropopause Tropical Cirrus: Observations and Radiative Impacts. *Journal of the Atmospheric Sciences*, *57*(12), 1841–1853. doi: 10.1175/1520-0469(2000)057¡1841:TASTTC¿2.0.CO;2

Mitchell, D. L., Mishra, S., & Lawson, R. P. (2011). Representing the ice fall speed in climate models: Results from tropical composition, cloud and climate coupling (tc4) and the indirect and semi-direct aerosol campaign (isdac). *Journal of Geophysical Research: Atmospheres*, *116*(D1). doi: 10.1029/2010JD015433

Mitchell, D. L., Rasch, P., Ivanova, D., McFarquhar, G., & Nousiainen, T. (2008). Impact of small ice crystal assumptions on ice sedimentation rates in cirrus clouds and gcm simulations. *Geophysical Research Letters*, *35*(9). doi: 10.1029/2008GL033552

Morrison, H., & Milbrandt, J. A. (2015). Parameterization of Cloud Microphysics Based on the Prediction of Bulk Ice Particle Properties. Part I: Scheme Description and Idealized Tests. *Journal of the Atmospheric Sciences*, *72*(1), 287–311. doi: 10.1175/JAS-D-14-0065.1

Morrison, H., van Lier-Walqui, M., Fridlind, A. M., Grabowski, W. W., Harrington, J. Y., Hoose, C., … Xue, L. (2020). Confronting the challenge of modeling cloud and precipitation microphysics. *Journal of Advances in Modeling Earth*

Systems, *12*(8). doi: 10.1029/2019MS001689

Möhler, O., Field, P. R., Connolly, P., Benz, S., Saathoff, H., Schnaiter, M., … Heymsfield, A. J. (2006). Efficiency of the deposition mode ice nucleation on mineral dust particles. *Atmospheric Chemistry and Physics*, *6*(10), 3007–3021. doi: 10.5194/acp-6-3007-2006

Naumann, A. K., Esch, M., & Stevens, B. (2024). How the representation of microphysical processes affects tropical condensate in a global storm-resolving model. *EGUsphere*, *2024*, 1–19. Retrieved from `https://egusphere.copernicus.org/preprints/2024/egusphere-2024-2268/` doi: 10.5194/egusphere-2024-2268

Nugent, J. M., Turbeville, S. M., Bretherton, C. S., Blossey, P. N., & Ackerman, T. P. (2022). Tropical Cirrus in Global Storm-Resolving Models: 1. Role of Deep Convection. *Earth and Space Science*, *9*(2). doi: 10.1029/2021EA001965

Paukert, M., Hoose, C., & Simmel, M. (2017). Redistribution of ice nuclei between cloud and rain droplets: Parameterization and application to deep convective clouds. *Journal of Advances in Modeling Earth Systems*, *9*(1), 514–535. doi: 10.1002/2016MS000841

Pradhan, R. K., Markonis, Y., Vargas Godoy, M. R., Villalba-Pradas, A., Andreadis, K. M., Nikolopoulos, E. I., … Hanel, M. (2022). Review of GPM IMERG performance: A global perspective. *Remote Sensing of Environment*, *268*, 112754. doi: 10.1016/j.rse.2021.112754

Putman, W. M., & Lin, S.-J. (2007). Finite-volume transport on various cubed-sphere grids. *Journal of Computational Physics*, *227*(1), 55–78. doi: 10.1016/j.jcp.2007.07.022

Putman, W. M., & Suarez, M. (2011). Cloud-system resolving simulations with the NASA Goddard Earth Observing System global atmospheric model (GEOS-5). *Geophysical Research Letters*, *38*(16). doi: 10.1029/2011GL048438

Randall, D., Khairoutdinov, M., Arakawa, A., & Grabowski, W. (2003, November).

Breaking the cloud parameterization deadlock. *Bullet of the American Meterological Society*, *84*(11). doi: 10.1175/BAMS-84-11-1547

Romps, D. M. (2014). An analytical model for tropical relative humidity. *Journal of Climate*, *27*(19), 7432–7449. doi: 10.1175/JCLI-D-14-00255.1

Saito, M., Iwabuchi, H., Yang, P., Tang, G., King, M. D., & Sekiguchi, M. (2017). Ice particle morphology and microphysical properties of cirrus clouds inferred from combined caliop-iir measurements. *Journal of Geophysical Research: Atmospheres*, *122*(8), 4440–4462. doi: 10.1002/2016JD026080

Sanderson, B. M., Piani, C., Ingram, W. J., Stone, D. A., & Allen, M. R. (2008). Towards constraining climate sensitivity by linear analysis of feedback patterns in thousands of perturbed-physics gcm simulations. *Climate Dynamics*, *30*(2), 175–190. doi: 10.1007/s00382-007-0280-7

Sassen, K., Wang, Z., & Liu, D. (2009). Cirrus clouds and deep convection in the tropics: Insights from CALIPSO and CloudSat. *Journal of Geophysical Research*, *114*, D00H06. doi: 10.1029/2009JD011916

Satoh, M., Noda, A. T., Seiki, T., Chen, Y.-W., Kodama, C., Yamada, Y., … Sato, Y. (2018). Toward reduction of the uncertainties in climate sensitivity due to cloud processes using a global non-hydrostatic atmospheric model. *Progress in Earth and Planetary Science*, *5*(1), 67. doi: 10.1186/s40645-018-0226-1

Satoh, M., Stevens, B., Judt, F., Khairoutdinov, M., Lin, S.-J., Putman, W. M., & Düben, P. (2019). Global cloud-resolving models. *Current Climate Change Reports*, *5*(3), 172–184. doi: 10.1007/s40641-019-00131-0

Schneider, J., Höhler, K., Wagner, R., Saathoff, H., Schnaiter, M., Schorr, T., … Möhler, O. (2021). High homogeneous freezing onsets of sulfuric acid aerosol at cirrus temperatures. *Atmospheric Chemistry and Physics*, *21*(18), 14403–14425. Retrieved from `https://acp.copernicus.org/articles/21/14403/2021/` doi: 10.5194/acp-21-14403-2021

Schoeberl, M. R., Jensen, E. J., Pfister, L., Ueyama, R., Avery, M., & Dessler, A. E.

(2018). Convective Hydration of the Upper Troposphere and Lower Stratosphere. *Journal of Geophysical Research: Atmospheres*, *123*(9), 4583–4593. doi: 10.1029/2018JD028286

Schumacher, C., & Houze, R. A. (2003). Stratiform Rain in the Tropics as Seen by the TRMM Precipitation Radar. *Journal of Climate*, *16*(11), 1739–1756. doi: 10.1175/1520-0442(2003)016¡1739:SRITTA¿2.0.CO;2

Seeley, J. T., Jeevanjee, N., Langhans, W., & Romps, D. M. (2019). Formation of tropical anvil clouds by slow evaporation. *Geophysical Research Letters*, *46*(1), 492–501. doi: 10.1029/2018GL080747

Seiki, T., & Ohno, T. (2022). Improvements of the double-moment bulk cloud microphysics scheme in the nonhydrostatic icosahedral atmospheric model (nicam). *Journal of the Atmospheric Sciences*, *80*(1), 111–127. doi: 10.1175/JAS-D-22-0049.1

Seiki, T., Roh, W., & Satoh, M. (2022, August). Cloud microphysics in global cloud resolving models. *Atmosphere-Ocean*, *60*(3–4), 477–505. doi: 10.1080/07055900.2022.2075310

Sherwood, S. C., Webb, M. J., Annan, J. D., Armour, K. C., Forster, P. M., Hargreaves, J. C., … Zelinka, M. D. (2020). An assessment of earth's climate sensitivity using multiple lines of evidence. *Reviews of Geophysics*, *58*(4), e2019RG000678. doi: 10.1029/2019RG000678

Skamarock, W. C., Klemp, J. B., Duda, M. G., Fowler, L. D., Park, S.-H., & Ringler, T. D. (2012). A Multiscale Nonhydrostatic Atmospheric Model Using Centroidal Voronoi Tesselations and C-Grid Staggering. *Monthly Weather Review*, *140*(9), 3090–3105. doi: 10.1175/MWR-D-11-00215.1

Sokol, A. B., & Hartmann, D. L. (2020). Tropical Anvil Clouds: Radiative Driving Toward a Preferred State. *Journal of Geophysical Research: Atmospheres*, *125*(21). doi: 10.1029/2020JD033107

Sokol, A. B., Wall, C. J., & Hartmann, D. L. (2024). Greater climate sensitivity implied by anvil cloud thinning. *Nature Geoscience*, 1–6. doi: 10.1038/s41561-024-01420-6

Solomon, S., Rosenlof, K. H., Portmann, R. W., Daniel, J. S., Davis, S. M., Sanford, T. J., & Plattner, G.-K. (2010). Contributions of Stratospheric Water Vapor to Decadal Changes in the Rate of Global Warming. *Science*, *327*(5970), 1219–1223. doi: 10.1126/science.1182488

Song, J., Song, F., Feng, Z., Leung, L. R., Li, C., & Wu, L. (2024). Realistic precipitation diurnal cycle in global convection-permitting models by resolving mesoscale convective systems. *Geophysical Research Letters*, *51*(13), e2024GL109945. doi: 10.1029/2024GL109945

Stevens, B., Acquistapace, C., Hansen, A., Heinze, R., Klinger, C., Klocke, D., ... Zängl, G. (2020). The Added Value of Large-eddy and Storm-resolving Models for Simulating Clouds and Precipitation. *Journal of the Meteorological Society of Japan. Ser. II*, *98*(2), 395–435. doi: 10.2151/jmsj.2020-021

Stevens, B., Satoh, M., Auger, L., Biercamp, J., Bretherton, C. S., Chen, X., ... Zhou, L. (2019). DYAMOND: the DYnamics of the Atmospheric general circulation Modeled On Non-hydrostatic Domains. *Progress in Earth and Planetary Science*, *6*(1), 61. doi: 10.1186/s40645-019-0304-z

Su, H., Jiang, J. H., Neelin, J. D., Shen, T. J., Zhai, C., Yue, Q., ... Yung, Y. L. (2017). Tightening of tropical ascent and high clouds key to precipitation change in a warmer climate. *Nature Communications*, *8*(1), 15771. doi: 10.1038/ncomms15771

Sulia, K. J., Morrison, H., & Harrington, J. Y. (2014). Dynamical and microphysical evolution during mixed-phase cloud glaciation simulated using the bulk adaptive habit prediction model. *Journal of the Atmospheric Sciences*, *71*(11), 4158–4180. doi: 10.1175/JAS-D-14-0070.1

Sullivan, S., & Voigt, A. (2021). Ice microphysical processes exert a strong control on the simulated radiative energy budget in the tropics. *Communications Earth &*

Environment, *2*(1), 1–8. doi: 10.1038/s43247-021-00206-7

Sullivan, S., Voigt, A., Miltenberger, A., Rolf, C., & Krämer, M. (2022). A lagrangian perspective of microphysical impact on ice cloud evolution and radiative heating. *Journal of Advances in Modeling Earth Systems*, *14*(11), e2022MS003226. doi: 10.1029/2022MS003226

Tan, I., & Storelvmo, T. (2016). Sensitivity study on the influence of cloud microphysical parameters on mixed-phase cloud thermodynamic phase partitioning in cam5. *Journal of the Atmospheric Sciences*, *73*(2), 709–728. doi: 10.1175/JAS-D-15-0152.1

Tan, J., Huffman, G. J., Bolvin, D. T., & Nelkin, E. J. (2019). IMERG V06: Changes to the Morphing Algorithm. *Journal of Atmospheric and Oceanic Technology*. doi: 10.1175/JTECH-D-19-0114.1

Turbeville, S. M., Nugent, J. M., Ackerman, T. P., Bretherton, C. S., & Blossey, P. N. (2022). Tropical Cirrus in Global Storm-Resolving Models: 2. Cirrus Life Cycle and Top-of-Atmosphere Radiative Fluxes. *Earth and Space Science*, *9*(2). doi: 10.1029/2021EA001978

Virts, K. S., Wallace, J. M., Fu, Q., & Ackerman, T. P. (2010). Tropical Tropopause Transition Layer Cirrus as Represented by CALIPSO Lidar Observations. *Journal of the Atmospheric Sciences*, *67*(10), 3113–3129. doi: 10.1175/2010JAS3412.1

Voldoire, A., Decharme, B., Pianezze, J., Lebeaupin Brossier, C., Sevault, F., Seyfried, L., . . . Riette, S. (2017). SURFEX v8.0 interface with OASIS3-MCT to couple atmosphere with hydrology, ocean, waves and sea-ice models, from coastal to global scales. *Geoscientific Model Development*, *10*(11), 4207–4227. doi: 10.5194/gmd-10-4207-2017

Wall, C. J., & Hartmann, D. L. (2018). Balanced Cloud Radiative Effects Across a Range of Dynamical Conditions Over the Tropical West Pacific. *Geophysical Research Letters*, *45*(20). doi: 10.1029/2018GL080046

Walters, D., Baran, A. J., Boutle, I., Brooks, M., Earnshaw, P., Edwards, J., … Zerroukat, M. (2019). The Met Office Unified Model Global Atmosphere 7.0/7.1 and JULES Global Land 7.0 configurations. *Geoscientific Model Development*, *12*(5), 1909–1963. doi: 10.5194/gmd-12-1909-2019

Wang, Y., Su, H., Jiang, J. H., Xu, F., & Yung, Y. L. (2020). Impact of cloud ice particle size uncertainty in a climate model and implications for future satellite missions. *Journal of Geophysical Research: Atmospheres*, *125*(6), e2019JD032119. doi: 10.1029/2019JD032119

Weng, H., Han, Y., Deng, X., Dong, L., & Liu, Y. (2024). Physical characteristics of convective and non-convective cirrus clouds from CALIPSO data over the South China Sea. *Atmospheric and Oceanic Science Letters*, 100510. doi: 10.1016/j.aosl.2024.100510

Wilson, D. R., & Ballard, S. P. (1999). A microphysically based precipitation scheme for the UK meteorological office unified model. *Quarterly Journal of the Royal Meteorological Society*, *125*(557), 1607–1636. doi: 10.1002/qj.49712555707

Windmiller, J. M., & Hohenegger, C. (2019). Convection On the Edge. *Journal of Advances in Modeling Earth Systems*, *11*(12), 3959–3972. doi: 10.1029/2019MS001820

Wing, A. A., & Cronin, T. W. (2016). Self-aggregation of convection in long channel geometry. *Quarterly Journal of the Royal Meteorological Society*, *142*(694), 1–15. doi: 10.1002/qj.2628

Wing, A. A., Emanuel, K., Holloway, C. E., & Muller, C. (2017). Convective self-aggregation in numerical simulations: A review. *Surveys in Geophysics*, *38*(6), 1173–1197. doi: 10.1007/s10712-017-9408-4

Wing, A. A., Reed, K. A., Satoh, M., Stevens, B., Bony, S., & Ohno, T. (2018). Radiative–convective equilibrium model intercomparison project. *Geoscientific Model Development*, *11*(2), 793–813. doi: 10.5194/gmd-11-793-2018

Wing, A. A., Stauffer, C. L., Becker, T., Reed, K. A., Ahn, M., Arnold, N. P.,

… Zhao, M. (2020). Clouds and convective self-aggregation in a multimodel ensemble of radiative-convective equilibrium simulations. *Journal of Advances in Modeling Earth Systems*, *12*(9). doi: 10.1029/2020MS002138

Woods, C. P., Stoelinga, M. T., & Locatelli, J. D. (2007). The improve-1 storm of 1–2 february 2001. part iii: Sensitivity of a mesoscale model simulation to the representation of snow particle types and testing of a bulk microphysical scheme with snow habit prediction. *Journal of the Atmospheric Sciences*, *64*(11), 3927–3948. doi: 10.1175/2007JAS2239.1

Yang, Q., Fu, Q., & Hu, Y. (2010). Radiative impacts of clouds in the tropical tropopause layer. *Journal of Geophysical Research: Atmospheres*, *115*(D4). doi: 10.1029/2009JD012393

Zhang, C., & Harrington, J. Y. (2015). The effects of surface kinetics on crystal growth and homogeneous freezing in parcel simulations of cirrus. *Journal of the atmospheric sciences*. doi: 10.1175/JAS-D-14-0285.1

Zhang, C., Wang, M., Morrison, H., Somerville, R. C. J., Zhang, K., Liu, X., & Li, J.-L. F. (2014). Investigating ice nucleation in cirrus clouds with an aerosol-enabled multiscale modeling framework. *J. Adv. Model. Earth Syst.*, *6*, 998–1015. doi: 10.1002/2014MS000343

Zhao, X., Lin, Y., Peng, Y., Wang, B., Morrison, H., & Gettelman, A. (2017). A single ice approach using varying ice particle properties in global climate model microphysics. *Journal of Advances in Modeling Earth Systems*, *9*(5), 2138–2157. doi: 10.1002/2017MS000952

Zhou, L., Harris, L., Chen, J.-H., Gao, K., Guo, H., Xiang, B., … Morin, M. (2022). Improving Global Weather Prediction in GFDL SHiELD Through an Upgraded GFDL Cloud Microphysics Scheme. *Journal of Advances in Modeling Earth Systems*, *14*(7). doi: 10.1029/2021MS002971

Zängl, G., Reinert, D., Rípodas, P., & Baldauf, M. (2015). The ICON (ICOsahedral Non-hydrostatic) modelling framework of DWD and MPI-M: Description of the non-hydrostatic dynamical core. *Quarterly Journal of the Royal Meteorological Society*, *141*(687), 563–579. doi: 10.1002/qj.2378